Thomas Rinder

Precipitation of Calcium Carbonates - Field Studies and Laboratory Experiments

DOCTORAL THESIS

For obtaining the academic degree of

Doktor der Naturwissenschaften

Graz University of Technology

Institute of Applied Geosciences

Assessors:

Univ.-Prof. Dipl.-Min. Dr.rer.nat. Martin Dietzel

Dipl.-Chem. Dr. Albrecht Leis

Graz, July 2012

Acknowledgments

First off all I want to thank my supervisor Martin Dietzel for constant support, good advice and stimulating discussion throughout my time on this institute. Albrecht Leis is thanked for providing the carbon and oxygen isotopic measurements. Florian Mittermayr and Arthur Deditius are thanked for scientific collaboration, microprobe analysis and exceptionally inspiring lunch breaks. I would also like to thank Maria Hierz, Daniel Höllen, Judith Jernej, Dietmar Klammer, Kurt Krenn, Christine Latal and Andrea Wolf for providing all sorts of analysis needed for the completion of this thesis as well as Anna Pendl for her help in administrative issues. Othmar Nestroy and Rashid Abdalla are especially thanked for times of relief and off-topic discussion, when working on the thesis became exhausting. Cheers!

I greatly appreciate the financial support of Graz University of Technology, the NAWI Graz through the Graz Advanced School of Science and the Austrian Federal Railways (ÖBB) as well as co-workers from 3G consulting and U.C.M. Heidelberg for their support during sampling.

At last I would like to thank my family for their support and encouragement along the way.

Statutory declaration

I declare that I have authored this thesis independently, that I have not used other than the declared sources / resources, and that I have explicitly marked all material which has been quoted either literally or by content from the used sources.

…… ……..

date (signature)

Abstract

Calcium carbonate formation on the field scale by means of tunnel drainage clogging and in flow through experiments for precipitation in porous media is investigated within this thesis.

Drainage systems of tunnels may get clogged by calcite precipitates, resulting in cost intensive maintenance for the operating company. Dissolved Ca^{2+} derives from groundwater and from dissolution of portlandite at the shotcrete. The carbonate in the sinter is obtained from the groundwater or from absorption of atmospheric CO_2. Here an elemental, isotopic and modelling approach is introduced to decipher the evolution of alkaline tunnel drainage solutions and sinter formation mechanisms. Interaction of local groundwater and shotcrete/concrete is indicated by a positive correlation of K^+ content and pH and a loss of aqueous Mg^{2+} by brucite formation (pH > 10.5). Variability in Ca^{2+} and DIC is attributed to portlandite dissolution, calcite precipitation and CO_2 exchange with the atmosphere, where $^{13}C/^{12}C$ and $^{18}O/^{16}O$ distribution of calcite clearly traces the origin of carbonate. The internal P_{CO2} value of a solution is a reliable proxy to evaluate whether uptake of CO_2 results in an increase or decrease of calcite saturation degree with a threshold value of $10^{-6.15}$ atm at 25°C (pH ≈ 11). Precipitation rates of calcite are highest at pH ≈ 10, which may cause relatively low abundance of respective moderate drainage solutions. Mixing of groundwater-like solutions with strong alkaline drainage solutions has to be considered as a crucial factor for evaluating apparent composition of drainage solutions and calcite precipitation capacities.

In the laboratory experiments for precipitation in porous media calculation of overall distribution coefficients D_{Sr} and D_{Mn} for the formation of calcite results in 0.68 and 6.1 at $SI_{Calcite}$ values of 1.1 and 1.5, respectively. For both, the Sr^{2+} and Mn^{2+} bearing experiment D values calculated from aqueous solutions are in good agreement with literature values, whereas actual incorporation of the trace elements from microprobe analysis is very heterogeneous delivering a maximum D_{Sr} and D_{Mn} value of 18 and 163, respectively. Despite the fact that the concentrations of Ca^{2+} and Sr^{2+} in the experimental solution were in the range of seawater, D_{Sr} values of the newly formed precipitates are much higher than reported for precipitates from natural environments. High amounts of Sr^{2+} in calcite are referred to recrystallisation of aragonite to calcite, whereas our results indicate that such incorporation occurred without transformation.

Conclusively precipitation environmental conditions for $CaCO_3$ formation, like mixing behaviour, precipitation rate and polymorphism, have a huge impact on Sr^{2+} and Mn^{2+} incorporation in $CaCO_3$ which has to be taken into account for their applicability as tracers for spatial and temporal evolution of precipitations in porous media.

Kurzfassung

In dieser Arbeit wird die Kalziumkarbonatbildung im angewandten und experimentellen System anhand der Versinterung von Tunneldrainagen und über Durchflussversuche zur Charakterisierung der Zementation poröser Medien untersucht.

Die Versinterung von Tunneldrainagen führt zu kostenintensiven Wartungsarbeiten für die Betreibergesellschaft. Das Kalzium in den Ablagerungen kommt aus dem Grundwasser sowie aus der Auflösung von Portlandit aus dem Spritzbeton. Das Karbonat wird aus dem Grundwasser oder aus der Absorption von atmosphärischen CO_2 erhalten. In dieser Arbeit wird über die Interpretation der (isotopen)geochemischen Zusammensetzung und hydrochemischer Modellierungen versucht die Herkunft und Entwicklung alkalischer Lösungen und die damit verbundenen Reaktionsmechanismen aufzuklären. Die Interaktion des örtlichen Grundwassers mit Spritzbeton wird über eine positive Korrelation der K^+ Konzentration mit dem pH-Wert und einen Verlust von gelösten Mg^{2+} Ionen über Bruzitbildung (pH> 10,5) angezeigt. Variationsbereiche im Gehalt an gelöstem Kalzium und DIC resultieren aus der Portlanditauflösung, der $CaCO_3$ Ausfällung und dem CO_2 Austausch mit der umgebenden Atmosphäre, wobei die Verteilung der stabilen Isotope des $^{13}C/^{12}C$ and $^{18}O/^{16}O$ die Herkunft des Karbonats entschlüsseln kann.

Die interne P_{CO2}-Wert einer Lösung ist ein zuverlässiger Proxy um zu beurteilen, ob die Aufnahme von CO_2 in eine stark alkalische Lösung zu einer Zu- oder Abnahme der Kalzitsättigung führt. Der Pco_2 Grenzwert liegt diesbezüglich bei $10^{-6.15}$ atm für 25 °C (pH ≈ 11).

Die Abscheidungsraten an Kalzit sind bei einem pH-Wert um 10 am höchsten anzusetzen. Dadurch ergibt sich eine mögliche Erklärung für das relativ geringe Auftreten von Wässern im letzteren pH Bereich in von uns beprobten Drainagesystemen. Die Mischung von Grundwässern mit hochalkalischen Lösungen muss als wichtiger Faktor bei der Evaluierung tatsächlicher Versinterungspotentiale berücksichtigt werden.

In den Versuchen zur Zementation poröser Medien ergab die anhand der Änderung der Gehalte an gelösten Ionen durchgeführte Berechnung D_{Sr} und D_{Mn} Werte von 0.68 und 6.08, bei einem SI_{Kalzit} von 1.1 und 1.5 für die jeweiligen Versuche mit Strontium und Mangan.

Während die so errechneten D-Werte n guter Übereinstimmung mit denen vergleichbarer Arbeiten sind, ist die tatsächliche über Mikrosondenmessung erhaltene Aufnahme der Spurenelemente sehr heterogen liefert einen maximale D_{Sr} und D_{Mn}-Wert von 18 bzw. 163.

Trotz der Tatsache, dass die Konzentrationen von Ca^{2+} und Sr^{2+} in der Lösung im Bereich von Meerwasser lagen, liegen die Strontiumgehalte in den neu gebildeten Festphasen weit über denen natürlicher Umfelder. Hohe Mengen an Sr^{2+} im Kalzit werden meist der Rekristallisation von Aragonit zugeschrieben, während die vorhandenen Ergebnisse nahelegen, dass hohe

Strontiumgehalte auch direkt im Kalzit auftreten können. Zusammenfassend scheinen kleine Mengen von Sr^{2+} und Mn^{2+} einen großen Einfluss auf Geschwindigkeit und Polymorphismus bei der Bildung von Kalziumkarbonat zu haben. Es gilt daher kritisch zu hinterfragen ob sie aufgrund dieser Eigenschaften als Tracer für räumliche und zeitliche Entwicklung von Ausfällungsprozessen in porösen Medien infrage kommen.

Table of contents

1. Introduction

The formation conditions of calcium carbonate have been widely addressed in research due to the wide abundance of $CaCO_3$ on the Earth's surface and its potential for the reconstruction of paleoenvironments and for technical applications like the evidential impact on the operational reliability of e.g. wells, pipelines, drainage systems and heat exchangers.

Lithification of unconsolidated carbonate material in marine and freshwater environments has been studied by (Dravis, 1996; Friedman, 1998) for characterisation and evolution of carbonate platforms. Calcium carbonate cementation of sandstone leads to a loss in permeability and porosity thus negatively influencing the potential quality of the host rock as a hydrocarbon reservoir (Taylor and Machent, 2011). The spatial distribution and evolution of such concretions has been studied by (Bjorkum and Walderhaug, 1990) and (Molenaar and Zijlstra, 1997), where cementation of marine sediments is attributed to precipitation from supersaturated seawater on the one hand as well as redistribution of bioclastic material on the other.

Within the increasing efforts to reduce CO_2 emission into the atmosphere the possibility of long term storage by means of fixation in carbonates receives more attention in recent years (Gislason et al., 2010; Matter et al., 2009). Such a CO_2 sequestration and accompanied precipitation of carbonates causes a change in permeability of the host rock (Xu et al., 2011) and therefore addresses research fields comparable to the investigation of natural environments.

Negative effects of calcium carbonate formation have been addressed by (Dietzel et al., 2008; Girmscheid et al., 2003), where clogging of drainage tubes in tunnels may significantly affect the functional efficiency of a drainage system. Additionally, according to (Molenaar and Venmans, 1993), cementation of sand may bear problems for dredging operations, where slightly lithified layers may inhibit the failure of underwater slopes and therefore largely reduce production rates. On the other hand (Lioliou et al., 2007) also pointed out positive effects like softening of water supersaturated with respect to calcite by addition of seed crystals. Additionally the same mechanisms that are responsible for cementation of sandstones might be attractive to achieve stabilisation of soils and embankments.

The effect of potential inhibitors such as Mg^{2+} and SO_4^{2-} (Flaathen et al., 2011; Zhang and Dawe, 2000) on the distribution and morphology of calcium carbonates as well as the effect of precipitation rate, temperature and solution composition on trace element incorporation into aragonite and calcite has been extensively studied (Fairchild and Treble, 2009; Franklin and Morse, 1983; Lorens, 1981; Mucci and Morse, 1983).

For all of these scientific fields an approach, interpreting major down to trace element behaviour is considered a promising to tool to decipher the individual formation conditions and water-rock interactions that lead to the apparent mineralogical and chemical composition of the precipitated material.

1.1 Aims and structure of the thesis

The two main research projects of my PhD thesis deal with the formation conditions and behaviour of calcium carbonates. On the one hand I am investigating the $CaCO_3$ precipitation in alkaline tunnel drainage systems, where I develop my scientific conclusions from field research. On the other hand I am studying the cementation of porous media on the laboratory scale, using column experiments.

Within the study of the applied system my research objective is to identify the processes responsible for tunnel drainage scaling in individual tunnel buildings and the overall mechanisms responsible for the formation of calcium carbonate under moderate to strongly alkaline conditions. Scaling can be related to water-concrete interaction. But it can also be a result of groundwater interaction with the atmosphere, e.g. at a high internal partial pressure of CO_2 and the precipitation of $CaCO_3$ in analogy to speleothem formation. $^{13}C/^{12}C$ signatures, Mg/Ca and Sr/Ca signatures in solids and solutions as well as leaching of K^+ and Na^+ from concrete of the tunnel wall are reliable proxies to identify the responsible mechanisms.

This part comprises the manuscript -*Rinder, T., Dietzel, M., Leis, A. Calcium Carbonate formation under Alkaline conditions - Case studies and hydrogeochemical modelling,* which is submitted *to Applied Geochemistry (chapter 2),* the conference contribution *F. Mittermayr , Rinder T., Klammer, D., Leis A., and Dietzel, M. (2012) A carbon isotope study of thaumasite and calcite sinter formation in underground constructions. Int. Con. Dur. Con. 1-14 (in press)* (chapter 3), which takes a closer look on the application of the stable isotopes of $^{13}C/^{12}C$ on the interpretation of tunnel drainage clogging and the publication *M. Dietzel, T. Rinder, A. Leis, P. Reichl, P. Sellner, C. Draschitz, G. Plank, D. Klammer, and H. Schöfer (2008) Koralm tunnel as a case study for sinter formation in drainage systems - precipitation mechanisms and retaliatory action. Geomechik und Tunnelbbau, 1(4), 271-278* (chapter 4) which deals with monitoring and evaluation of sinter formation potential in an Austrian railway tunnel by means of in situ experiments in the tunnel, carried out during my PhD thesis. This first part is concluded by mixing calculations (chapter 5), carried out by using the computer code PHREEQC (Parkhurst and Apello, 1999). By expanding the concept of mixing corrosion as presented first by (Bögli,

1964), the mixing of calcite saturated waters under alkaline conditions may lead to oversaturated solutions thus precipitate $CaCO_3$. Such a process might be also relevant for mixing of waters that derive from closed system during calcite dissolution.

The second part of my thesis deals with experiments for the precipitation of $CaCO_3$ in porous media (chapter 6). This part is represented by the manuscript *Rinder, T., Dietzel, M., Deditius, A. Sr^{2+} and Mn^{2+} incorporation during $CaCO_3$ cementation on calcitic and aragonitic shells*. Herein I am studying the trace element incorporation of, Sr^{2+} and Mn^{2+} in $CaCO_3$ druing precipitation from solution, and their effects on precipitation kinetics as well as polymorphism. Additionally periodical trace element addition of, e.g. Mn^{2+} and Sr^{2+} is be used to decipher the evolution of calcium carbonate formation over time by analysis of polished thin sections.

Conclusively for field studies as well as laboratory experiments the investigation of trace element behaviour with respect to $CaCO_3$ formation by means of aqueous solution and solid analysis, as well as PHREEQC calculations are the major tools to contribute to the understanding of evolution and spatial distribution carbonates formed under alkaline man-made and natural conditions.

1.2 References

Bjorkum, P.A., Walderhaug, O., 1990. Geometrical arrangement of calcite cementation within shallow marine sandstones. Earth-Science Reviews 29, 145-161.

Bögli, A., 1964. Mischungskorrosion: ein Beitrag zum Verkastungsproblem. Erkunde 18, 83–92.

Dietzel, M., Rinder, T., Niedermayr, A., Mittermayr, F., Leis, A., Klammer, D., Köhler, S., Reichl, P., 2008. Mechanisms of Sinter Formation in Drainage Systems. BHM Berg- und Hüttenmännische Monatshefte 153, 369-372.

Dravis, J.J., 1996. Rapidity of freshwater calcite cementation and implications for carbonate diagenesis and sequence stratigraphy. Sedimentary Geology 107, 1-10.

Fairchild, I.J., Treble, P.C., 2009. Trace elements in speleothems as recorders of environmental change. Quaternary Science Reviews 28, 449-468.

Flaathen, T.K., Oelkers, E.H., Gislason, S.u.R., Aagaard, P., 2011. The effect of dissolved sulphate on calcite precipitation kinetics and consequences for subsurface CO_2 storage. Energy Procedia 4, 5037-5043.

Franklin, M.L., Morse, J.W., 1983. The interaction of manganese(II) with the surface of calcite in dilute solutions and seawater. Marine Chemistry 12, 241-254.

Friedman, G.M., 1998. Rapidity of marine carbonate cementation â€" implications for carbonate diagenesis and sequence stratigraphy: perspective. Sedimentary Geology 119, 1-4.

Girmscheid, G., Gamisch, T., Klein, T., Meinlschmidt, A., 2003. Scale sintering in tunnel drainages - Mechanisms of scale formation. Bauingenieur 78, 292-300.

Gislason, S.R., Wolff-Boenisch, D., Stefansson, A., Oelkers, E.H., Gunnlaugsson, E., Sigurdardottir, H.l., Sigfusson, B., Broecker, W.S., Matter, J.M., Stute, M., Axelsson, G., Fridriksson, T., 2010. Mineral sequestration of carbon dioxide in basalt: A pre-injection overview of the CarbFix project. International Journal of Greenhouse Gas Control 4, 537-545.

Lioliou, M.G., Paraskeva, C.A., Koutsoukos, P.G., Payatakes, A.C., 2007. Heterogeneous nucleation and growth of calcium carbonate on calcite and quartz. Journal of Colloid and Interface Science 308, 421-428.

Lorens, R.B., 1981. Sr, Cd, Mn and Co distribution coefficients in calcite as a function of calcite precipitation rate. Geochimica et Cosmochimica Acta 45, 553-561.

Matter, J.M., Broecker, W.S., Stute, M., Gislason, S.R., Oelkers, E.H., StefÃ¡nsson, A., Wolff-Boenisch, D., Gunnlaugsson, E., Axelsson, G., BjÃ¶rnsson, G., 2009. Permanent Carbon Dioxide Storage into Basalt: The CarbFix Pilot Project, Iceland. Energy Procedia 1, 3641-3646.

Molenaar, N., Venmans, A.A.M., 1993. Calcium carbonate cementation of sand: A method for producing artificially cemented samples for geotechnical testing and a comparison with natural cementation processes. Engineering Geology 35, 103-122.

Molenaar, N., Zijlstra, J.J.P., 1997. Differential early diagenetic low-Mg calcite cementation and rhythmic hardground development in Campanian-Maastrichtian chalk. Sedimentary Geology 109, 261-281.

Mucci, A., Morse, J.W., 1983. The incorporation of Mg2+ and Sr2+ into calcite overgrowths: influences of growth rate and solution composition. Geochimica et Cosmochimica Acta 47, 217-233.

Parkhurst, D.L., Apello, C.A.J., 1999. User's guide to PHREEQC (V2). U.S. Geol. Sur, 312.

Taylor, K.G., Machent, P.G., 2011. Extensive carbonate cementation of fluvial sandstones: An integrated outcrop and petrographic analysis from the Upper Cretaceous, Book Cliffs, Utah. Marine and Petroleum Geology 28, 1461-1474.

Xu, T., Zheng, L., Tian, H., 2011. Reactive transport modeling for CO2 geological sequestration. Journal of Petroleum Science and Engineering 78, 765-777.

Zhang, Y., Dawe, R.A., 2000. Influence of Mg^{2+} on the kinetics of calcite precipitation and calcite crystal morphology. Chemical Geology 163, 129-138.

Chapter 2

Calcium Carbonate Scaling under Alkaline Conditions - Case Studies and Hydrochemical Modelling

Thomas Rinder , Martin Dietzel , Albrecht Leis

(Submitted to Applied Geochemistry, 2012)

Calcium Carbonate Scaling under Alkaline Conditions - Case Studies and Hydrochemical Modelling

Thomas Rinder [a,] *, Martin Dietzel [a], Albrecht Leis [b]

[a] *Institute of Applied Geosciences, Graz University of Technology, Rechbauerstraße 12, 8010 Graz, Austria*

[b] *Institute of Water, Energy and Suistainability, Joanneum Research, Elisabethstraße 18, 8010 Graz, Austria*

***Corresponding author.** Tel.: +43 (0)650-4360765.
E-mail address: rinder.thomas@gmx.net

Abstract

Calcium carbonate scaling comprises highly challenging tasks for its prediction, prevention, and retaliatory action. Here we used an elemental, isotopic and modelling approach to decipher the evolution of alkaline tunnel drainage solutions and sinter formation mechanisms for 3 sites in Austria. Drainage solutions are originated from local groundwater and in particular by interaction with shotcrete/concrete, which is indicated by a positive correlation of K^+ content and pH (up to 12.3), and a loss of aqueous Mg^{2+} by brucite formation (pH > 10.5). Variability in Ca^{2+} and DIC is strongly attributed to portlandite dissolution, calcite precipitation and CO_2 exchange with the atmosphere, where $^{13}C/^{12}C$ and $^{18}O/^{16}O$ distribution of calcite clearly traces the origin of carbonate. The internal P_{CO2} value is a reliable proxy to evaluate whether uptake of CO_2 results in an increase or decrease of calcite saturation degree with a threshold value of $10^{-6.15}$ atm at 25°C (pH ≈ 11). Precipitation rates of calcite are highest at pH ≈ 10, which may cause relatively low abundance of respective moderate drainage solutions. Mixing of groundwater-like solutions with strong alkaline drainage solutions has to be considered as a crucial factor for evaluating apparent composition of drainage solutions and calcite precipitation capacities. Aspects of scaling prevention are conclusively discussed.

2.1 Introduction

Calcium carbonate scaling in tunnel drainage systems can induce serious problems due to the reduction of the cross section of drainage tubes and the pollution of receiving streams by suspended $CaCO_3$ particles and ongoing sinter formation (Dietzel et al., 2008). Both drainage systems and receiving streams have to be cleaned periodically to provide a proper discharge of the drainage solutions and to fulfil environmental protection assignments. Cleaning of drainage tubes is accompanied with reduced transfer capacities or even no passage for e.g. trains and cars. Consequently scaling in tunnel drainage systems is a challenging economical task for a huge number of tunnels during construction of a tunnel and especially for building maintenance like treatment with scaling inhibitors and mechanical cleaning tools (Girmscheid et al., 2003a; Girmscheid et al., 2003b). For instance the estimated proportion of drainage maintenance charges of Austrian railway tunnels reaches up to about 40% of total maintenance charges for the whole tunnel during the expected life time of 100 years (Draschitz, 2008).

In general the formation of calcium carbonate in tunnel drainage systems is induced by groundwater reacting with the hydraulic cement phases of shotcrete at the outer lining of the tunnel, hydraulic binder used for e.g. anchor stabilization, and/or concrete used for construction, in the following referred to as water-cement interaction. Highly soluble phases such as portlandite ($Ca(OH)_2$) are dissolved in the groundwater, which results in elevated Ca^{2+} concentrations and an alkaline environment of the drainage solutions. Although water-cement reactions are complex, $CaCO_3$ precipitation directly at the shotcrete/concrete is mostly caused by the redistribution of dissolved inorganic carbon (DIC) of the groundwater induced by an increase of pH. Carbonate sinter formation in the drainage system is quite more complicated as exchange reactions between atmospheric and aqueous CO_2 as well as mixing of solutions with different chemistry have to be considered.

In former case studies tools like mineralogical, chemical or isotope signatures of the carbonate sinter and reacting solutions were successfully applied to obtain further insight in aspects like leaching of ions from shotcrete/concrete, source of trace elements in drainage solutions, sulphate attack of concrete, and source of carbonate in precipitates (Gineys et al., 2010; Hillier et al., 1999; Marion et al., 2005; Mittermayr et al., 2012a). However there is a high need to develop further proxies and to combine such kind of signatures within a multi-proxy approach to discover apparent water-cement interaction, reaction mechanisms and kinetics of $CaCO_3$ formation and the chemical evolution of drainage solutions.

An advanced understanding of the above aspects is essentially required to prevent carbonate sinter formation by application of tailored material for tunnel construction and to design a proper drainage system as well as to develop strategies for suitable counteracting against scaling.

Therefore three Austrian tunnel buildings were selected for analysing the composition of carbonate sinter in the drainage, the drainage solutions and the locally occurring groundwater. Hydrogeochemical modelling approaches are used to decipher impacts of various physicochemical parameters, individual reaction paths, $CO_{2(aq)}$ - $CO_{2(g)}$ exchange, mixing of solutions, precipitation capacities and rates for ongoing scaling.

2.2 Study area and methodology

The Grünburg (GB), Wienerwald (WW), and Koralm tunnel (KA) were selected for case studies. As a requirement local groundwater had to be available for sampling to decipher changes in its composition due to water-cement interaction, which results in individual ranges of drainage solution chemistry. The above tunnel buildings are located within the Austrian Alps, but are related to somewhat different local geological settings. GB cuts through parts of the "Flyschzone" with a typical mixture of sandstone, limestone, siltstone, shale and mudstone. WW penetrates also geological sections of the "Flyschzone", but with less calcareous rocks compared to GB. KA, which is still under construction, cuts through the crystalline basement of metamorphic rocks like gneiss, quartzite, mica schist as well as silt- and sandstones within the Quaternary basins.

However for the present task the chemical composition of the local occurring groundwater in the respective study area is most decisive. For each case study we sampled two groundwaters from wells in the vicinity of the sampling sites for tunnel drainage solution and precipitates. Sampling of drainage solutions comprises 10, 13, and 23 solutions from GB, WW and KA, respectively. Immediately after sampling the solutions were filtered through 0.45 µm membranes (cellulose acetate) to avoid suspended particles remaining in the solution. Subsequently to the filtration the solution was stored in gas-tight glass vessels (0.5L) for alkalinity and in PE vessels for ion analyses (0.5L). The sampled solutions were placed in a cooled box and subsequently transferred to the lab for measurements. 25 precipitates in total were gathered from the drainage for mineralogical, chemical and isotope analyses, where 2, 11 and 12 samples are referred to GB, WW and KA, respectively.

Field data of water samples, including pH, electrical conductivity and temperature, was recorded during sampling. Alkalinity was measured in the lab by potentiometric titration with 0.05n HCl within 6 hours after sampling. Concentration of cations (Na^+, K^+, Mg^{2+}, Ca^{2+}) and anions (Cl^-, NO_3^-, and SO_4^{2-}) was analysed by ion chromatography (Dionex ICS-3000) with an analytical error of ±3%. The computer code PHREEQC (Parkhurst and Apello, 1999) with the database minteq.dat was used to calculate saturation indices with respect to calcite ($SI_{Calcite}$) and brucite ($SI_{Brucite}$), and the internal partial pressure of CO_2 (P_{CO2} in atm) as well as for hydrogeochemical

modelling. Main focus of modelling was given on CO_2 exchange between the solution and the atmosphere, mixing of solutions and precipitation of calcite.
Mineralogical analyses of the precipitates were carried out by X-Ray Diffraction (XRD) pattern using a PANalytical X'Pert Pro series diffractometer equipped with a cobalt-target tube. Chemical digestion of selected precipitates was carried out by using 10wt. % ultrapure double distilled HNO_3 to check the chemical composition in comparison to the mineralogical content. Chemical analysis of acid digestions was done by ICP-OES (Perkin Elmer 4300) with an analytical precision of ±5%. Distribution of stable carbon and oxygen isotopes of the $CaCO_3$ precipitates was analyzed using a fully automated peripheral continuous-flow gas preparation device (Gasbench II), which was connected to a Finnigan DELTA^{plus} XP Mass Spectrometer (Dietzel et al., 2009). Respective $\delta^{13}C$ and $\delta^{18}O$ values are given in ‰ relative to VPDB (Vienna Pee Dee Belemnite).

2.3 Mechanisms of $CaCO_3$ formation

In principle the formation of calcium carbonate in tunnel drainage systems can be induced by groundwater, which is enriched in bicarbonate and calcium at a high internal partial pressure of CO_2 (P_{CO2} > $10^{-3.45}$ atm; value of the Earth's atmosphere). The degassing of CO_2 from the corresponding drainage solution into the atmosphere leads to an increase of pH. Elevated pH shifts the DIC species from HCO_3^- to CO_3^{2-}. Accordingly saturation degree with respect to $CaCO_3$ increases and precipitation according to the overall reaction

$$Ca^{2+} + 2HCO_3^- = CaCO_3 + H_2O + CO_{2(g)} \quad (1)$$

can be obtained. Such kind of scaling or sinter formation can be seen in analogy to e.g. travertine or speleothem formation in natural environment. For spontaneous precipitation of calcite, $SI_{Calcite}$ > 1 is assumed from field investigations (Dandurand et al., 1982). On the other side groundwater reacting with the shotcrete/concrete of tunnel buildings before entering the drainage system, can dissolve highly soluble compounds from the cement matrix like portlandite ($Ca(OH)_2$) as well as sodium and potassium hydroxides. For instance portlandite dissolution results in an increase of calcium ions and in particular of pH (up to ≈ 13), which - in analogy to CO_2 degassing - shifts DIC species from HCO_3^- to CO_3^{2-}. Accordingly precipitation of $CaCO_3$ according to the expressions

$$Ca(OH)_2 = Ca^{2+} + 2OH^- \quad (2a)$$

$$2Ca^{2+} + 2OH^- + 2HCO_3^- = 2CaCO_3 + 2H_2O \quad (2b)$$

$$Ca(OH)_2 + Ca^{2+} + 2HCO_3^- = 2CaCO_3 + 2H_2O \quad (2)$$

can occur within the matrix of the shotcrete/concrete, in the drainage system or in the receiving stream. For both overall reactions (1) and (2) the carbonate ion for the formation of $CaCO_3$ is generated from the groundwater and therefore corresponds to the uptake of soil CO_2 during infiltration of meteoric solutions and subsequent dissolution of carbonate minerals (e.g. calcite, dolomite) in the aquifer.

Calcium carbonate scaling in high alkaline environments can also be induced by the absorption of atmospheric CO_2. In this case, the sinter formation is based on the hydroxylation of atmospheric CO_2, subsequent transformation to CO_3^{2-} and its precipitation as $CaCO_3$ according to the reactions

$$CO_{2(g)} + OH^- = HCO_3^- \quad (3a)$$

$$HCO_3^- + = CO_3^{2-} + H^+ \quad (3b)$$

$$OH^- + H^+ = H_2O \quad (3c)$$

$$Ca(OH)_2 = Ca^{2+} + 2OH^- \quad (3d)$$

$$Ca^{2+} + CO_3^{2-} = CaCO_3 \quad (3e)$$

$$Ca(OH)_2 + CO_{2(g)} = CaCO_3 + H_2O \quad (3)$$

2.4 Composition of scalings and solutions

2.4.1 Scaling

The X-Ray pattern of all precipitates from the above 3 tunnels accounts for calcite as the main component with minor amounts of detrital quartz and silicates such as mica and feldspar. No additional $CaCO_3$ polymorph like aragonite and vaterite was found. In one sample from WW brucite ($Mg(OH)_2$) was detected as minor component. The average chemical composition of the precipitates from chemical analyses of acid digestions is: 89.8 ±4.8 wt.% $CaCO_3$, 1.6 ±0.9 wt.% $MgCO_3$, 0.22 ±0.03 wt.% $SrCO_3$ and 0.03 ±0.01 wt. $BaCO_3$. Remained solids after acid digestion consist of quartz and silicates at about 5.8 ±4.1 wt.%. As given by the above formula, Mg^{2+}, Sr^{2+} and Ba^{2+} ions can be incorporated into the calcite structure by isomorphic substitution (Boettcher and Dietzel, 2010), but may be also related to XRD non-detectable individual solid phases. For instance high Mg^{2+} content may indicate additional solid $Mg(OH)_2$, which was detected by XRD as brucite only once.

Mineralogical and chemical analyses clearly reveal the precipitation of calcite. But to decipher the origin of the carbonate ions according to the overall reactions (1) and (2) or (3) the distribution of stable carbon and oxygen isotopes has to be evaluated. The measured $\delta^{13}C_{Calcite}$ values range from -12.4 to -14.7, -13.5 to -20.5, and -9.1 to -20.7 ‰ (VPDB) for GB, WW and KA, respectively (Fig.1). The upper $\delta^{13}C$ limit of calcite precipitates can be explained by the fixation of DIC from groundwater. The $\delta^{13}C_{DIC}$ value of groundwater depends on the isotopic composition of the soil CO_2 (C_3 vegetation in the study area results in $\delta^{13}C_{CO2,\ soil} \approx -25 \pm 3$ ‰) and dissolved carbonate minerals in the aquifer (mostly marine limestone: $\delta^{13}C_{limestone} \approx 0 \pm 3$ ‰). Assuming a closed system with respect to limestone dissolution, as valid in most aquifers, a value of $\delta^{13}C_{DIC} \approx \delta^{13}C_{Calcite} = -13 \pm 3$ ‰ (= 0.5 · (-25 + 0) ‰) is obtained, which covers the above upper $\delta^{13}C_{Calcite}$ limit (Dietzel et al., 1992). The lower limit of about -21 ‰ cannot be predicted from groundwater composition, but from absorption of CO_2. This approach is based on a kinetic isotope fractionation of about -18 ‰ via the individual hydroxylation of $^{12}CO_2$ and $^{13}CO_2$ at high pH (see reaction (3a)) (Clark et al., 1992; Usdowski and Hoefs, 1986). Modern atmospheric CO_2 with $\delta^{13}C_{CO2,\ atm} \approx -8$ ‰ leads to typical $\delta^{13}C_{Calcite}$ values of about -26 ‰. Thus the different $\delta\ ^{13}C_{Calcite}$ values in Fig.1 indicate carbonate in calcite from groundwater and from the absorption of CO_2. Individual values are referred to various amounts of carbonate from reactions (1) and (2) versus (3). Besides carbon isotope also oxygen isotope values can be used to decipher the carbonate sources (see Fig.1), although fractionation mechanisms are different and limits depend also on $\delta\ ^{18}O_{H2O}$ of the solution (Dietzel, 2000).

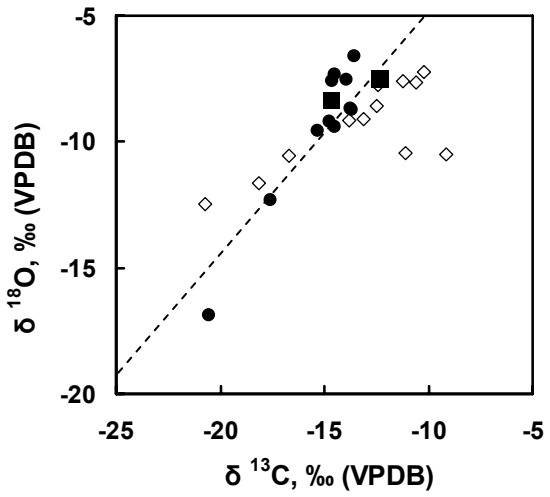

Fig. 1. $\delta^{13}C$ versus $\delta^{18}O$ values of calcium carbonate scaling from the tunnel drainage. Dotted line denotes the regression line for calcium carbonate scaling from a German railway tunnel drainage (Dietzel, 2000). ■: GB, ●: WW, ◊: KA

Interestingly $\delta^{13}C_{Calcite}$ versus $\delta^{18}O_{Calcite}$ values display a positive trend, which is similar to former studies. The individual slope is related to (i) local $\delta\ ^{13}C_{DIC}$ and (ii) $\delta\ ^{18}O_{H2O}$ as well as (iii) variability in isotopic composition of atmospheric CO_2. For instance diesel-engines may produce lower $\delta\ ^{13}C_{CO2}$ values of the tunnel atmosphere due to combustion of fossil hydrocarbon. The latter aspect is traced by a shift in isotope values for precipitates from KA, where diesel-engines are recently and frequently used for ongoing construction. In conclusion isotopic composition clearly indicates that absorption of CO_2 besides carbonate from groundwater has to be taken into account for sinter formation and hydrogeochemical modelling. However sampled sinter material from consolidated horizons and mud comprises an accumulation of solids gained from precipitation in various drainage solutions, where also transport and sedimentation have to be considered.

2.4.2 Groundwater and drainage solutions

The chemical composition of drainage solutions is highly variable in particular with regards to pH, alkali and Mg^{2+} concentration (Tab.A1). In general elevated pH values of drainage solutions are observed in comparison to the local groundwater from GB, WW and KA. The pH ranges from 7.67 to 12.25 and from pH 7.00 to 7.38 for drainage solutions and groundwater, respectively. Based on pH values, 3 water types can be distinguished. Type 1 represents drainage solutions with chemical composition similar to the local groundwater at pH < 7.5. The groundwater itself varies in chemical composition according to the aquifer composition in respect to the local geology (Tab.A1). In contrast to type 1 the drainage solutions of type 2 are highly alkaline (i.e. pH > 10) caused by strong interaction with the shotcrete/concrete. Type 2 solutions are usually characterized by low discharge or flow rates
(< 0.1 L s^{-1}). Type 3 represents drainage solutions with pH values between 7.5 and 10. These solutions can be deduced from less water-cement interaction, mixing of drainage solutions of types 1 and 2, as well as ongoing degassing of CO_2 and/or calcite precipitation from pristine groundwater. Type 3 solutions are most frequent at elevated up to moderate discharge or flow rates (> 0.1 L s^{-1}).

Water-cement interaction results in elevated alkali concentration in the solution due to the dissolution of alkali and calcium hydroxides and/or by mixing with already existing high mineralized interstitial solutions of the shotcrete/concrete. Alkali ions are a part of clinker materials at concentrations from 0.1 to 1.5 and from 0.1 to 1 wt.% of K_2O and Na_2O, respectively (Stark and Wicht, 2000). Alkali can be incorporated into the crystal lattice of cement phases (Jawed and Skalny, 1978) or can form alkali soluble salts like sulphate minerals. Furthermore alkali based accelerators, if used e.g. for shotcrete application, result in an

increase of alkali and hydroxide content of the cement. The overall correlation between potassium hydroxide from accelerators can be expressed by the reaction

$$K_2OSiO_2 + Ca(OH)_2 + CO_{2(g)} \rightarrow CaCO_3 + 2KOH + SiO_2 \quad (4)$$

where highly soluble portlandite and potassium (sodium) silicate combined with carbonatisation end up in KOH (NaOH) in the interstitial solutions of e.g. shotcrete (Stark and Wicht, 2001). Accordingly the concentrations of alkali ions increase with pH in the drainage solution, which is displayed in respect to $[K^+]$ in Fig.2a. For a given set of drainage solutions individual regression lines can be obtained (see Fig.2a).

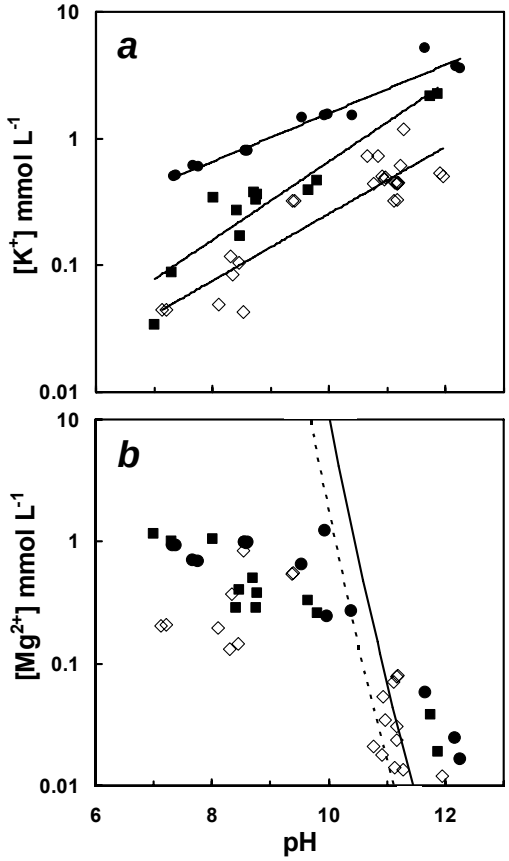

Fig. 2. K^+ (a) and Mg^{2+} concentration (b) versus pH of groundwater and drainage solutions. (a) Regression lines obtained for GB, WW and KA, respectively:
$Log[K^+]_{GB} = 0.31 \cdot pH - 3.28$ (R^2 =0.88)
$Log[K^+]_{WW} = 0.19 \cdot pH - 1.71$ (R^2 =0.96)
$Log[K^+]_{KA} = 0.26 \cdot pH - 3.24$ (R^2 =0.83)
(b): concentration of Mg^{2+} in equilibrium with brucite at 10 (solid line) and 20°C (dotted line). ■: GB, ●: WW, ◊: KA.

Less pronounced $[Na^+]$ - pH correlation in our case studies is addressed to elevated $[Na^+]$ versus low $[K^+]$ in the groundwater and low $[Na^+]$ versus high $[K^+]$ values from water-cement interaction (Tab.A1).

The decrease of Mg^{2+} concentration in the drainage solutions at pH above ≈ 10.5 indicates the formation of $Mg(OH)_2$ (Fig.2b). The solid and dashed lines in Fig.2b denote the concentration of Mg^{2+} in equilibrium with respect to brucite ($SI_{Brucite}$ = 0) at 10 and 20 °C, respectively. A shift of the chemical composition below the brucite saturation line can be induced by a drop in temperature or a decrease of pH caused e.g. by calcite precipitation. Data points above the brucite saturation line display drainage solutions with distinct $Mg(OH)_2$ precipitation capacities (see $SI_{Brucite}$ > 0; Tab.A1).

By combining Figs.2a and b the molar $[K^+]/[Mg^{2+}]$ ratio is given as a function of pH in Fig.3. Ratios above 1 are unlikely to appear in the local groundwater of our case studies. Thus $[K^+]/[Mg^{2+}]$ > 1 can be used as a combined elemental proxy for a significant impact of water-cement interaction on drainage solution chemistry for type 2 and 3 solutions. For the solutions 6-KA-DS, 7-KA-DS and 8-KA-DS (highlighted area in Fig.3) the $[K^+]/[Mg^{2+}]$ ratio is very similar to the respective groundwater, although a shift to higher pH is observed. In these cases the shift of pH is rather caused by degassing of CO_2 from the local groundwater than by water-cement interaction.

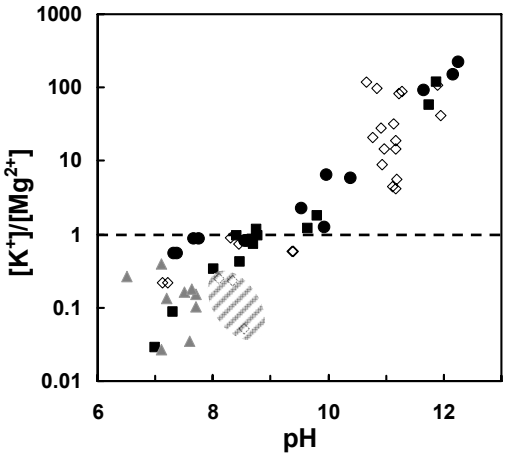

Fig. 3. Molar $[K^+]/[Mg^{2+}]$ ratio of groundwater and drainage solutions. ■: GB, ●: WW, ◊: KA, ▲ : shallow groundwaters for different geological units of the Austrian Alps (data not given in Tab.A1). Highlighted area indicates solutions 6-KA-DS, 7-KA-DS and 8-KA-DS (see text).

In Figures 4a and b the saturation index with respect to calcite is displayed as a function of Ca^{2+} and CO_3^{2-} concentration. All except 6 drainage solutions are supersaturated with respect to

calcite. The limit for spontaneous precipitation of calcite (about $SI_{Calcite} > 1$) is reached only for ≈ 50% of the solutions. Obviously the correlation of $SI_{Calcite}$ values versus CO_3^{2-} concentration is much more concise than that versus Ca^{2+} (Figs. 4a and b).

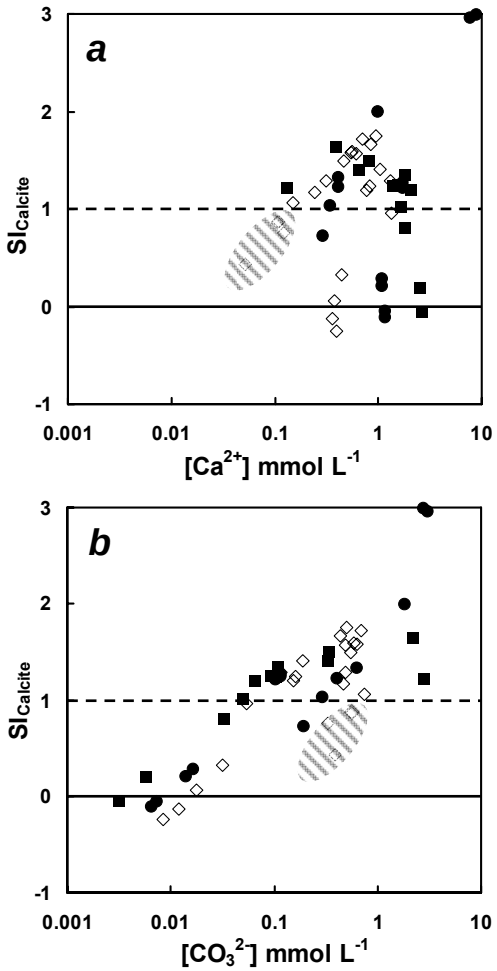

Fig. 4. Saturation index with respect to calcite ($SI_{Calcite}$) versus Ca^{2+} concentration (a) and CO_3^{2-} concentration (b). ■: GB, ●: WW, ◊: KA. Highlighted area indicates drainage solutions 17-KA-DS, 18-KA-DS, 20-KA-DS and 21-KA-DS (see text).

The CO_3^{2-} concentration is highly variable by redistribution of DIC species from changing pH. Accordingly the pH can be clearly identified as major parameter controlling the CO_3^{2-} content and thus $SI_{Calcite}$ values. An increase of pH can be caused by both degassing of CO_2 or dissolution of hydroxides as discussed above. Four drainage solutions from KA (17-KA-DS, 18-KA-DS, 20-KA-DS, 21-KA-DS; highlighted area in Figs. 4a and b) with high $[CO_3^{2-}]$ values show an unexpected low $SI_{Calcite} < 1$ due to very low Ca^{2+} concentration. These low Ca^{2+}

concentrations can be explained by precipitation of calcite from such kind of type 2 drainage solutions before sampling.

Although individual water-cement interactions for SO_4^{2-} are well known, in the present studies the SO_4^{2-} concentrations do not trace water-cement interaction due to complex dissolution and precipitation behaviour of sulphate containing solids like ettringite, thaumasite and gypsum(Mittermayr et al., 2012a; Mittermayr et al., 2012b). Moreover concentrations of dissolved NO_3^- and Cl^- are not significantly correlated with those of other dissolved species (Tab.A1).

2.5 Mixing of solutions

In the drainage system of a tunnel individual solutions are mixed within the drainage tubes. Such mixing may result in solutions (MX) with calcite saturation degrees different from the initial end member solutions. In the following two individual end member solutions, the groundwater with the lowest pH value (GW^*) and the drainage solution with the highest pH and/or highest [K^+] concentration (DS^*), were used for modelling of mixtures at various proportions. For GB highest pH and K^+ concentration is measured in a single solution, whereas for WW and KA two drainage solutions are valid for highest pH and highest K^+ concentration. The chemical composition of the mixed solution is obtained according to equation

$$[\ ]_{MX} = [\ ]_{GW^*} \cdot (1-x) + [\ ]_{DS^*} \cdot x \qquad (5)$$

where [ ] denotes the concentration of the individual component (e.g. Ca^{2+}, Mg^{2+}, Na^+, K^+, Cl^-, SO_4^{2-}, DIC) and x the fraction of DS* on MX. The pH value of the mixed solution is derived from PHREEQC modelling. In the first modelling approach neither exchange with atmospheric CO_2 nor precipitation of calcite is considered for any solution before and after mixing (dotted lines in Fig.5). In the second approach, groundwater is equilibrated with atmospheric CO_2 ($P_{CO2} = 10^{-3.45}$ atm) and calcite before mixing (GW_{eq}*). This pre-calculation leads to degassing of CO_2 into the atmosphere (pH increase) and precipitation of calcite down to $SI_{Calcite} = 0$. The “equilibrated” groundwater GW_{eq}* is in analogy to the original GW* mixed with DS^* according to equation 5 (dashed lines in Fig.5).

Modelled pH and K^+ concentration of the MX solutions as well as data of drainage solutions are plotted in Fig.5. Nearly all drainage solutions of GB plot between the dotted and dashed line and thus could be obviously explained by mixing of the end member solutions (Fig.5a). Analogous calculations were carried out for WW and KA with the given two DS^* end member solutions. For

WW the modelling results are also quite consistent with the composition of the solutions found in the drainage (Fig.5b).

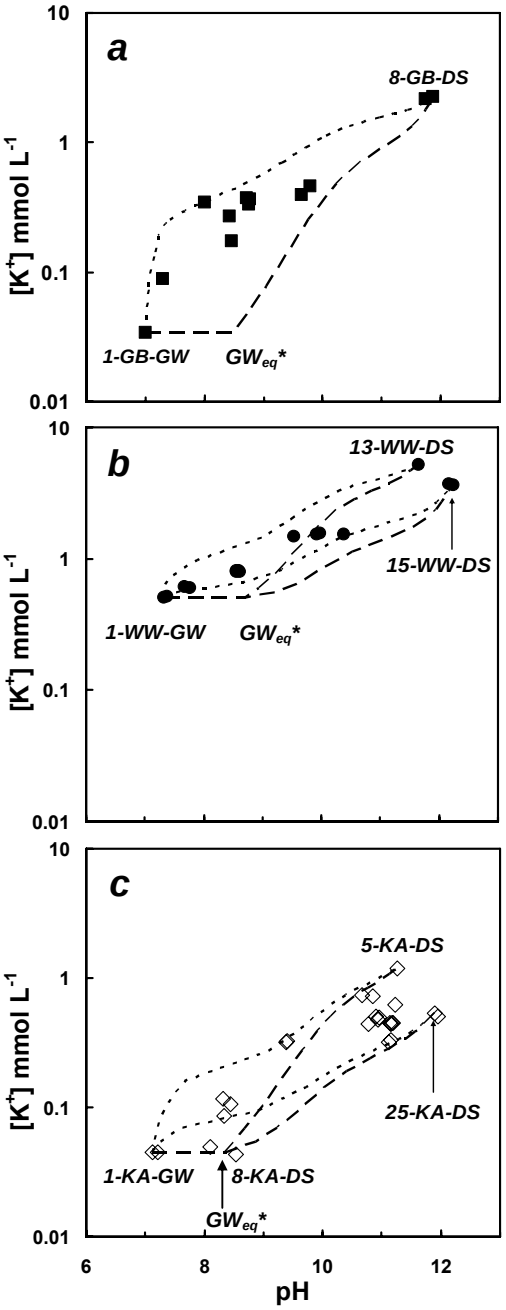

Fig. 5. K^+ concentration versus pH for groundwater and drainage solutions of GB (a), WW (b) and KA (c). Dotted lines: Mixed solutions (MX) from groundwater (lowest pH: GW^*) and type 2 drainage solution (highest pH and/or highest $[K^+]$: DS^*).

Dashed line: Mixed solutions (MX), where for GW_{eq}^* equilibration with atmospheric CO_2 (degassing) and precipitation of calcite is considered before mixing with DS^*.

Modelling results for KA are rather inconsistent with analysed drainage solution chemistry, in particular at elevated pH and K^+ concentration (Fig.5c). Deviations can be best explained by the occurrence of strong alkaline solutions with chemical content between the two drainage solutions with highest pH or highest K^+ concentration (DS^*) used for mixing. The pH of drainage solution of type 1 (e.g. 8-KA-DS) with a K^+ concentrations similar to the local groundwater can be modelled precisely by means of degassing of CO_2 (see also Fig.5c).

In Figure 6 mixing results are given for Ca^{2+} concentration and $SI_{Calcite}$ values as a function of pH. In contrast to [K^+] and [Ca^{2+}] values the evolution of $SI_{Calcite}$ as a function of pH for mixing is not necessarily within the limiting values of the end member solutions. In the case of GB and KA the $SI_{Calcite}$ values of MX solutions are calculated to be significant above those of DS^* (e.g. $SI_{Calcite}$(DS*) = 1.6 versus $SI_{Calcite}$(MX) ≤ 2.2; Fig.6b). Thus a strong increase of $SI_{Calcite}$ in drainage solutions and respective higher calcite precipitation capacities can be obtained if mixing is considered instead of separately discharging drainage solutions.

In particular until pH ≈ 8.5 is reached most consistent results are obtained for the mixing approach without considering CO_2 degassing and calcite precipitation (GW^*; dotted line). At pH ≈ 8.5 $SI_{Calcite}$ = 1 for spontaneous calcite precipitation is reached. At $SI_{Calcite}$ > 1 the “dotted line” for mixing seems to be no longer valid as $SI_{Calcite}$ decreases by precipitation of calcite.

In analogy to GB, the Ca^{2+} concentration of the MX solutions of WW and KA are modelled, yielding four individual mixing lines in Figs. 6c and e. Modelling results are somewhat inconclusive with analysed data concerning $SI_{Calcite}$ of the alkaline solutions around pH 10.5 and 11, respectively (Figs. 6d and f). This may be caused by ongoing precipitation of calcite or variability in chemical composition of DS* (see also Fig.5c).

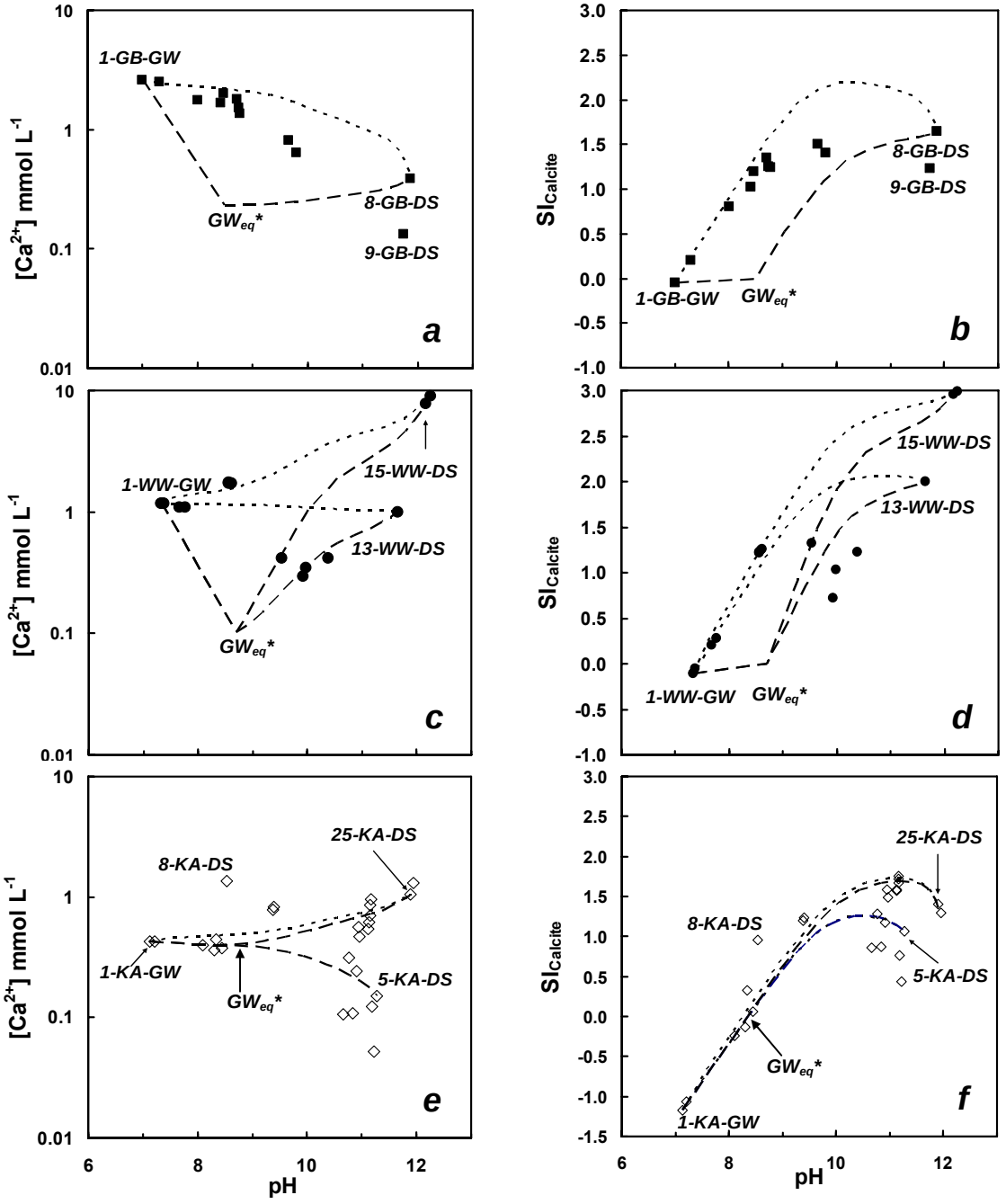

Fig. 6. *Calcium concentration and saturation indices of calcite versus pH for GB (a and b), WW (c and d) and KA (e and f). Dotted lines: Mixing of groundwater (lowest pH: GW*) with type 2 drainage solution (highest pH and/or highest [K^+]: DS*).*
Dashed lines: Equilibration with atmospheric CO_2 (degassing) and precipitation of calcite for GW$_{eq}$ before mixing with DS*.*

2.6 CO_2 absorption

The uptake of atmospheric CO_2 into a solution requires an internal P_{CO2} less than the apparent P_{CO2} (Earth's atmosphere: $10^{-3.45}$ atm). This is valid in particular for strong alkaline type 2 solutions (Tab.A1). The absorption of CO_2 from the atmosphere as a function of time or along a flow path may result in a change of saturation degree with respect to calcite. For instance at pH = 12 the absorbed CO_2 is quasi-quantitatively transformed to CO_3^{2-} ions. Thus the increase of CO_3^{2-} concentration by CO_2 absorption can result a significant increase of the saturation degree with respect to calcite. According to the overall reaction

$$CO_{2(g)} + 2OH^- = CO_3^{2-} + H_2O \quad (6)$$

each CO_2 consumes two OH^- ions for a CO_3^{2-} ion formation. However accompanied ongoing decrease of pH will subsequently cause reactions $CO_2 + OH^- = HCO_3^-$ and $CO_2 + H_2O = H_2CO_3$ to be dominant. Whether an increase or decrease of CO_3^{2-} concentration during CO_2 absorption is valid, depends on the interrelation between [DIC] and pH.

To discover this interrelationship hydrogeochemical modelling was carried out for 0.00625, 0.025, and 0.1 mol L^{-1} KOH solutions with calculated pH values of 11.9, 12.4 and 13.0, respectively (25°C). As ongoing CO_2 absorption into the above KOH solutions is modelled without any initial dissolved [DIC], the pH decreases and simultaneously [DIC] increases. CO_3^{2-} concentration reaches a maximum value, $[CO_3^{2-}]_{max}$, at pH 10.84, 11.11 and 11.32, respectively, where 81, 91 and 96 % of the absorbed DIC are converted to CO_3^{2-} under the present conditions (Fig.7). By reaching this pH any further absorption of CO_2 will lower the CO_3^{2-} concentration. At $[CO_3^{2-}]_{max}$ the absorbed CO_2 is about half of the initial OH^- concentration according to the stoichiometry of the overall reaction (6). Additionally at $[CO_3^{2-}]_{max}$ the stoichiometric requirements for concentrations of HCO_3^- and OH^- to be equal have to be met according to the reaction

$$CO_{2(g)} + 2OH^- = HCO_3^- + OH^- \quad (7)$$

(see dotted lines in Fig.7). At $[HCO_3^-]/[OH^-] = 1$ a constant P_{CO2} value is obtained according to the equation

$$P_{CO2} = K_W / (K_{H_2CO_3-HCO_3^-} \cdot K_H) \quad (8)$$

where K_w, $K_{H2CO3-HCO3}$ and K_H denote dissociation constants for water, carbonic acid and $CO_{2(g)}$. At 25°C $P_{CO2} = 10^{-6.15}$ atm marks the $[CO_3^{2-}]_{max}$ value for any alkaline solution in the given

system (K values from minteq.dat). Therefore the internal P_{CO2} value is a reliable proxy to evaluate whether uptake of CO_2 will increase or decrease the CO_3^{2-} concentration.

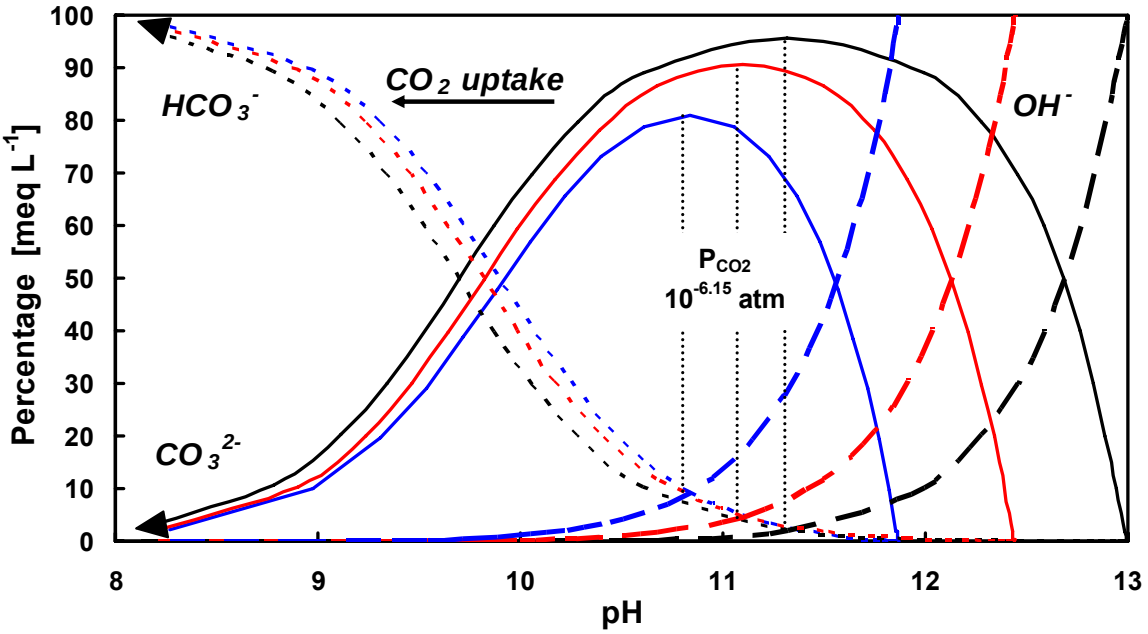

Fig. 7. Contribution of CO_3^{2-} (solid lines), OH^- (dashed lines) and HCO_3^- ions (dotted lines) to total alkalinity. Ongoing absorption of CO_2 into 0.00625 (blue), 0.025 (red) and 0.1 mol L^{-1} KOH solutions (black). Maximum CO_3^{2-} percentage (equal to concentration) is reached for $[OH^-] = [HCO_3^-]$ at $P_{CO2} = 10^{-6.15}$ atm (25°C).

2.7 Overall precipitation capacities and kinetics

The maximum CO_3^{2-} concentration, $[CO_3^{2-}]_{max}$, reached through the absorption of CO_2 into alkaline solutions finds its analogy in reaching a maximum supersaturation degree with respect to calcite ($SI_{Calcite}$) at a given Ca^{2+} concentration. Respective hydrogeochemical modelling is exemplarily carried out by defining an initial model solution using the groundwater 1-KA-GW ($SI_{Calcite}$ = -1.12; 12.5 °C; see Tab.A1). This groundwater is suggested to leach alkali hydroxide from shotcrete/concrete, which is finally yielding in a strong alkaline drainage solution. The modelled addition of 0.0022, 0.00625 and 0.025, mol L^{-1} of KOH to the groundwater 1-KA-GW results in $SI_{Calcite}$ of 1.65, 1.65 and 1.51 at pH 10.93, 11.98 and 12.71, respectively. Note that the $SI_{Calcite}$ values decrease as function of pH due to the strong $CaOH^+$ aquo-complex formation. The initial model solutions are obtained by precipitation of calcite down to $SI_{Calcite}$ = 1, which simulates a partial formation of calcite direct at the shotcrete/concrete (see dashed lines in Fig.8a). The internal P_{CO2} values of the initial model solutions are $10^{-6.69}$, $10^{-8.74}$ and $10^{-10.24}$ atm,

respectively. In Fig.8a the calculated $SI_{Calcite}$ and pH values during ongoing uptake of CO_2 into the three model solutions are shown until equilibrium with the P_{CO2} of the Earth's atmosphere is reached (solid lines in Fig.8a). Final pH values are 8.6, 9.0 and 9.4.

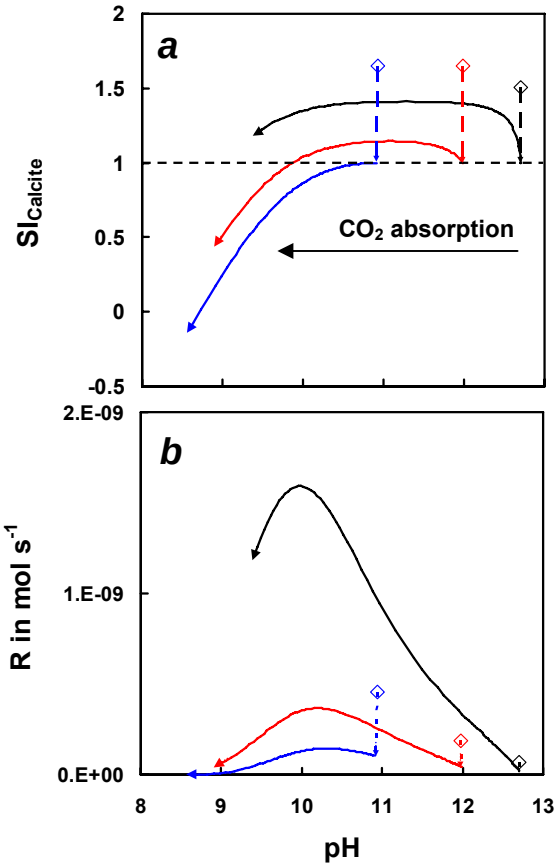

Fig. 8. Saturation index of calcite versus pH (a), precipitation rate of calcite calculated according to equation (9) versus pH (b). Precipitation of calcite from initial solutions (◊) until $SI_{Calcite}$ = 1 (dashed lines) and subsequent CO_2 absorption until equilibrium the Earth's atmosphere is reached (solid lines). The initial solutions are obtained by the addition of 0.025 (black), 0.00625 (red) and 0.0022 (blue) mol L^{-1} of KOH to groundwater 1-KA-GW.

At relatively low initial pH (10.93) the saturation degrees with respect to calcite continuously decreases by the uptake of CO_2, whereas at higher initial pH (11.98 and 12.71) an increase is followed by a decrease of $SI_{Calcite}$ values. The maximum $SI_{Calcite}$ is directly referred to the evolution of CO_3^{2-} concentration and defined by $P_{CO2} = 10^{-6.70}$ atm at 12.5 °C (equation 8). Note that in the case of low initial pH 10.93 the P_{CO2} of the initial solution is already below $10^{-6.70}$ atm. From calcite saturation degrees calcite precipitation capacities (CPC) can be calculated by assuming precipitation of $CaCO_3$ until equilibrium with respect to calcite and the P_{CO2} of the

Earth's atmosphere is reached ($SI_{Calcite}$ = 0 and P_{CO2} = $10^{-3.45}$ atm). Initial pH values of 10.93, 11.98 and 12.71 result in overall calcite precipitation capacities of 31, 40 and 42 mg L^{-1} of $CaCO_3$, respectively. As the Ca^{2+} concentration of the pristine groundwater 1-KA-GW amounts to 43 mg L^{-1} $CaCO_3$, nearly all dissolved Ca^{2+} can be precipitated in order to reach equilibrium with calcite and the Earth's atmosphere. Assuming a discharge of 0.1 L s^{-1} and a CPC of 31 mg L^{-1} a precipitation of ≈ 250 kg $CaCO_3$ is calculated for each year from this single drainage solution.

Although CPC and scaling amounts can be calculated, the apparent amount of precipitated calcite in the drainage depends on a huge number of parameters, like the flow rate through the drainage, CO_2 exchange behaviour and in particular on calcite precipitation kinetics. High CO_2 absorption rates are related to concentration of OH^- (Danckwerts and Kennedy, 1958); (Back et al., 2011). The uptake rate of gaseous CO_2 into the solution is controlled by the CO_2 gradient and the pH, but also by the provided gas-liquid area (Back et al., 2011). From theoretical and empirical approaches elevated calcite growth rates are obtained at high $SI_{Calcite}$ values (Plummer et al., 1978); (Inskeep and Bloom, 1985), but additional parameters like the ionic strength (I) and $(Ca^{2+})/(CO_3^{2-})$ activity ratio have to be considered (Nehrke et al., 2007). By combining available kinetic data the overall calcite growth rate can be calculated by the empirical expression

$$R_{Calcite} = I^{-0.004} \cdot pH^{-10.71} \cdot ((Ca^{2+})/(CO_3^{2-}))^{-0.35} \cdot (S^{0.5} - 1)^2 \quad (9)$$

(Wolthers et al., 2012). S is the saturation degree ($SI_{Calcite}$ = log (S)). Interestingly calcite growth rate maximum for $(Ca^{2+})/(CO_3^{2-})$ ≈ 1, as reported by (Nehrke et al., 2007) and (Wolthers et al., 2012), results in highest precipitation rates in the initial model solution with lowest pH (see dashed blue line in Fig.8b). This is in accordance with (Ruiz-Agudo et al., 2011) where in alkaline solutions the calcite growth rate decreased with increasing pH values at given $(Ca^{2+})/(CO_3^{2-})$ ratio and constant value of $SI_{Calcite}$. Through CO_2 absorption pH decreases and calcite precipitation rate increases and reaches a maximum value close to pH 10.2, although the overall CPC is highest close to pH ≈ 11 (P_{CO2} = $10^{-6.70}$ atm; Fig.8a). The kinetic aspect may explain the infrequent occurrence of solutions with pH 10.2 ±0.3. (see Tab.A1) as pH instantaneously decreased by rapid calcite precipitation.

2.8 Summary and conclusions

The main mechanisms, which are responsible for calcium carbonate scaling in the present alkaline environments, were successfully discovered by using multi-proxy and modelling

approaches. In Figure 9 three elemental proxies, Ca^{2+}, Mg^{2+} and K^{+}, are presented using a triplot diagram. The arrows indicate reaction paths from groundwater reacting with shotcrete/concrete to yield drainage solutions as follows: (I) Water-cement interaction is primarily connected to an increase of pH and in particular of highly soluble K^{+} (Na^{+}) ions. (IIa) [Ca^{2+}] increases by the dissolution of portlandite. (IIb) Once precipitation of calcite starts the [Mg^{2+}]/[Ca^{2+}] ratio increase in the remaining solution, even if co-precipitation of Mg^{2+} with calcite is assumed as the distribution coefficient of Mg^{2+} into calcite is << 1 (Boettcher and Dietzel, 2010). Thus reaction paths (IIa) and (IIb) denote an increase and decrease of Ca^{2+} due to $Ca(OH)_2$ dissolution and $CaCO_3$ precipitation, respectively. (III) Considering type 2 solutions (pH > 10.5) and ongoing dissolution of alkali and calcium hydroxide, supersaturation with respect to brucite can be reached even at very low Mg^{2+} concentrations. (IV) Although calcite formation can occur at any of the above described stages, the limited solubility of calcite at highly alkaline conditions can lead to a significant removal of dissolved Ca^{2+}, but leaving K^{+} (Na^{+}) in the solution. Independently on the geological site and groundwater composition a K(Na)-OH solution marks the “final” high alkaline conditions.

Calcium carbonate scaling shows evidence for uptake of atmospheric CO_2 in strong alkaline solutions by means of low $\delta^{13}C_{Calcite}$ and $\delta^{18}O_{Calcite}$ values. Interestingly the uptake of CO_2 in alkaline solutions can either lead to an increase or decrease of the saturation index with respect to calcite, where the internal P_{CO2} ($10^{-6.70}$ and $10^{-6.15}$ atm at 12.5 and 25°C) marks the respective boundary conditions.

Mixing of highly alkaline solutions with groundwater-like type 1 solutions in the drainage can cause a dramatic increase of calcite supersaturation in the resulting solution, which stimulates calcite formation. A similar mixing effect is known for karstic groundwater for the dissolution of $CaCO_3$, so-called mixing corrosion (Bögli, 1964). The latter behaviour can trigger ongoing limestone dissolution even if the primary groundwaters are in equilibrium with calcite. Both the increase and decrease of $SI_{Calcite}$ values through mixing is caused by the non-linear behaviour of re-distribution of DIC species as a function of pH.

In general calcite precipitation capacities (CPC) of drainage solutions increase at elevated pH. But the apparent amount of calcite formation in a tunnel drainage depends on additional parameters, like CO_2 uptake rate, calcite precipitation rates and the residence time of drainage solution in the tunnel. Highest calcite precipitation rates are estimated at pH 10.2 ±0.3, which may cause relatively low abundance of moderate alkaline drainage solutions due to rapid calcite formation and corresponding pH decrease. The mixing of alkaline solutions and groundwater-type solutions increases both, calcite precipitation capacities and rates.

In conclusion a sustainable prevention of calcium carbonate scaling in tunnel drainage systems can be reached by (i) the use of hydraulic cements for concrete and shotcrete application with reduced content of portlandite and leachable alkalies, e.g. by adding fly ash with latent hydraulic silica, (ii) avoiding mixtures of high alkaline type 1 and type 3 solutions, e.g. by separating flow channels, (iii) decreasing residence times of solutions within the tunnel, e.g. by tailored design of the drainage system, (iv) increasing the CO_2 exchange rates between the solution and the atmosphere for solutions with internal P_{CO2} values between $10^{-3.45}$ and $10^{-6.70}$ atm (12.5°C), e.g. by ventilation with air, (v) decreasing the respective CO_2 exchange rates for solutions with internal P_{CO2} values $<10^{-6.70}$ and $> 10^{-3.45}$ atm (12.5°C), e.g. by laminar flow and (vi) adding substances to inhibit calcium carbonate formation, like polyaspartic acid, if applicable.

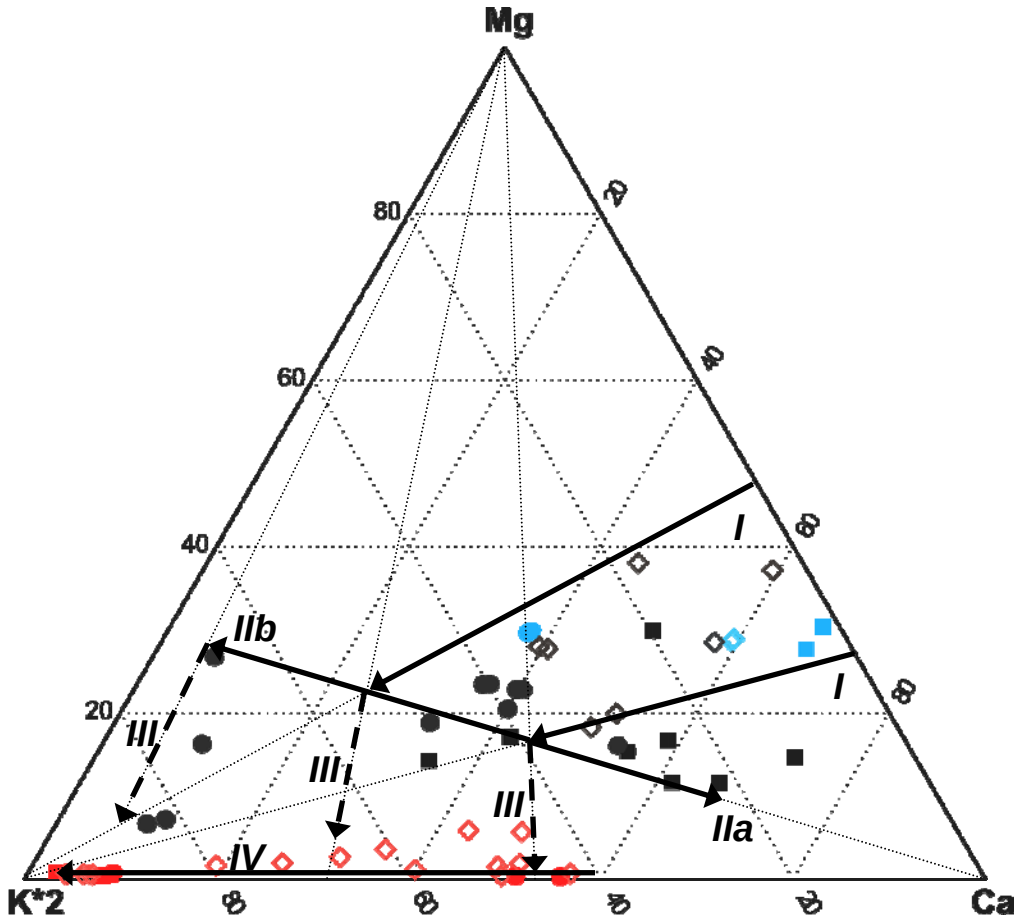

Fig. 9. Triplot of molar K^+ (·2), Mg^{2+} and Ca^{2+} content. Blue symbols denote local groundwater. Red symbols denote type 3 solutions (pH > 10.5). Arrows indicate reaction paths (I, II, III and IV) as discussed in the text. ■: GB, ●: WW, ◊: KA.

2.9 Acknowledgements

The authors greatly appreciate funding of this study by Graz University of Technology, the NAWI Graz network and the Austrian Federal Railways (ÖBB). We thank Arthur Deditius, Andrea Niedermayr, Dietmar Klammer, Florian Mittermayr and Daniel Höllen for stimulating discussion as well as co-workers from 3G consulting and U.C.M. Heidelberg for support during sampling.

2.10 References

Back, M., Bauer, M., Stanjek, H., Peiffer, S., 2011. Sequestration of CO_2 after reaction with alkaline earth metal oxides CaO and MgO. Applied Geochemistry 26, 1097-1107.

Boettcher, M.E., Dietzel, M., 2010. Metal-ion partitioning during low-temperature precipitation and dissolution of anhydrous carbonates and sulfates. EMU notes in mineralogy 10.

Bögli, A., 1964. Mischungskorrosion: ein Beitrag zum Verkastungsproblem. Erkunde 18, 83–92.

Clark, I.D., Fontes, J.-C., Fritz, P., 1992. Stable isotope disequilibria in travertine from high pH waters: Laboratory investigations and field observations from Oman. Geochimica et Cosmochimica Acta 56, 2041-2050.

Danckwerts, P.V., Kennedy, A.M., 1958. The kinetics of absorption of carbon dioxide into neutral and alkaline solutions. Chemical Engineering Science 8, 201-215.

Dandurand, J.L., Gout, R., Hoefs, J., Menschel, G., Schott, J., Usdowski, E., 1982. Kinetically controlled variations of major components and carbon and oxygen isotopes in a calcite-precipitating spring. Chemical Geology 36, 299-315.

Dietzel, M., 2000. Measurement of the stable carbon isotopes in calcite sinters on concrete, Cement-Lime-Gypsum. Bauverlag GmbH, pp. 544-548.

Dietzel, M., Rinder, T., Niedermayr, A., Mittermayr, F., Leis, A., Klammer, D., Köhler, S., Reichl, P., 2008. Mechanisms of Sinter Formation in Drainage Systems. BHM Berg- und Hüttenmännische Monatshefte 153, 369-372.

Dietzel, M., Tang, J., Leis, A., Köhler, S.J., 2009. Oxygen isotopic fractionation during inorganic calcite precipitation • Effects of temperature, precipitation rate and pH. Chemical Geology 268, 107-115.

Dietzel, M., Usdowski, E., Hoefs, J., 1992. Chemical and $^{13}C/^{12}C$- and $^{18}O/^{16}O$-isotope evolution of alkaline drainage waters and the precipitation of calcite. Applied Geochemistry 7, 177-184.

Draschitz, C., 2008. Zur Erhöhung der Gebrauchssicherheit von Eisenbahntunneln - Ziel, aufwand, Erfordernisse, Drainagesysteme im Tunnelbau - Design, Versinterung und Instandhaltung. Gruppe Geotechnik Graz, Graz, p. 16.

Gineys, N., Aouad, G., Damidot, D., 2010. Managing trace elements in Portland cement – Part I: Interactions between cement paste and heavy metals added during mixing as soluble salts. Cement and Concrete Composites 32, 563-570.

Girmscheid, G., Gamisch, T., Klein, T., Meinlschmidt, A., 2003a. Scale sintering in tunnel drainages - Mechanisms of scale formation. Bauingenieur 78, 292-300.

Girmscheid, G., Gamisch, T., Meinlschmidt, A., 2003b. Scale sintering in tunnel drainages – Recommendations for maintenance of tunnels. Bauingenieur 78, 562-570.

Hillier, S.R., Sangha, C.M., Plunkett, B.A., Walden, P.J., 1999. Long-term leaching of toxic trace metals from Portland cement concrete. Cement and Concrete Research 29, 515-521.

Inskeep, W.P., Bloom, P.R., 1985. An evaluation of rate equations for calcite precipitation kinetics at pCO2 less than 0.01 atm and pH greater than 8. Geochimica et Cosmochimica Acta 49, 2165-2180.

Jawed, I., Skalny, J., 1978. Alkalies in cement: A review: II. Effects of alkalies on hydration and performance of Portland cement. Cement and Concrete Research 8, 37-51.

Marion, A.-M., De Lanève, M., De Grauw, A., 2005. Study of the leaching behaviour of paving concretes: quantification of heavy metal content in leachates issued from tank test using demineralized water. Cement and Concrete Research 35, 951-957.

Mittermayr, F., Bauer, C., Klammer, D., Böttcher, M.E., Leis, A., Escher, P., Dietzel, M., 2012a. Concrete under Sulphate Attack: An Isotope Study on Sulphur Sources Isotopes in Environmental & Health Studies 48, 105 - 117.

Mittermayr, F., Klammer, D., Höllen, D., Köhler, S., Böttcher, M.E., Leis, A., Dietzel, M., 2012b. Deterioration of concrete – application of stable isotopes, in: Broekmans, M.A.T.M. (Ed.), 10th International Congress for Applied Mineralogy, Trondheim, pp. 435-445.

Nehrke, G., Reichart, G.J., Van Cappellen, P., Meile, C., Bijma, J., 2007. Dependence of calcite growth rate and Sr partitioning on solution stoichiometry: Non-Kossel crystal growth. Geochimica et Cosmochimica Acta 71, 2240-2249.

Parkhurst, D.L., Apello, C.A.J., 1999. User's guide to PHREEQC (V2). U.S. Geol. Sur, 312.

Plummer, L.N., Wigley, T.M.L., Parkhurst, D.L., 1978. Kinetics of calcite dissolution in CO_2-water systems at 5 degree to 60 degree C and 0. 0 to 1. 0 ATM CO_2. Am J Sci 278, 179-216.

Ruiz-Agudo, E., Putnis, C.V., Rodriguez-Navarro, C., Putnis, A., 2011. Effect of pH on calcite growth at constant ratio and supersaturation. Geochimica et Cosmochimica Acta 75, 284-296.

Stark, J., Wicht, B., 2000. Zement und Kalk - Der Baustoff als Werkstoff. Birkhäuser Verlag, Basel.

Stark, J., Wicht, B., 2001. Dauerhaftigkeit von Beton. Birkhäuser Verlag, Basel.

Usdowski, E., Hoefs, J., 1986. $^{13}C/^{12}C$ partitioning and kinetics of CO_2 absorption by hydroxide buffer solutions. Earth and Planetary Science Letters 80, 130-134.

Wolthers, M., Nehrke, G., Gustafsson, J.P., Van Cappellen, P., 2012. Calcite growth kinetics: Modeling the effect of solution stoichiometry. Geochimica et Cosmochimica Acta 77, 121-134.

2.11 Appendix

Table A1: In-situ parameters, concentrations of dissolved components, internal partial pressure of CO_2 (P_{CO2}) and saturation indices with respect to calcite and brucite. Temperature, specific conductivity (SpC), and individual concentrations are given in °C, µS cm^{-1} and mmol L^{-1}, respectively. GB: Grünberg; WW: Wienerwald; KA: Koralm; GW: groundwater; DS: drainage solution.

Sample ID	Temp	SpC	pH	K^+	Na^+	Ca^{2+}	Mg^{2+}	Cl^-	NO_3^-	SO_4^{2-}	DIC	P_{CO2}	$SI_{Calcite}$	$SI_{Brucite}$
1-GB-GW	9.6	615	7.00	0.03	0.22	2.62	1.16	0.23	0.25	0.06	4.20	-1.86	-0.11	-7.0
2-GB-GW	9.8	567	7.30	0.09	0.16	2.49	1.02	0.07	0.24	0.13	1.93	-1.90	-0.05	-6.4
3-GB-DS	12.3	454	8.77	0.36	0.83	1.36	0.38	0.17	0.08	0.13	2.58	-2.19	0.21	-3.7
4-GB-DS	6.5	323	9.80	0.46	0.92	0.64	0.26	0.46	0.09	0.18	8.56	-2.30	0.28	-2.2
5-GB-DS	6.8	367	9.65	0.39	0.91	0.81	0.33	0.23	0.09	0.14	7.28	-3.12	1.21	-2.4
6-GB-DS	11.2	542	8.47	0.17	0.56	2.01	0.40	0.16	0.09	0.12	5.32	-3.11	1.23	-4.3
7-GB-DS	13.9	694	8.01	0.34	1.62	1.76	1.04	0.35	0.19	0.21	6.76	-3.16	1.25	-4.7
8-GB-DS	15.3	1851	11.87	2.23	7.58	0.39	0.02	0.29	0.05	0.27	2.52	-3.17	1.26	1.1
9-GB-DS	15.3	1663	11.74	2.16	7.74	0.13	0.04	0.28	0.04	0.29	3.14	-4.26	1.33	1.1
10-GB-DS	11.0	563	8.71	0.37	1.41	1.79	0.50	0.10	0.13	0.12	5.11	-5.57	0.73	-3.8

Sample ID	Temp	SpC	pH	K^+	Na^+	Ca^{2+}	Mg^{2+}	Cl^-	NO_3^-	SO_4^{2-}	DIC	P_{CO2}	$SI_{Calcite}$	$SI_{Brucite}$
11-GB-DS	13.0	422	8.75	0.33	0.75	1.53	0.29	0.12	0.06	0.11	3.85	-5.46	1.03	-3.8
12-GB-DS	12.8	454	8.42	0.27	0.66	1.65	0.29	0.14	0.06	0.12	4.36	-6.14	1.23	-4.5
1-WW-GW	13.0	939	7.33	0.51	5.34	1.18	0.93	0.98	0.34	1.08	6.89	-8.06	2.00	-6.2
2-WW-GW	13.0	937	7.38	0.52	5.34	1.18	0.93	0.99	0.35	1.09	6.93	-8.93	2.95	-6.1
3-WW-DS	13.4	-	7.67	0.61	4.85	1.08	0.70	0.74	0.24	0.92	6.58	-9.13	2.99	-5.6
4-WW-DS	13.3	840	7.76	0.59	4.81	1.09	0.69	0.72	0.21	0.92	6.27	-3.49	1.24	-5.4
5-WW-DS	14.1	981	8.56	0.80	4.52	1.73	0.98	0.65	0.16	1.86	5.97	-5.01	1.40	-3.7
6-WW-DS	14.3	975	8.56	0.80	4.55	1.75	0.98	0.63	0.15	1.86	6.06	-4.71	1.50	-3.6
7-WW-DS	14.0	989	8.60	0.80	4.63	1.71	0.98	0.68	0.16	1.87	6.03	-1.50	-0.05	-3.6
8-WW-DS	14.1	983	8.61	0.80	4.53	1.73	0.98	0.67	0.16	1.86	6.01	-1.83	0.20	-3.6
9-WW-DS	15.3	877	9.53	1.47	5.39	0.41	0.65	0.51	0.04	1.47	4.57	-3.10	1.20	-1.9
10-WW-DS	15.0	773	9.93	1.53	2.54	0.29	1.22	1.94	0.05	2.44	0.76	-2.51	0.81	-0.8
11-WW-DS	15.0	618	9.98	1.55	2.47	0.35	0.24	1.86	0.11	1.23	1.02	-8.42	1.64	-1.3
12-WW-DS	15.0	630	10.39	1.53	2.47	0.41	0.27	1.68	0.11	1.22	0.88	-8.05	1.23	-0.5
13-WW-DS	15.0	1480	11.65	5.18	5.35	1.00	0.06	2.13	0.27	1.24	2.45	-3.36	1.35	1.1
14-WW-DS	15.0	4980	12.17	3.73	4.25	7.74	0.02	2.08	bdl	0.72	7.12	-3.50	1.25	1.7
15-WW-DS	15.0	5510	12.25	3.60	4.13	9.00	0.02	2.01	bdl	0.57	7.24	-3.11	1.02	1.6
1-KA-GW	12.4	176	7.21	0.04	0.48	0.43	0.21	0.02	bdl	0.08	1.49	-3.45	-1.07	-7.0
2-KA-GW	12.6	174	7.13	0.04	0.48	0.43	0.21	0.02	bdl	0.08	1.63	-3.56	-1.17	-7.1
3-KA-DS	12.3	158	8.31	0.12	0.50	0.36	0.13	0.02	0.02	0.04	0.90	-7.60	-0.13	-5.0
4-KA-DS	12.1	168	8.45	0.10	0.49	0.38	0.14	0.02	0.01	0.04	1.72	-3.18	0.06	-4.7
5-KA-DS	11.8	460	11.27	1.19	1.28	0.15	0.01	0.03	0.02	0.06	3.02	-3.13	1.06	-0.3
6-KA-DS	12.0	164	8.10	0.05	0.47	0.40	0.20	0.02	0.01	0.04	2.04	-2.26	-0.25	-5.3
7-KA-DS	18.3	322	8.34	0.09	1.74	0.44	0.37	0.03	bdl	0.14	1.96	-2.20	0.32	-4.1
8-KA-DS	14.7	441	8.53	0.04	0.21	1.35	0.84	0.21	bdl	0.50	3.53	-3.30	0.96	-3.7
9-KA-DS	13.0	350	9.40	0.32	0.43	0.82	0.56	0.24	0.29	0.28	1.75	-4.54	1.24	-2.2
10-KA-DS	12.9	341	9.38	0.32	0.44	0.78	0.55	0.24	0.28	0.29	1.74	-4.52	1.20	-2.3
11-KA-DS	18.1	538	11.17	0.45	0.70	0.96	0.03	0.03	0.01	0.04	0.79	-7.61	1.73	0.3
12-KA-DS	18.1	439	11.16	0.44	0.69	0.85	0.02	0.03	0.01	0.04	0.68	-7.64	1.65	0.2
13-KA-DS	18.3	431	11.13	0.45	0.69	0.61	0.01	0.03	0.02	0.04	0.70	-7.53	1.55	-0.1
14-KA-DS	18.3	336	10.94	0.48	0.73	0.56	0.05	0.04	0.02	0.04	0.89	-7.06	1.57	0.1
15-KA-DS	18.6	334	10.96	0.49	0.74	0.47	0.03	0.03	0.02	0.03	0.79	-7.13	1.47	0.0
16-KA-DS	18.5	285	10.91	0.50	0.75	0.24	0.02	0.03	0.02	0.03	0.62	-7.10	1.15	-0.3
17-KA-DS	18.4	276	10.66	0.73	0.82	0.11	0.01	0.03	0.03	0.03	0.82	-6.51	0.85	-1.3
18-KA-DS	17.9	280	10.84	0.73	0.82	0.11	0.01	0.03	0.03	0.03	0.74	-6.88	0.85	-0.9
19-KA-DS	15.8	239	10.77	0.44	0.71	0.31	0.02	0.03	0.01	0.03	0.73	-6.79	1.27	-0.7
20-KA-DS	13.7	215	11.19	0.45	0.68	0.12	0.08	0.00	bdl	0.02	0.39	-7.80	0.73	0.6
21-KA-DS	13.4	236	11.22	0.62	0.77	0.05	0.01	0.03	0.03	0.03	0.43	-7.79	0.41	-0.4
22-KA-DS	11.2	309	11.16	0.33	0.69	0.71	0.08	0.03	bdl	0.02	1.02	-7.42	1.70	0.3
23-KA-DS	10.9	280	11.12	0.32	0.68	0.54	0.07	0.02	bdl	0.02	0.90	-7.38	1.57	0.1
24-KA-DS	9.3	706	11.95	0.50	0.76	1.31	0.01	0.02	bdl	0.02	0.16	-9.88	1.20	0.9
25-KA-DS	9.3	610	11.90	0.53	0.79	1.05	0.005	0.03	bdl	0.02	0.27	-9.52	1.35	0.4

bdl: below detection limit

Chapter 3

A Carbon isotope study of thaumasite and calcite sinter formation in underground constructions

Florian Mittermayr, Thomas Rinder, Dietmar Klammer, Albrecht Leis and Martin Dietzel

(Conference paper for the International Congress on Durability of Concrete, 2012)

A CARBON ISOTOPE STUDY OF THAUMASITE AND CALCITE SINTER FORMATION IN UNDERGROUND CONSTRUCTIONS

Florian Mittermayr[1], Thomas Rinder[1], Dietmar Klammer[1], Albrecht Leis[2] and Martin Dietzel[1]

[1]Graz University of Technology, Graz, Austria
[2]Joanneum Research, Graz, Austria

ABSTRACT

Secondary formation of sulphate and carbonate minerals (e.g. thaumasite, ettringite, gypsum, and calcite) may cause serious problems concerning the durability of concrete and the overall lifespan of man-made constructions. Thereby high costs for servicing and renovation are incurring. A key to understand the reactions involving deterioration of concrete constructions is to decipher the causes for its appearance by identifying the individual sources. The occurrence of sulphate attack on concrete and drainage clogging is well known and documented from field and laboratory studies. However reactions that lead to the formation of secondary minerals as well as the origin of the involved ions such as carbonate (CO_3^{2-}) and sulphate (SO_4^{2-}) are poorly understood and still hotly debated. In the presented study we highlight the application of stable carbon isotopes ($^{13}C/^{12}C$) to get further insights about potential sources for carbonate minerals. The study comprises results from calcite sinters ($CaCO_3$) which cause drainage clogging and from concrete that suffered severe sulphate attack leading to the formation of thaumasite ($Ca_3Si(OH)_6(CO_3)(SO_4)\cdot 12H_2O$). Carbon for $CaCO_3$ sinter formation is either originating from the absorption of atmospheric CO_2 into high alkaline drainage solutions or stemming from dissolved inorganic carbon (DIC) mainly present as bicarbonate (HCO_3^-) in the ground water. This results in typical $\delta^{13}C$ values (VPDB) of -25‰ ± 3 and -11‰ ± 3, respectively. Isotope data from 3 tunnel case studies indicate DIC of the local ground water to be the main source of CO_3^{2-} for thaumasite formation with $\delta^{13}C$ values of about -8‰. In contrary to calcite sinter formation no clear evidence for absorption of atmospheric CO_2 is found and the dissolution of carbonate fillers/aggregates could not be verified as the proper CO_3^{2-} source for thaumasite formation.

Key-words: Thaumasite, calcite, sulphate attack, drainage clogging, stable carbon isotopes, $^{13}C/^{12}C$.

INTRODUCTION

Concrete has become the most important building material resulting in a fast increasing cement production. In 2006 the cement production was about 2.5 Gt and almost double of this amount is predicted for 2050 [1]. As this trend is continuing less space will be available e.g. in agglomerations leading to taller buildings. The increasing demand will shift the construction into the underground. Furthermore traffic routes are subject for future optimization of infrastructures especially in regions difficult to pass and with little space available like in mountainous areas. Thus traffic routes for rail road and highways are also built in the underground. For instance many trans-alpine projects are in construction and some are close to finishing. Prior to these mega underground projects long lasting intensive planning is needed to meet the requirements of subsurface conditions and to assure the intended lifespans.

A crucial aspect for the initiative of the present study is how to deal with undesired and negative effects concerning the interaction of concrete used in underground construction with the adjacent natural environment. This comprises chemical interaction in the system concrete – ground water – underground atmosphere which leads to leaching of certain elements and precipitation elsewhere such as in drainage systems (Figure 1). Thus it is highly challenging to understand the processes that cause potential problems. Promising studies on this task are investigations on existing underground buildings where chemical interaction provokes serious alterations of concrete itself or performance limitations of the whole construction. An advanced approach to gain further knowledge on how certain elements react under the apparent conditions is the application of stable isotopes, which was pointed out in several former studies [2-9]. In the present study we focus on the use of stable carbon isotopes which already have a wide field of applications in the aspect of environmental, biological and geological tasks [10-13].

Figure 1 – Calcite sinter formation in a drainage tube.

$CaCO_3$ sinter formation in drainage systems

Calcium carbonate scaling in tunnel drainage systems may be caused by different reaction mechanisms. In a first approach calcium and bicarbonate from ground water has to be considered as a potential source for $CaCO_3$ formation. Following the overall reaction

$$CaCO_3 + H_2O + CO_{2(soil)} \leftrightarrow Ca^{2+} + 2HCO_3^- \quad (1a)$$

Limestone within the catchment area of ground water is dissolved which is stimulated by the uptake of CO_2 from soil horizons. Ongoing limestone dissolution results in calcium and bicarbonate rich ground water. Subsequently dissolved calcium and bicarbonate may precipitate causing scaling in drainage systems by $CaCO_3$ precipitates when entering the tunnel atmosphere [14-18]. This can be induced by CO_2 degassing from the solution which results in an increase of pH and a redistribution of dissolved inorganic carbon (DIC). As a critical supersaturation with respect to calcite is reached, precipitation of calcite is triggered comparable to natural speleothem formation in karst systems. Moreover, the reaction of ground water with shotcrete of the tunnel wall has to be considered as a crucial mechanism for $CaCO_3$ formation. Dissolution of the highly soluble mineral portlandite (equation 1b) from the shotcrete results in alkaline solutions with elevated CO_3^{2-} / DIC ratios (equation 1c) and consequently calcite can be precipitated in the drainage system (equation 1d).

$$Ca(OH)_2 \rightarrow Ca^{2+} + 2OH^- \quad (1b)$$

$$2OH^- + 2HCO_3^- \rightarrow 2CO_3^{2-} + 2H_2O \quad (1c)$$

$$2Ca^{2+} + 2CO_3^{2-} \rightarrow 2CaCO_3 \quad (1d)$$

$$CaCO_3 + Ca(OH)_2 + CO_{2(soil)} = 2CaCO_3 + H_2O \quad (1)$$

In this case the carbonate ion for the formation of calcite according to the overall reaction (1) is gained from the ground water as a mixture of soil CO_2 and carbonate from the dissolved limestone. A third mechanism for $CaCO_3$ formation in drainage solutions is valid for high alkaline solutions with low internal CO_2 partial pressures, where absorption of atmospheric CO_2 occurs. According to the overall reaction

$$Ca^{2+} + 2OH^- + CO_{2(g)} = CaCO_3 + H_2O \quad (2)$$

the absorbed CO_2 reacts with OH^- to form HCO_3^- which is mostly converted to CO_3^{2-} in strong alkaline solutions. If Ca^{2+} ions are present from dissolution of e.g. primary limestone or portlandite from the concrete, $CaCO_3$ can precipitate. Such precipitates contain carbon from atmospheric CO_2.

Sulphate attack and thaumasite formation

A well-known "concrete disease" is accounted to sulphate attack and the formation of thaumasite according to the overall reaction

$$Ca_3Si_2O_7 3H_2O + 2\{CaSO_4 2H_2O\} + CaCO_3 + CO_2 + 23H_2O \rightarrow Ca_6[Si(OH)_6]_2(CO_3)_2(SO4)_2\ 24H_2O) \quad (3)$$

besides that of ettringite and gypsum [19, 20]. Neo-formation of such minerals in concretes is accompanied with softening, cracking and in extreme cases with a complete loss of stability and failure of the concrete construction [21, 22]. The sulphate for mineral formation can be gained from internal and external sources stemming from the cement, aggregates, additives, atmosphere or ground water generated from catchment areas with sulphate and sulphide bearing host rocks and soils [23-26]. For the identification of individual sources the application of stable sulphur isotopes has revealed confirming results [27-29]. However the origin of the carbonate (CO_3^{2-}) in thaumasite is still debated by absorption of atmospheric CO_2, DIC of the ground water, carbonate from aggregates and cement fillers [30-32]. For instance Bensted [33] suggests both calcite and atmospheric CO_2 as carbonate source for thaumasite formation in accordance to equations 3.

CASE STUDIES

Sampling of solids comprises drainage sinter, deteriorated shotcrete and concrete from the tunnel linings as well as local host rocks. Aqueous solutions were collected from drainage solution (DS), ground water (GW) and drip water (DW). Compositions of typical solids and aqueous solutions from the case studies are given in Tables 1 and 2 in the Appendix, respectively. For drainage sinter formation 5 solids were collected from the drainage system of an Austrian tunnel. Additionally 4 speleothem-like sinters from the concrete wall were sampled. Moreover, 6 solutions from the drainage system have been taken, as well as one ground water sample and a drip water from a speleothem, formed on the shotcrete lining. Sampling of damaged concrete was conducted at 3 Austrian railroad and highway tunnels running through the eastern Alps, where it is possible to investigate concrete that has suffered intensive deterioration due to sulphate attack in distinct areas (Figure 2).

Figure 2 – Concrete heavily damaged by thaumasite form of sulphate attack (TSA).

MATERIALS AND METHODS

Solid samples were dried at 40°C and grinded for phase identification by X-ray powder diffraction (XRD). XRD patterns were recorded with a PANalytical X'Pert PRO diffractometer with an X'Celerator detector (CoKα radiation, 45 kV and 40 mA). Secondary electron images (SEI) were obtained using a Zeiss DSM 982 Gemini scanning electron microscope (SEM) and

insitu chemical analyses were acquired by electron microprobe analyzer (EPMA) Jeol JXA-8200 at 10kV and 5nA with wavelength dispersive X-ray spectroscopy measurements (WDX). In order to remove aggregates or consolidated concrete from damaged concrete material, samples were treated by ultrasonic and sedimentation techniques to increase the content of thaumasite for carbon isotope analyses in analogy to [28]. During sampling of aqueous solutions in the field temperature and pH of ground and drainage waters were measured. Potentiometric titration was used to determine the alkalinity with 0.001M HCl. Concentrations of major dissolved cations and anions (Na^+, K^+, Mg^{2+}, Ca^{2+}, Cl^-, NO_3^- and SO_4^{2-}) were quantified by ion chromatography with Dionex ICS-3000. The computer code PHREEQC (Version 2.17.01) was used to calculate the saturation indices with respect to calcite and gypsum as well as internal CO_2 partial pressures (P_{CO2}) and DIC speciations [34]. Ion charge balance was checked by deviations from electric charge neutrality being generally < ±3%.

Results from stable carbon isotope measurements ($^{13}C/^{12}C$) are given in the δ-notation as $\delta^{13}C_{VPDB}$ values in ‰ relative to the Vienna Pee Dee Belemnite standard. Isotopic composition of DIC and solid carbonates was analyzed using a fully automated peripheral continuous-flow gas preparation device (Gasbench II), which was connected to a Finnigan DELTA^{plus} XP Mass Spectrometer. The analytical setup is comparable to previous studies and reproducibility of measurements is better than ±0.03‰ [35].

RESULTS AND DISCUSSION

$CaCO_3$ sinter formation in drainage systems

XRD pattern and SEM images of drainage sinters indicate almost pure calcite with small quantities of detritus like quartz or mica. On the macroscopic scale sinters mostly precipitate as white dense or brownish-white layered hard crusts. Figure 3 images a typical sinter under the SEM. Besides hard crusts speleothem-like tubes hanging from the concrete linings or soft mushy or sometimes egg-shaped accumulations can be found in the studied tunnel. In principle, the macroscopic sinter shape and microscopic crystal shape is related to the solution properties [36].

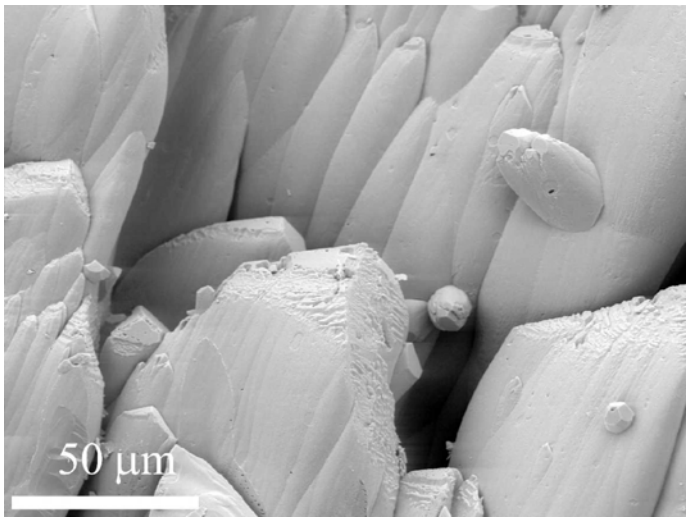

Figure 3 – Secondary electron image of calcite crystals from a drainage scaling.

Solution GW-KAT 8 resembles the chemical composition of local ground water with Na^+ and K^+ concentrations of 4.9 and 1.7 mg/l, respectively. In contrast solution DW-KAT 7 presents the opposite end-member, a highly alkaline solution derived from intensive water – shotcrete interaction. At the high pH of the solution DW-KAT 7 typically elevated concentrations of Na^+ (19.1 mg/l) and K^+ (30.1 mg/l) and a strong depletion of magnesium ions due to brucite ($Mg(OH)_2$) formation are obtained [37-39]. Drainage solutions DS-KAT 1 to DS-KAT 6 are collected along the flow path of the tunnel drainage. Generally these solutions can be considered as mixtures between end member solutions GW and DW. The evolution of K^+ and Na^+ concentrations from DS-KAT 1 to DS-KAT 6 suggests only minor inflow of GW into the drainage along the given flow path with values ranging from 11.6 to 15.8 mg/l and 9.3 to 11.0 mg/l, respectively (see Table 2). Thus, $CaCO_3$ formation and CO_2 exchange between solution and atmosphere has to be considered as the main reasons for continuous change of physicochemical parameters. Obviously, the decrease in concentration of dissolved Ca^{2+} (Figure 4a) and the evolution of saturation index with respect to calcite ($SI_{calcite}$, Figure 4b) give evidence of ongoing calcite formation. The decrease of CO_3^{2-} along the flowpath is to some extent due to the pH decrease and the accompanied shift of the DIC species toward bicarbonate and to the consumption of CO_3^{2-} by $CaCO_3$ formation. Accordingly almost constant DIC concentrations reflect nearly zero net C-balance for CO_2 uptake from the atmosphere and precipitation of $CaCO_3$.

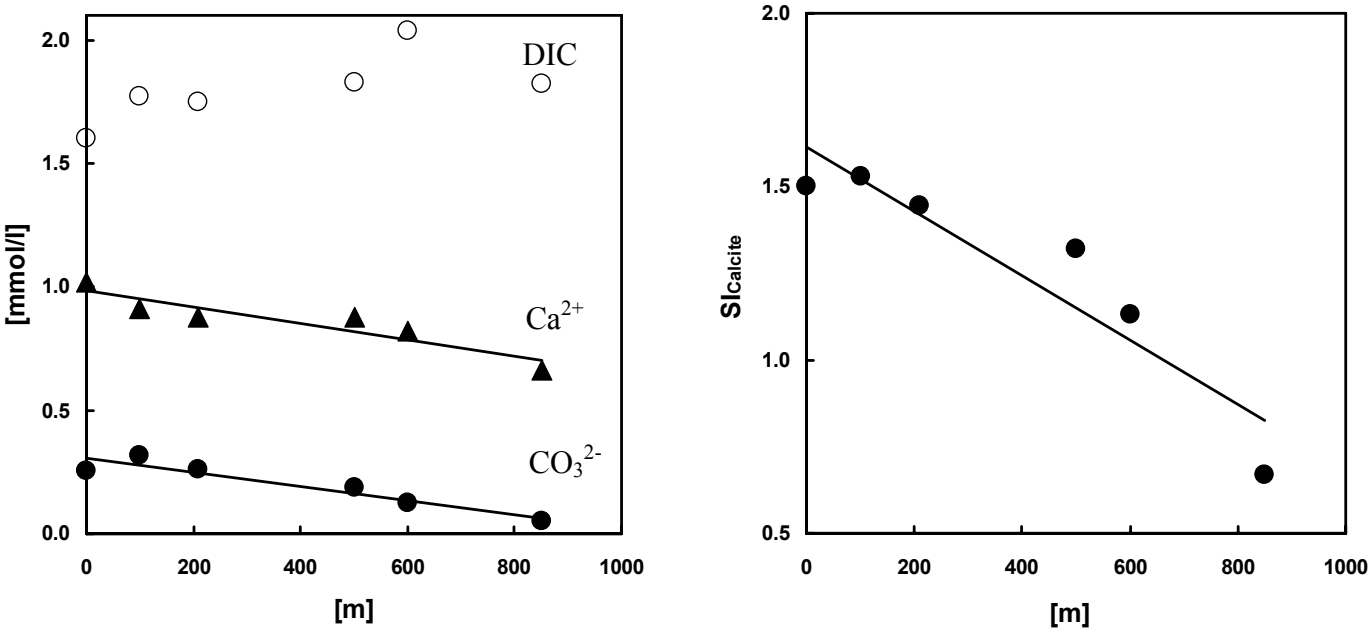

Figure 4 – Evolution of Ca^{2+}-, CO_3^{2-}- and DIC - content of solutions KAT 1-DS to KAT 6-DS along the flow path of the drainage system (4a) and $SI_{Calcite}$ (4b).

Sulphate attack and thaumasite formation

Petrological investigations (XRD, SEM and EPMA) indicate concrete damage from sulphate attack which is mainly due to the formation of thaumasite (Figure 5). However the presence of ettringite could not be clearly distinguished from thaumasite by XRD pattern due to the dominance of thaumasite and structural similarities. Quantitative chemical analyses by WDX

indicate a solid solution between ettringite and thaumasite with a maximum molar Si/Al ratio from 8 to 1. Higher Al contents were particularly found in areas of damaged concrete with less intensive damage or transition horizons to non-altered concrete. However in intensively damaged mushy materials the composition of thaumasite was mostly very pure and almost free of Al. As described in a former study on the present altered concretes, incongruent dissolution of dolomite aggregates and partial replacement by calcite and brucite was found in most of the samples [38].

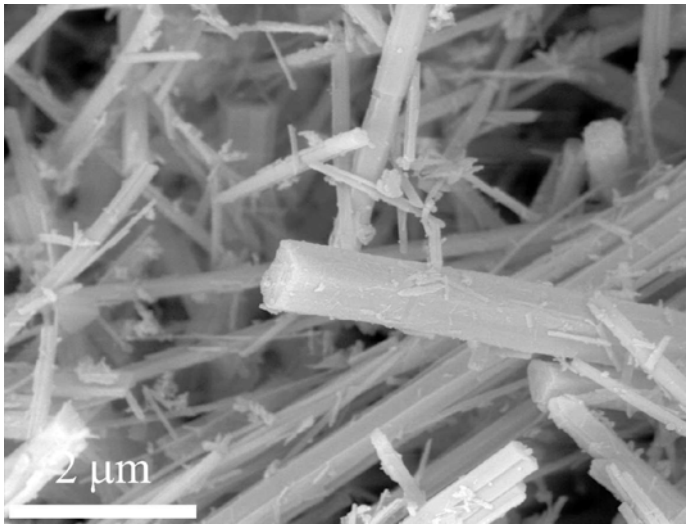

Figure 5 – Secondary electron image showing thaumasite needles (purified sample).

The compositions of typical local ground (GW) and drainage water (DW) inside the tunnels are given in Table 2. In general GW and DW are enriched in SO_4^{2-} (500-1500 mg/l) due to the local geological units containing sulphate minerals. However ground water with a high discharge (>10 l/s) within limestone and dolomite horizons displays very low SO_4^{2-} contents of less than 10 mg/l. In contrast DW with less discharge and drip waters are nearly saturated with respect to gypsum with SO_4^{2-} concentration up to about 4000 mg/l. Latter solutions is therefore being a potential threat for sulphate attack. Na^+ and Cl^- are partly to be accounted to rock salt dissolution but also to intensive concrete and shotcrete interaction when molar Na^+/Cl^- ratios exceed 1 as for solution TT_2-DW. Ca^{2+} concentrations reach up to 600 mg/l, but are limited to the solubility of gypsum. Mixing of Ca^{2+} and SO_4^{2-} rich GW or DW with high alkaline DW from the interaction with concrete has a high potential for drainage clogging due to $CaCO_3$ sinter formation at a high supersaturation degree.

Stable carbon isotopes

As conventional chemical analyses are not suitable to decipher the individual source of CO_3^{2-} in the precipitated solids, stable carbon isotopes are introduced for both calcite and thaumasite formation issues.

The mechanisms responsible for precipitation of calcite can be identified by the use of stable carbon isotope analysis ($^{13}C/^{12}C$) of the DIC and solids. Hydroxilation of CO_2 at high pH conditions leads to a depletion of ^{13}C vs. ^{12}C with a kinetic isotope fractionation of about -18 ‰ [40, 41]. This results in $\delta^{13}C_{CaCO3} \approx$ -26 ‰ for the fixation of atmospheric CO_2 ($\delta^{13}C_{atm\ CO2} \approx$ -8 ‰). The $^{13}C/^{12}C$ isotope values in precipitated calcite gained from ground water

bicarbonate is indicated by a 1:1 mixture of soil CO_2 ($\delta^{13}C_{soil\ CO2} \approx$ -25 ‰) and dissolved local marine limestone ($\delta^{13}C \approx 0$ ‰) leading to $\delta^{13}C_{CaCO3} \approx$ -13 ‰ [41].

The $\delta^{13}C_{DIC}$ value of the local ground water is -11.1 ‰, whereas analysis of highly alkaline drip water from the tunnel wall shows a value of -19.8 ‰ (dominated by absorption of atmospheric CO_2) giving the range of carbon isotope values in the present system (Table 2). The solutions from the drainage system show a continuous uptake of CO_2 from the Earth`s atmosphere by means of decreasing $\delta^{13}C_{DIC}$ values from -12.6 to -14.1 ‰ (Figure 6). Apparent stable carbon isotope fractionation between $\delta^{13}C_{DIC}$ and $\delta^{13}C_{CaCO3}$ is close to the known equilibrium fractionation [42] as $CaCO_3$ solids in the drainage are between 2.0 and 3.2 ‰ isotopically heavier than the associated DIC. For drainage solution KAT 6 at the end of the tunnel, the analyzed solid results in a $\delta^{13}C_{CaCO3}$ value which is 2.7 ‰ isotopically lighter than the corresponding DIC. In the latter case the solution KAT 6-DS was sampled from the outlet of the main drainage into a storage basin. The basin itself receives drainage solutions from various origins. Thus precipitated $CaCO_3$ in the storage basin cannot be directly related to the drainage solution KAT 6-DS.

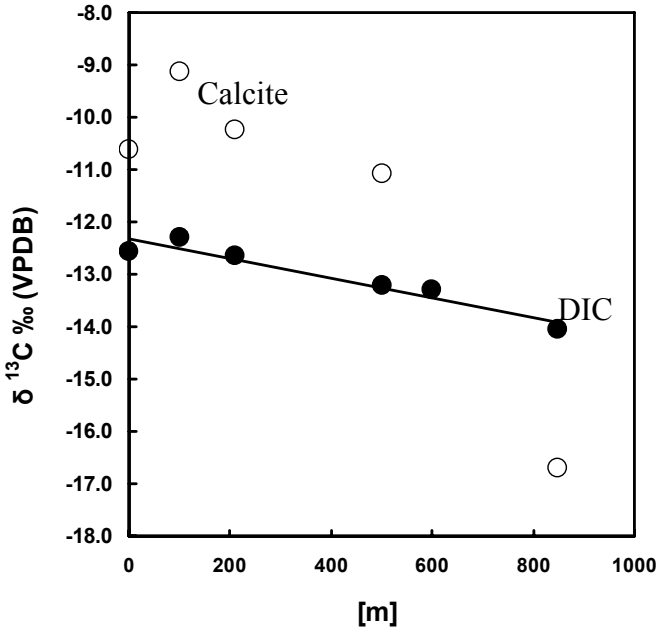

Figure 6 – Evolution of stable carbon isotopes of the solution and the corresponding calcite along the flowpath of the drainage.

Although fractionation mechanisms of stable carbon isotope in the system CO_2-H_2O-$CaCO_3$ are mostly well understood, knowledge of such aspects is very limited for thaumasite formation [27, 43]. Iden and Hagelia [27] reported a high overall variability with respect to the isotopic composition on a micro scale basis due to fine grained materials. Our presented approach is in accordance with results from Iden and Hagelia to use small sample volumes of solids and if possible monomineralic material to exclude variation due to inhomogeneities. By purifying damaged concrete material with ultrasonic treatment the final material consists of almost pure thaumasite (>95 wt.%) with less than 3 wt.% calcite or dolomite, which may slightly disrupt $\delta^{13}C$ results. Tables 1 and 2 comprise $\delta^{13}C$ values of solid carbonate samples and of the DIC, respectively. Obviously given ranges of isotope data in Figure 7 indicate DIC of the local ground

water as carbon source accounted to thaumasite formation. However other carbon sources like atmospheric CO_2 or carbon from dissolution of carbonate filler and aggregates may also be likely carbon source as postulated by [30, 31, 44, 45]. In this study carbon isotope results show that the impact of atmospheric CO_2 can be almost ruled out as a shift of $\delta^{13}C$ values to -25 ‰ was not detected in any case. Dissolution of carbonate aggregates and fillers in the concrete due to CO_2 from interacting ground water is also very unlikely. The local ground water is already close to saturation with respect to calcite and dolomite with P_{CO2} values near the Earth`s atmosphere level at slightly alkaline conditions. Thus CO_2 from soil uptake cannot be assumed for potential aggregate dissolution. Nevertheless for dolomite aggregates, dedolomitization has to be considered, resulting in precipitation of brucite and calcite. This would lead to lower $\delta^{13}C$ isotopic signals in DIC and thaumasite as $\delta^{13}C$ of dolomite aggregates is close to 0 ‰ (see carbonate aggregates in Fig.7). However a shift of $\delta^{13}C$ of thaumasite to 0 ‰ is not shown in Fig.7. Therefore within a first approach we believe that bicarbonate of the ground water is the major source for thaumasite formation. Interestingly, an analogous behavior was obtained for SO_4^{2-} in thaumasite from the same tunnels by using stable sulphur isotope signals where SO_4^{2-} from ground water was identified for thaumasite formation[28, 46].

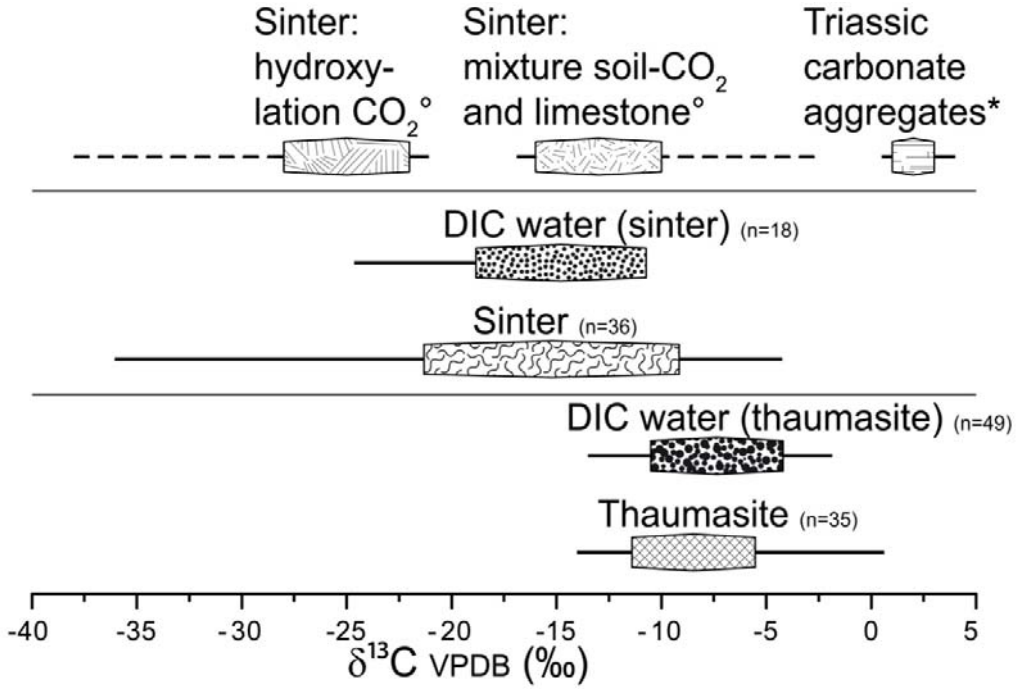

*Figure 7 – Range of $\delta^{13}C_{VPDB}$ values from studies of drainage sinter formation and thaumasite formation. °denotes $\delta^{13}C_{VPDB}$ values of $CaCO_3$ sinter from the literature [36, 41, 47]. *denotes $\delta^{13}C_{VPDB}$ values from this study and the literature[48].*

CONCLUSIVE REMARKS

The application of stable carbon isotope distribution has shown to be a very useful tool to gain an advanced understanding of the formation of carbonate containing minerals like $CaCO_3$ and thaumasite induced by cement-water reactions. $CaCO_3$ sinter formation is referred to both the bicarbonate of the ground water and the absorption of atmospheric CO_2. Absorption phenomena were studied by $CaCO_3$ sinter formation in the drainage along a flow path via isotopic $^{13}C/^{12}C$ evolution in the DIC and in the $CaCO_3$ precipitates. In the case of thaumasite the CO_3^{2-} is mainly

derived from DIC of the ground water. Ongoing experiments for thaumasite formation are carried out to verify the latter findings by involving stable carbon isotope distribution.

ACKNOWLEDGMENT

The authors greatly appreciate financial support of the present study by NAWI Graz (Graz Advanced School of Science, GASS) and Österreichische Forschungsförderungsgesellschaft (FFG, 828476). The authors also want thank Prof. Josef Tritthart for the helpful comments and discussions.

REFERENCES

1. Schneider, M., et al., *Sustainable cementproduction—present and future.* Cement and Concrete Research, 2011. **41**(7): p. 642-650.
2. Rafai, N., et al., *Carbonation-decarbonation of concretes studied by the way of carbon and oxygen stable isotopes.* Cement and Concrete Research, 1992. **22**(5): p. 882-890.
3. Rafai, N., et al., *Isotope geochemistry (13C, 18O) of carbonation processes in concretes.* Cement and Concrete Research, 1991. **21**(2-3): p. 368-377.
4. Kosednar-Legenstein, B., et al., *Stable carbon and oxygen isotope investigation in historical lime mortar and plaster - Results from field and experimental study.* Applied Geochemistry, 2008. **23**(8): p. 2425-2437.
5. Létolle, R., et al., *Stable isotopes of carbon and oxygen for the study of carbonation/decarbonation processes in concretes.* Cement and Concrete Research, 1992. **22**(2-3): p. 235-240.
6. Graham, I.J., R.L. Goguel, and D.A. St John, *Use of strontium isotopes to determine the origin of cement in concretes: Case examples from New Zealand.* Cement and Concrete Research, 2000. **30**(7): p. 1105-1111.
7. Kloppmann, W., et al., *Building materials as intrinsic sources of sulphate: A hidden face of salt weathering of historical monuments investigated through multi-isotope tracing (B, O, S).* Science of The Total Environment, 2011. **409**(9): p. 1658-1669.
8. Clark, I.D., R. Dayal, and H.N. Khoury, *The Maqarin (Jordan) natural analogue for 14C attenuation in cementitious barriers.* Waste Management, 1994. **14**(5): p. 467-477.
9. Dotsika, E., et al., *Isotopic analysis for degradation diagnosis of calcite matrix in mortar.* Analytical and Bioanalytical Chemistry, 2009. **395**(7): p. 2227-2234.
10. Górka, M., et al., *Carbon isotope signature of dissolved inorganic carbon (DIC) in precipitation and atmospheric CO_2.* Environmental Pollution, 2011. **159**(1): p. 294-301.
11. Hoefs, J., *Stable Isotope Geochemistry*. 6th ed. 2008, Berlin: Springer. 288.
12. O'Neil, J.R. and I. Barnes, *C13 and O18 compositions in some fresh-water carbonates associated with ultramafic rocks and serpentinites: western United States.* Geochimica et Cosmochimica Acta, 1971. **35**(7): p. 687-697.
13. Wilson, S.A., et al., *Isotopic Disequilibrium during Uptake of Atmospheric CO(2) into Mine Process Waters: Implications for CO(2) Sequestration.* Environmental Science & Technology, 2010. **44**(24): p. 9522-9529.
14. Dietzel, M., *C-13/C-12-Signatures and O-18/O-16-signatures of calcite precipitations in drainage systems.* Acta Hydrochimica Et Hydrobiologica, 1995. **23**(4): p. 180-184.
15. Dietzel, M., *Measurement of the stable carbon isotopes in calcite sinters on concrete.* ZKG International, 2000. **53**(9): p. 544-548.
16. Dietzel, M., *C-13/C-12-signatures of calcite-sinter onto concrete.* Applied Mineralogy, Vols 1 and 2, 2000: p. 747-748.
17. Girmscheid, G., et al., *Scale sintering in tunnel drainages - Mechanisms of scale formation.* Bauingenieur, 2003. **78**: p. 292-300.
18. Girmscheid, G., T. Gamisch, and A. Meinlschmidt, *Scale sintering in tunnel drainages – Recommendations for maintenance of tunnels.* Bauingenieur, 2003. **78**: p. 562-570.
19. Bensted, J., *Thaumasite - background and nature in deterioration of cements, mortars and concretes.* Cement & Concrete Composites, 1999. **21**(2): p. 117-121.
20. Jallad, K.N., M. Santhanam, and M.D. Cohen, *Stability and reactivity of thaumasite at different pH levels.* Cement and Concrete Research, 2003. **33**(3): p. 433-437.

21. Romer, M., *Steam locomotive soot and the formation of thaumasite in shotcrete.* Cement and Concrete Composites, 2003. **25**(8): p. 1173-1176.
22. Schlegel, M.C., et al., *Deciphering the sulfate attack of cementitious materials by high-resolution micro-X-ray diffraction.* Analytical Chemistry, 2011. **83**(10): p. 3744-3749.
23. Glasser, F.P., J. Marchand, and E. Samson, *Durability of concrete — Degradation phenomena involving detrimental chemical reactions.* Cement and Concrete Research, 2008. **38**(2): p. 226-246.
24. Tritthart, J., et al., *A Casestudy of Thaumasite Formation in an Austrian Tunnel*, in *13th International Congress on the Chemistry of Cement*. 2011: Madrid. p. 431.
25. Bellmann, F., W. Erfurt, and H.M. Ludwig, *Field performance of concrete exposed to sulphate and low pH conditions from natural and industrial sources.* Cement and Concrete Composites, in Press.
26. Blanco-Varela, M.T., et al., *Thaumasite formation due to atmospheric SO2-hydraulic mortar interaction.* Cement & Concrete Composites, 2003. **25**(8): p. 983-990.
27. Iden, I.K. and P. Hagelia, *C, O and S isotopic signatures in concrete which have suffered thaumasite formation and limited thaumasite form of sulfate attack.* Cement and Concrete Composites, 2003. **25**(8): p. 839-846.
28. Mittermayr, F., et al., *Concrete under Sulphate Attack: An Isotope Study on Sulphur Sources* Isotopes in Environmental & Health Studies, in Press.
29. Pye, K. and N. Schiavon, *Cause of Sulfate Attack on Concrete, Render and Stone indicated by Sulfur Isotope Ratios.* Nature, 1989. **342**(6250): p. 663-664.
30. Collett, G., et al., *The role of carbon dioxide in the formation of thaumasite.* Cement and Concrete Research, 2004. **34**(9): p. 1599-1612.
31. Thomas, M.D.A., C.A. Rogers, and R.F. Bleszynski, *Occurrences of thaumasite in laboratory and field concrete.* Cement and Concrete Composites, 2003. **25**(8): p. 1045-1050.
32. Hagelia, P. and R.G. Sibbick, *Thaumasite Sulfate Attack, Popcorn Calcite Deposition and acid attack in concrete stored at the "Blindtarmen" test site Oslo, from 1952 to 1982.* Materials Characterization, 2009. **60**(7): p. 686-699.
33. Bensted, J., *Thaumasite—direct, woodfordite and other possible formation routes.* Cement and Concrete Composites, 2003. **25**(8): p. 873-877.
34. Parkhurst, D.L. and C.A.J. Apello, *User's guide to PHREEQC (V2).* U.S. Geol. Sur, 1999. **312**.
35. Spotl, C., *A robust and fast method of sampling and analysis of delta C-13 of dissolved inorganic carbon in ground waters.* Isotopes in Environmental and Health Studies, 2005. **41**(3): p. 217-221.
36. Dietzel, M., et al., *Mechanisms of Sinter Formation in Drainage Systems.* BHM Berg- und Hüttenmännische Monatshefte, 2008. **153**(10): p. 369-372.
37. Chen, W. and H.J.H. Brouwers, *Alkali binding in hydrated Portland cement paste.* Cement and Concrete Research, 2010. **40**(5): p. 716-722.
38. Mittermayr, F., et al., *Dissolution of Dolomite in alkaline cementitious media*, in *13th International Congress on the Chemistry of Cement*. 2011: Madrid. p. 445.
39. Pokrovsky, O.S. and J. Schott, *Experimental study of brucite dissolution and precipitation in aqueous solutions: surface speciation and chemical affinity control.* Geochimica et Cosmochimica Acta, 2004. **68**(1): p. 31-45.
40. Usdowski, E. and J. Hoefs, *$^{13}C/^{12}C$ partitioning and kinetics of CO_2 absorption by hydroxide buffer solutions.* Earth and Planetary Science Letters, 1986. **80**(1-2): p. 130-134.

41. Dietzel, M., E. Usdowski, and J. Hoefs, *Chemical and $^{13}C/^{12}C$- and $^{18}O/^{16}O$-isotope evolution of alkaline drainage waters and the precipitation of calcite.* Applied Geochemistry, 1992. **7**(2): p. 177-184.
42. Dandurand, J.L., et al., *Kinetically controlled variations of major components and carbon and oxygen isotopes in a calcite-precipitating spring.* Chemical Geology, 1982. **36**(3-4): p. 299-315.
43. French, W.J., *Presidential Address 2003: Why concrete cracks - geological factors in concrete failure.* Proceedings of the Geologists Association, 2005. **116**: p. 89-105.
44. Justnes, H., *Thaumasite formed by sulfate attack on mortar with limestone filler.* Cement and Concrete Composites, 2003. **25**(8): p. 955-959.
45. Torres, S.M., et al., *Microstructure of 5-year-old mortars containing limestone filler damaged by thaumasite.* Cement and Concrete Research, 2006. **36**(2): p. 384-394.
46. Mittermayr, F., et al., *Deterioration of concrete – application of stable isotopes*, in *10th International Congress for Applied Mineralogy*, M.A.T.M. Broekmans, Editor. 2011: Trondheim. p. 435-445.
47. Clark, I. and P. Fritz, *Environmental Isotopes in Hydrogeology*. 1997, Boca Raton: Lewis Publishers. 328.
48. Schroll, E., *V. Geochemische und geochronologische Daten und Erläuterungen*, in *Archiv für Lagerstätten Forschung*, L. Weber, Editor. 1997, Geologische Bundesanstalt: Wien. p. 395-537.

APPENDIX

Table 1 – Typical $\delta^{13}C$ values of carbonate minerals.

Sample ID	Position Tunnel [m]	$\delta^{13}C$ [‰]	Comment
KAT 1-DS	0	-10.6	calcite sinter
KAT 2-DS	100	-9.1	calcite sinter
KAT 3-DS	209	-10.2	calcite sinter
KAT 4-DS	500	-11.1	calcite sinter
KAT 6-DS	850	-16.7	calcite sinter
KAT 7-DW	-	-18.2	calcite sinter
KAT 9-DW	-	-13.8	calcite sinter
KAT 10-DW	-	-35.0	calcite sinter
KAT 11-DW	-	-20.7	calcite sinter
Bos_Tha1	211	-8.7	thaumasite
Bos_Tha2	3269	-4.5	thaumasite
Bos_Tha3	4206	-6.0	thaumasite
TT_Tha1	0	-8.8	thaumasite
TT_Tha2	1860	-9.3	thaumasite
TT_Tha3	3316	-6.7	thaumasite
TT_Cal	3541	-3.2	calcite host rock
TT_Agg	-	1.0	dolomite aggregate
TT_DolGy	1754	3.9	dolomite host rock
TT_GyDol	5921	0.3	dolomite host rock

Table 2 – Chemical composition of aqueous solutions from various sampling sites; TDS: Total dissolved solids; n.d.: not detectable; DIC: dissolved inorganic carbon ; DIC, Internal partial pressure of CO_2 (P_{CO2}) and saturation indices(SI) were calculated with PHREEQC [34].

Sample ID [No.]	pH	Na [mg/l]	K [mg/l]	Mg [mg/l]	Ca [mg/l]	Cl [mg/l]	NO_3 [mg/l]	SO_4 [mg/l]	DIC [mmol/l]
KAT 1-DS	9.71	11.0	15.8	14.7	40.9	9.0	23.8	22.2	1.6
KAT 2-DS	9.77	10.4	15.1	14.8	36.5	9.1	20.9	24.1	1.77
KAT 3-DS	9.66	10.4	14.6	14.5	35.2	8.7	19.4	25.9	1.75
KAT 4-DS	9.46	10.1	13.2	13.8	35.3	8.6	18.1	26.7	1.83
KAT 5-DS	9.20	9.8	12.7	13.6	33.0	8.7	17.9	26.9	2.04
KAT 6-DS	8.83	9.3	11.6	11.3	26.5	9.1	15.8	36.6	1.82
KAT 7-DW	12.06	19.8	30.1	0.24	112.5	11.5	55.8	14.7	0.36
KAT 8-GW	8.23	4.9	1.7	20.4	54.0	7.3	0.1	48.5	3.89
Bos_S1-DW	7.94	1328	44.0	604	502	1578	3.5	4256	1.44
Bos_S2-GW	8.31	0.2	0.3	7.9	27.6	0.3	2.3	5.1	1.93
Bos_S3-DS	8.18	48.6	5.6	57.8	234	60.7	1.3	650	3.47
Bos_R1-DS	8.34	6.7	0.3	10.0	38.0	7.4	3.0	22.1	2.27
Bos_R2-GW	8.32	0.9	0.3	10.8	40.3	0.9	4.0	18.1	2.46
Bos_R3-GW	7.60	3.8	0.9	32.9	206	4.9	1.0	505	2.8
TT_1-DS	8.28	650	34.3	18.9	144	656	12.0	820	2.03

TT_2-DW	7.49	1227	10.2	126	428	46.1	3.4	4072	1.37
TT_3-GW	7.60	2.0	0.8	35.4	554	0.8	n.d.	1298	2.65

Table 2 – Continued.

Sample ID [No.]	**Position** [m]	**T** [°C]	**TDS** [mg/l]	**$\delta^{13}C_{DIC}$** [‰]	**P_{CO2}** atm.	**SI_{Gp}**	**SI_{Cal}**	**Type**
KAT 1-DS	0	13.3	264	-12.6	-5.0	-2.0	1.5	drainage water
KAT 2-DS	100	13.1	274	-12.3	-5.0	-2.0	1.5	drainage water
KAT 3-DS	209	13.2	264	-12.7	-4.9	-2.0	1.4	drainage water
KAT 4-DS	500	12.9	258	-13.2	-4.6	-2.0	1.3	drainage water
KAT 5-DS	600	13.0	260	-13.3	-4.2	-2.0	1.1	drainage water
KAT 6-DS	850	14.3	236	-14.1	-3.9	-2.1	0.7	drainage water
KAT 7-DW	-	17.0	602	-19.8	-9.9	-2.0	1.7	drip water
KAT 8-GW	-	14.7	380	-11.1	-3.0	-1.7	0.7	ground water
Bos_S1-DW	750	10.9	8403	-7.0	-3.3	0.3	0.3	drip water
Bos_S2-GW	1600	6.9	162	-2.0	-3.4	-2.8	0.2	ground water
Bos_S3-DS	5425	10.3	1272	-8.8	-3.0	-0.3	1.0	drainage water
Bos_R1-DS	0	6.3	226	-5.5	-3.4	-2.1	0.4	drainage water
Bos_R2-GW	1196	8.5	226	-7.1	-3.3	-2.2	0.4	ground water
Bos_R3-GW	4766	7.2	919	-5.6	-2.6	-0.4	0.2	ground water
TT_1-DS	0	11.4	2460	-11.6	-3.4	-0.5	0.6	drainage water
TT_2-DW	1950	14.7	5993	-9.2	-2.8	0.3	-0.1	drip water
TT_3-GW	3117	5.6	2048	-7.0	-2.6	0.2	0.5	ground water

Chapter 4

Koralm tunnel as a case study for sinter formation in drainage systems - precipitation mechanisms and retaliatory action

Martin Dietzel, Thomas Rinder, Albecht Leis, Peter Reichl, Peter Sellner, Christian Draschitz, Gerhard Plank, Dietmar Klammer, Herwig Schöfer

(Published in Geomechanik und Tunnelbau, 2008)

Topics

DOI: 10.1002/geot.200800024

Martin Dietzel
Thomas Rinder
Albrecht Leis
Peter Reichl
Peter Sellner
Christian Draschitz
Gerhard Plank
Dietmar Klammer
Herwig Schöfer

Koralm Tunnel as a Case Study for Sinter Formation in Drainage Systems – Precipitation Mechanisms and Retaliatory Action

The drainage systems of several tunnels in Austria are heavily clogged with calcite precipitates. Cleaning and water conditioning are cost-intensive for the operating company. The results of the case study Koralm tunnel show that the dissolved calcium in the drainage solutions derives from the ground water and especially from the dissolution of portlandite at the shotcrete. Accordingly, the drainage solutions are often strongly alkaline and as sufficient supersaturation with respect to calcite is reached, calcite precipitates. The carbonate in the calcite sinter is obtained from the ground water or from the absorption of atmospheric CO_2. Extensive chemical, mineralogical, and isotopic analyses as well as hydrogeochemical modelling permit to decipher the effective parameters in order to develop recommendations for retaliatory action. In-situ experiments in the Koralm tunnel simulate the conditions for the designed drainage system, which should provide an appropriate evaluation of the sinter formation in the drainage and the application of inhibitors. Sinter formation will be reduced by using tailored construction materials.

Koralmtunnel als Fallbeispiel für Versinterungen in Dränagesystemen – Ablagerungsmechanismen und Gegenmaßnahmen

In den Dränagesystemen mehrer Tunnel in Österreich werden enorme Mengen an Kalzit abgelagert. Die Reinigung und Wasserkonditionierung sind für den Betreiber mit erheblichen Kosten verbunden. In dieser Arbeit konnte anhand der Fallstudie Koralmtunnel gezeigt werden, dass das gelöste Kalzium in dem Dränagewasser aus dem Bergwasser selbst und insbesondere aus der Auflösung von Portlandit im Spritzbeton bereitgestellt wird. Die so erhaltenen Lösungen sind häufig stark alkalisch. Hierdurch kommt es zu einer Übersättigung an Kalzit, wodurch in weiterer Folge die Abscheidung von Kalzit eingeleitet werden kann. Das Karbonat im Kalksinter kann entweder aus dem Grundwasser oder aus der Absorption von atmosphärischem CO_2 erhalten werden. Durch umfangreiche chemische, mineralogische und isotopenchemische Analysen sowie hydrogeochemische Modellierungen wurden die jeweils wirksamen Faktoren identifiziert, um auf deren Basis Ansätze für Gegenmaßnahmen entwickeln zu können. In-situ-Experimente im Koralmtunnel simulieren die Bedingungen in der geplanten Dränage. Hierüber soll eine Beurteilung der Versinterungen im Dränagesystem und der Anwendung von Inhibitoren ermöglicht werden. Versinterungen werden auch durch den Einsatz maßgeschneiderter Baustoffe verringert werden.

1 Introduction

The formation of carbonate sinter is a natural phenomenon as well as a challenge in the fields of engineering [3] [4]. Carbonate precipitation in drainage systems may cause serious problems due to the reduction of the cross section of drainage tubes (Figure 1) and the pollution of receiving streams by suspended carbonates and ongoing sinter formation.

The Koralm tunnel will be the longest tunnel in Austria and special effort is given to minimize costs for maintenance action such as cleaning of the drainage system and water conditioning. The time effort for maintenance of the Koralm tunnel drainage system with respect to cleaning of drainage pipes by high pressure flushing may comprise a couple of hundreds of hours for seven workmen. Additional costs for flushing equipment as well as for delays and rerouting of trains have to be considered. Simulations of cleaning procedures could yield in blocking of one tube for more than six weeks or nearly one-third of the weekends during one year. Furthermore, annual charges for conventional scale inhibiting may comprise up to about 15 % of the costs for one cleaning procedure.

In tunnel drainage systems calcium carbonates precipitate from aqueous solutions, which are mostly generated from local ground water and the reaction with the shot-

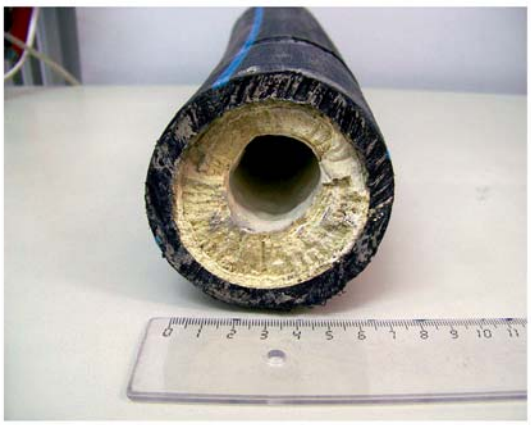

Fig. 1. Drainage tube from the Koralm tunnel with calcite sinter
Bild 1. Dränagerohr aus dem Koralmtunnel mit Kalzitinkrustierungen

crete of the tunnel construction. Accordingly, the chemical composition of the drainage solutions depends on the evolution of the local ground water as well as on the chemical composition and reactivity of the materials used for construction.

The aims of this study are to decipher the mechanisms of sinter formation and to develop strategies to minimize the quantity of precipitates. Crucial factors comprise a proper construction of the drainage system and the development of suitable recommendations for retaliatory action such as techniques for scale inhibition. For this purpose, experiments and field studies were carried out in the Koralm tunnel. Sampling of solids and solutions in the drainage system, of shotcrete and of ground water in the vicinity of the tunnel was conducted from 2005 to 2008.

2 Study area and methodology

In the final stage the Koralm tunnel will have two separate tubes, a maximum overburden of about 1.2 km, and a length of about 32.8 km. It will cross a mountain range, which mostly consists of a polymetamorphic crystalline basement with Tertiary basins on both sides. The crystalline basement is dominated by mylonitic gneisses and micaschists. Infrequently, marbles and amphibolites may occur. The Tertiary sedimentary basins encountered by the tunnel comprise clastic fluviatile and marine deposits. In the study area of the investigation tunnels Mitterpichling and Paierdorf mostly neogene sediments (clayey and silty sands) are encountered by the tunnel (Tertiary basin). The maximum overburden in this area reaches about 200 m.

The solids collected from the Koralm tunnel were analysed by x-ray diffraction, infrared spectroscopy, ion coupled plasma optical emission spectroscopy (ICP-OES) via digestion with diluted nitric acid, and mass spectroscopy. Aqueous solution analyses comprised pH, ion chromatography, titration, and ICP-OES. Hydrogeochemical modelling was carried out using the computer code PHREEQ C [5].

3 Drainage concept

Along the entire length of the Koralm tunnel two separate drainage systems are designed: One for the drainage of ground water and another for collecting condensation and spilled water from trains. Additionally, the main local inflows of ground water encountered during tunnel construction will be collected and drained in separate pipes and might be used as drinking water in a local supply system.

The reduction of maintenance works was a crucial factor to design the drainage system of the Koralm tunnel. Since cleaning of drainage pipes had been identified as the main factor for the maintenance costs of the tunnel, the ÖBB (Austrian Federal Railways) proposed only one drainage pipe at the tunnel invert. This would result in a total pipe length of only one-third of a conventional drainage system.

The 2 × 32.8 km long Koralm tunnel will predominantly be excavated by shield TBM. The outer lining will consist of prefabricated, reinforced concrete segments. For the conventionally excavated tunnel sections in the study area the outer lining consists of shotcrete. The inner lining will be made from in-situ concrete. Along tunnel sections in sound rock and without water inflow, the inner lining will be omitted.

A waterproof membrane separates the outer lining and the in-situ concrete along the tunnel roof and side walls. Ground water will enter the tunnel drainage also through drainage boreholes at invert level, which are drilled in radial direction through the lining segments in a systematic pattern (Figure 2). Subsequently, the solutions will flow by gravity in transversal direction along the

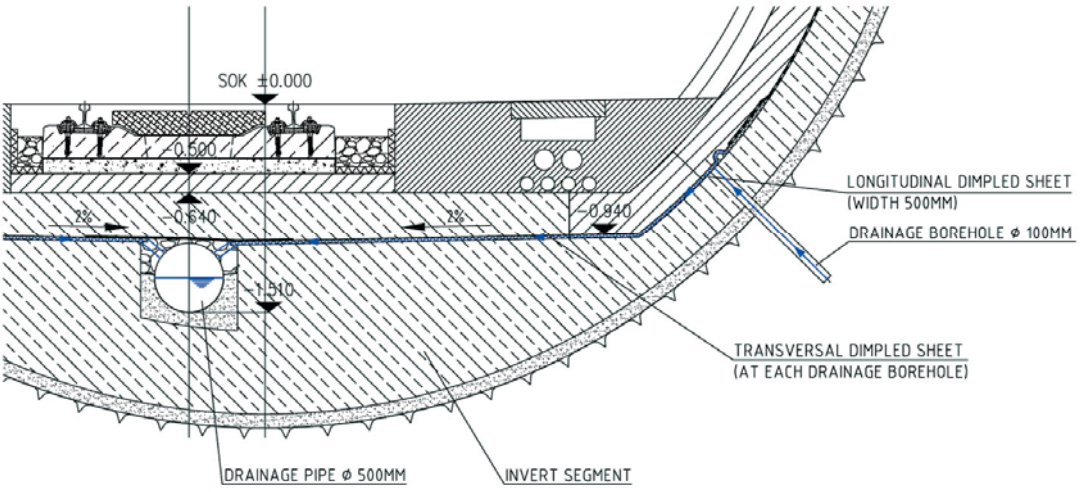

Fig. 2. Cross section of the drainage system of the Koralm tunnel
Bild 2. Querschnitt des Dränagesystems des Koralmtunnels

slightly inclined surface of the invert segment and underneath stripes of dimpled sheets towards the drainage pipe in the centre of the invert. Transversally installed dimpled sheets, covering 50 % of the invert segment surface, provide the cavities underneath the in-situ concrete slab required for the water to flow towards the drainage pipe and also enable a transfer of vertical loads onto the invert segment.

The drainage pipe at the centre of the invert has a diameter of 500 mm with cleaning manholes at a distance of 75 m. In each manhole a vertical 100 mm diameter pipe will be installed into the surrounding ground, thus providing an additional path for the ground water to enter into the tunnel drainage system. These vertical pipes are permanently accessible.

4 Sinter composition

The precipitates in Koralm tunnel mainly consist of the mineral calcite ($CaCO_3$), see Figure 1. Aragonite ($CaCO_3$) and brucite ($Mg(OH)_2$), which may also occur in such environments, were not found. In the precipitated calcite magnesium and strontium were detected as minor and trace components, respectively. Both ions co-precipitate with calcite by isomorphic substitution of calcium ions in the calcite crystal lattice. Detritus comprises rock fragments and silicates such as chlorite and quartz.

5 Composition of the drainage solutions

The analysed drainage solutions can be classified by three water types (Table 1). Type 1 represents drainage solutions with chemical compositions similar to the local ground water (e.g. solutions D-10 and D-15). In this case the interaction of the ground water with the shotcrete is low. The main cations are Ca^{2+} and Mg^{2+}, and main anions comprise HCO_3^-, SO_4^{2-} and Cl^-. Minor and trace components are Na^+ and K^+, and Sr^{2+}, respectively. Solutions of type 2 represent highly alkaline drainage solutions, which are obtained by strong interaction with the shotcrete (e.g. solutions D-1 and D-12). These solutions are usually characterised by low flow rates. Compared to the ground water, the solutions of type 2 are typically depleted in magnesium and sulphate but enriched in calcium, sodium and potassium at elevated pH. Type 3 represents solutions which are typically found as merged solutions at rather high flow rates in the drainage system (e.g. solutions D-2 and D-3). The chemical composition of type 3 solutions may be obtained by mixtures of type 1 and 2 solutions or by intermediate strength of interaction of the solutions with the shotcrete.

In general, low flow rates cause an increase in the residence time of the solution at the shotcrete. Therefore, in drainage solutions of type 2 high pH values are due to a significant dissolution of portlandite ($Ca(OH)_2$) from the

Table 1. Chemical composition of typical drainage solutions (D) and ground water (G) from the Koralm tunnel. Concentrations are given in mg L^{-1}. SpC: specific conductivity in µS/cm. T: temperature in °C. Alk: alkalinity. $SI_{calcite}$: modelled saturation index with respect to calcite. Pco_2: modelled internal partial pressure of CO_2 in atm. Sampling date: 13.11.2005 for solutions D-1 to D-10 and G; 20.11.2007 for solutions D-11 to D-15

Tabelle 1. Chemische Zusammensetzung von typischen Drainagelösungen (D) und Grundwasser (G) aus dem Koralmtunnel. Die Konzentrationen sind in mg L^{-1} angegeben. SpC: Spezifische Leitfähigkeit in µS/cm. T: Temperatur in °C. Alk: Alkalinität. $SI_{calcite}$: modellierter Sättigungsindex in Bezug auf Kalzit. Pco_2: modellierter interner CO_2 Partialdruck in atm. Zeitpunkt der Probennahme: 13.11.2005 für Lösungen D-1 bis D-10 und G; 20.11.2007 für Lösungen D-11 bis D-15

No.	SpC	T	pH	Ca^{2+}	K^+	Mg^{2+}	Na^+	SiO_2	Sr^{2+}	Cl^-	SO_4^{2-}	Alk	$SI_{calcite}$	P_{CO2}
D-1	1380	17.0	12.26	112.5	30.1	0.2	19.8	3.90	0.55	11.5	14.7	324.6	2.56	$10^{-9.01}$
D-2	341	12.9	9.38	31.1	12.5	13.2	10.1	8.26	0.19	8.6	27.9	123.6	1.19	$10^{-4.52}$
D-3	382	13.3	9.72	40.9	15.8	14.8	11.0	7.79	0.19	9.0	22.2	115.5	1.46	$10^{-5.01}$
D-4	377	13.1	9.67	36.5	15.1	14.8	10.4	7.63	0.18	9.1	24.1	129.6	1.49	$10^{-5.04}$
D-5	350	13.0	9.40	33.0	12.7	13.6	9.8	8.06	0.18	8.7	26.9	125.4	1.23	$10^{-4.54}$
D-6	305	14.3	9.14	26.5	11.6	11.3	9.3	6.90	0.15	9.1	36.6	105.3	0.64	$10^{-3.93}$
D-7	343	12.7	9.29	30.4	13.6	12.4	12.0	8.27	0.21	9.4	32.6	138.1	1.16	$10^{-4.36}$
D-8	348	12.5	9.36	30.6	13.6	12.3	12.5	8.30	0.21	9.6	32.8	136.7	1.20	$10^{-4.45}$
D-9	340	12.6	9.42	29.7	13.3	12.2	12.3	8.27	0.22	9.2	36.5	123.0	1.19	$10^{-4.57}$
D-10	441	14.7	7.99	54.0	1.7	20.4	4.9	8.45	0.13	7.3	48.5	221.0	0.45	$10^{-2.74}$
G	398	13.7	7.60	42.6	2.9	14.5	7.0	10.7	0.11	14.8	30.8	103.1	–0.26	$10^{-2.78}$
D-11	1030	9.4	12.06	64.2	22.4	0.4	19.3	11.0	0.52	1.2	2.7	279.4	1.66	$10^{-9.68}$
D-12	2330	9.0	12.45	156.1	45.6	0.1	26.1	1.4	1.10	0.8	2.2	572.4	0.84	$10^{-11.63}$
D-13	250	11.0	7.73	31.3	2.9	8.0	9.8	18.1	0.14	2.3	12.4	140.8	–0.24	$10^{-2.70}$
D-14	249	11.4	7.75	31.3	2.8	8.3	10.2	18.3	0.14	2.4	12.6	140.3	–0.21	$10^{-2.72}$
D-15	246	11.2	7.64	32.5	3.0	8.7	11.0	18.4	0.14	2.3	12.5	139.8	–0.31	$10^{-2.61}$

shotcrete. For the drainage solutions of type 1 and 3 with rather high flow rates the interaction of the solutions with the mineral phases of the shotcrete, e.g. portlandite dissolution, is less intensive. Thus, the pH values of drainage solutions of type 1 and 3 are lower than for solutions of type 2.

Several drainage solutions sampled in November 2007 are undersaturated with respect to calcite ($SI_{calcite} < 0$) indicating dissolution instead of precipitation of calcite. However, the occurrence of highly alkaline and highly supersaturated solutions such as D-14 and D-15 shows strong and ongoing interaction of the solutions with the shotcrete.

6 Evolution of drainage solutions

6.1 Dissolution of limestone

The drainage solutions are gained from ground water, which dissolves carbonate minerals from the natural rocks and sediments in the study area. The dissolution of carbonates is promoted by the uptake of carbon dioxide from the soil atmosphere. Calcium carbonates dissolve according to the overall reaction

$$CO_{2(gas)} + H_2O + CaCO_3 = Ca^{2+} + 2HCO_3^- \quad (1)$$

The dissolution usually results in slightly alkaline calcium bicarbonate solutions. The concentration of total dissolved carbonate strongly depends on the primary content of carbonic acid and the occurrence of solid carbonates. In the study area of the Koralm tunnel (Mitterpichling and Paierdorf) the rocks consist mostly of clayey and silty sands. Thus, the ground water contains moderate calcium and bicarbonate concentrations and is slightly undersaturated with respect to calcite (see solution G in Table 1; $SI_{calcite} < 0$).

6.2 Reactions at the shotcrete

As the ground water gets into contact with the shotcrete of the Koralm tunnel, complex mineral water reactions appear. Simplified, the portlandite of the shotcrete dissolves which results in an increase of the calcium concentration and pH. Drainage solutions can reach pH values between 12 and 13 (type 2 solutions; Table 1). On the other hand, calcium ions can be fixed by the precipitation of calcium carbonate and sulphate minerals directly at the shotcrete. The calcium concentrations in the drainage solutions may be even below the concentration of the ground water (type 3), whereas sulphate content is reduced in most of the drainage solutions (type 2 and 3). Figure 3 clearly shows that the sulphate content in the drainage solutions are negatively correlated to the pH of the solutions. Newly formed sulphate minerals at the shotcrete may comprise gypsum, ettringite, monosulfate, and thaumasite depending on the availability of aqueous sulphate ions. In highly alkaline solutions brucite can be precipitated (type 2 solution). The depletion of magnesium and sulphate ions in the drainage solutions vs. the ground water can be used as an indicator for the degree of solution-shotcrete interaction. Further proxies for the degree of this interaction are elevated strontium, sodium, and potassium concentrations (see Table 1).

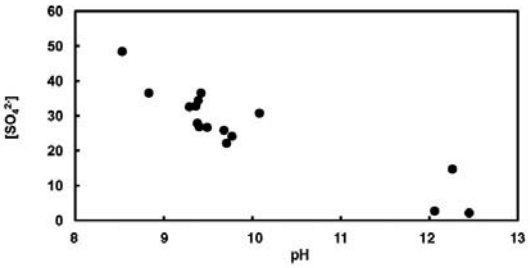

Fig. 3. Concentration of dissolved sulphate ions (mg L^{-1}) as a function of the pH of drainage solutions from the Koralm tunnel
Bild 3. Konzentrationen gelöster Sulfationen (mg L^{-1}) als Funktion des pH Werts von Dränagewasser aus dem Koralmtunnel

7 Mechanisms of carbonate sinter formation

Calcite precipitation from the drainage solutions can be induced by the dissolution of portlandite in the primary ground water at the shotcrete. The dissolved calcium and carbonate ion can be precipitated according the equation

$$Ca(OH)_2 + 2HCO_3^- + Ca^{2+} = 2CaCO_3 + 2H_2O \quad (2)$$

as supersaturation with respect to calcite is reached ($SI_{calcite} > 0$). However, once the solutions come into contact with the Earth's atmosphere, the internal partial pressures of CO_2 in the solutions control the CO_2 exchange with the atmosphere and ongoing carbonate precipitation.

As the internal P_{CO2} values of the drainage solutions are higher than the surrounding atmosphere (Earth's atmosphere: $Pco_2 = 10^{-3.5}$ atm), CO_2 is liberated from the solutions into the atmosphere (see solutions D-10 and D-13 in Table 1). The pH value increases and saturation with respect to calcite increases. If supersaturation is reached, calcite may precipitate according to equation (1) from the right to the left.

As the internal P_{CO2} values of the drainage solutions are lower than the surrounding atmosphere, CO_2 is absorbed from the atmosphere into the drainage solutions (see solutions D-1 and D-12). High CO_2 absorption rates are especially obtained for highly alkaline solutions. Precipitation of carbonates from the absorbed atmospheric CO_2 may be followed by the expression

$$CO_{2(gas)} + Ca^{2+} + 2OH^- = CaCO_3 + H_2O \quad (3)$$

The isotopic composition of the carbonate sinter can be used to decipher whether the carbonate is gained from the ground water carbonate (equation 2) or from the atmosphere (equation 3). In the case of CO_2 absorption the newly formed calcite is characterised by $\delta^{13}C_{calcite} \approx -25$ ‰, whereas fixation of ground water carbonate results in isotopic heavier $\delta^{13}C_{calcite}$ values in the range from −10 to −16 ‰ [2]. The latter isotope value depends on the conditions of carbonate dissolution during the evolution of the ground water [1]. In Figure 4 the analysed $\delta^{13}C_{calcite}$ versus $\delta^{18}O_{calcite}$ values of the precipitated calcite show a

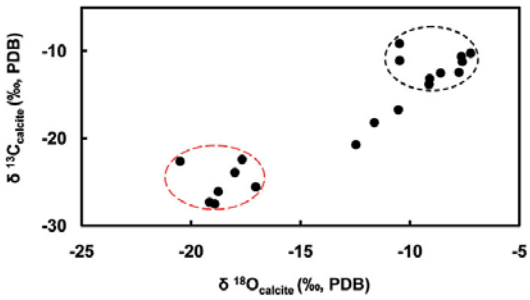

Fig. 4. $\delta^{13}C_{calcite}$ and $\delta^{18}O_{calcite}$ values of calcite sinter precipitated from the drainage solutions of the Koralm tunnel (e.g. $\delta^{13}C_{calcite} = (^{13}R_{sample}/^{13}R_{standard} - 1) \cdot 10^3$; isotope values are related to the PDB-standard and are given in ‰); Light and heavy isotope values indicate highly (red circle) and slightly alkaline solutions (black circle), respectively
Bild 4. $\delta^{13}C_{Kalzit}$ und $\delta^{18}O_{Kalzit}$ Werte von Kalzitsinter abgeschieden aus den Dränagelösungen des Koralmtunnels (z. B. $\delta^{13}C_{Kalzit} = (^{13}R_{Probe}/^{13}R_{Standard} - 1) \cdot 10^3$, die Isotopenwerte sind auf den PDB-Standard bezogen und in ‰ angegeben); isotopisch leichte und schwere Werte zeigen hochalkalische (roter Kreis) beziehungsweise schwach alkalische Dränagelösungen (schwarzer Kreis) an

good relationship. Light and heavy isotope values are obtained for highly and slightly alkaline solutions, respectively. At highly alkaline conditions the carbonate is mostly derived from the Earth's atmosphere, whereas at pH below 10 ground water carbonate is fixed in the carbonate sinter.

8 Retaliatory action

Carbonate sinter formation in the Koralm tunnel is closely related to the ground water-concrete interaction. Sinter formation can be reduced e.g. by using tailored shotcrete. Lab experiments show that shotcrete with low content of portlandite and sulphate active minerals as well as low permeabilities should be used for a sustainable reduction of carbonate sinter formation. Appropriate recipes for shotcrete are developed under construction site conditions using low hydraulic cement content to reduce portlandite formation during the hydration, alkali-free setting accelerators, and proper conditions to avoid fissure formation. A suitable composition was obtained by using around 280 kg m^{-3} of CEM I 52.2R, 140 kg m^{-3} of AHWZ (preprocessed latent hydraulic acting material such as fly ash), and about 7 wt.% of a aluminium sulphate containing setting accelerator. Results from water-shotcrete interaction experiments confirmed that such tailored shotcrete can significantly lower the liberation of Ca^{2+} and OH^- ions into the solution. The Ca^{2+} liberation can be reduced by about 65 % by the application of the above recipe in comparison to common shotcrete compositions. Analogous developments will also be prepared for further construction materials, e.g. grouting mortar.

Hydrogeochemical modelling indicates that the addition of even very low volumes of highly alkaline solutions, e.g. 1 to 3 vol.% of solution D-1, to the ground water of the Koralm tunnel (G) can result in solutions similar to the drainage solutions of type 3 of the Koralm tunnel [6]. High precipitation capacities can be generated by the addition of small volumes of type 2 to type 1 solutions.

The mechanisms of calcite precipitation in the drainage solutions, discussed in section 6, show that the drainage system should be designed to minimize the CO_2 exchange with the atmosphere. Turbulent flow of solutions has to be avoided. However, precipitation of calcium carbonate from solutions of type 2 cannot be significantly reduced by such an approach. In such a case the drainage solutions might be treated with scale inhibitors, e.g. "hardness stabilisation".

Once carbonate sinter is formed in the drainage system, a proper drainage design for the discharge of drainage solution and for cleaning actions is essential for cost-efficient maintenance of the tunnel building.

9 Drainage simulation construction

Five drainage constructions simulating the designed drainage system are installed in-situ in the Koralm tunnel to monitor the progress of sinter formation (Figures 5 and 6). These drainage constructions are supplied by merged drainage solutions of types 1 to 3, which are gained directly from the shotcrete or from temporary drainage tubes. Optionally, enhanced solution-shotcrete interaction can be simulated by the flow of the merged drainage solutions through a container packed with fragments of shotcrete of about 2 to 5 cm in diameter from the respective tunnel section (see Figure 5). Dimpled sheets with vents of about 2 cm will allow solutions to drain into the drainage pipe in the middle of the tunnel (see Figure 6). Once the tunnel is finalized the cleaning of the dimpled sheets is impractical.

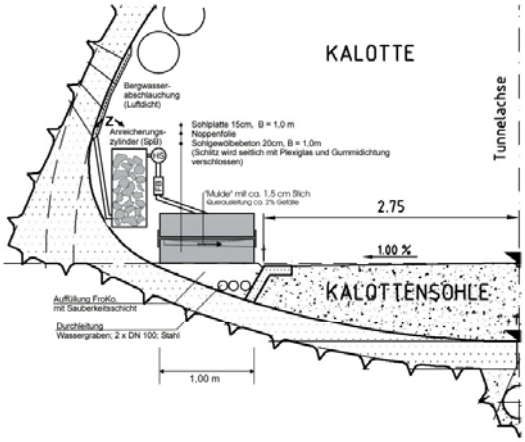

Fig. 5. Schematic cross section (top heading and temporary top heading invert) of the prospection tunnel Mitterpichling and Paierdorf with the drainage simulation construction for the monitoring of sinter formation
Bild 5. Schematischer Querschnitt (Kalotte und temporäre Kalottensohle) des Erkundungstunnels Mitterpichling bzw. Paierdorf mit dem Dränage-Testfeld für das Monitoring der Sinterbildung

Fig. 6. Dimpled sheet for the discharge of drainage solutions to the mid-pipe of the drainage system (Z, see also Figure 5)
Bild 6. Noppenfolie für die Ableitung des Dränagewassers in die mittlere Sammelleitung des Dränagesystems (Z, vgl. Bild 5)

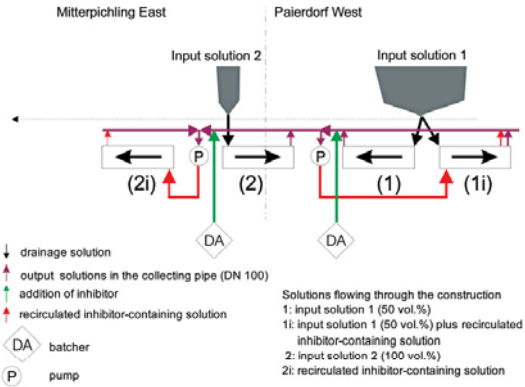

Fig. 7. Experimental setup for the drainage simulation construction
Bild 7. Experimenteller Aufbau für die Konstruktion zur Dränagesimulation

Besides the progress of calcium carbonate precipitation, special focus will be given on the effect of inhibitors on the precipitation behaviour. Simultaneous experimental runs for drainage solutions with and without inhibitor dosage will be carried out. In Figure 7 the experimental setup for two collected and merged drainage solutions (input solution) are shown. Concerning the drainage simulation construction (1) about half of the input solution volume flows through the construction without inhibitor dosage. After passing the construction (1) the output solution 1 is doped with inhibitor (e.g. polyaspartic acid). The other part of the input solution 1 is mixed with the recirculated inhibitor-containing output solution 1. The mixed solution enters the drainage simulation construction (1i) with inhibitor. The setups of the drainage simulation constructions (2) and (2i) are similar, except the exclusive use of recirculated inhibitor-containing output solution 2 for the construction (2i). In the latter constructions the input

solution 2 is not splitted into two fractions due to low flow rates.

The input solutions 1 and 2 comprise a drainage solution of type 3 and 2, respectively (see section 5). Various experimental runs will be carried out as the application of suitable inhibition techniques and proper dosage may play a decisive role for sustainable and cost-efficient retaliatory action.

10 Conclusions

Hydrogeochemical, mineralogical, and isotopic analyses permit to decipher the individual mechanisms of carbonate sinter formation in the Koralm tunnel. Modelling tools and proxies such as mixing calculations and isotope signatures can provide evidence for expected quantities of precipitation and indicators for environmental conditions and changes. From in-situ experiments at the drainage simulation constructions reliable data for prognosis of sintering, inhibitor dosage, and retaliatory action should be achieved for a cost-efficient maintenance of the tunnel building.

References

[1] *Clark, I. D. and Fritz, P.*: Environmental isotopes in hydrology. Lewis Publishers, 1997.
[2] *Dietzel, M.*: Messungen der stabilen Isotope des Kohlenstoffs an Kalk-Versinterungen von Beton. Cement-Lime-Gipsum 53 (2000), No. 9, pp. 544–548.
[3] *Gamisch, T. and Girmscheid, G.*: Versinterungsprobleme in Bauwerksentwässerungen. Berlin: Bauwerk Verlag, 2007.
[4] *Morse, J. W. and Mackenzie, F. T.*: Geochemistry of sedimentary carbonates. Develop. Sed. 48 (1990), pp. 707.
[5] *Parkhurst, D. L. and Appelo, C. A. J.*: User's guide to PHREEQC (version 2); a computer program for speciation, batch-reaction, one-dimensional transport, and inverse geochemical calculations. Water-Resources Investigations U.S. Geol. Sur.: 312 (1999).
[6] *Rinder, T.*: Versinterung von Tunneldränagen – Ursachen und Risikoabschätzung. Diploma Thesis, Graz University of Technology, 2007, 96 p.

Chapter 5

Mixing of aqueous solutions – Impact on dissolution and precipitation of calcium carbonate

Thomas Rinder, Martin Dietzel

(To be submitted upon completion of the study)

Mixing of aqueous solutions – Impact on dissolution and precipitation of calcium carbonate

5.1 Introduction

The potential for dissolution of calcium carbonate by mixing of waters, both saturated in respect to calcite, has been discussed at first by (Bögli, 1964). Main focus was given on its potential for limestone weathering and accompanied karst evolution. A similar rise in dissolution of limestone was observed in horizons, where seawater, supersaturated with respect to calcite, is mixed with freshwater. (Baceta et al., 2001; Romanov and Dreybrodt, 2006; Sanz et al., 2011) showed that such kind of mixing can yield solutions with high capacities to dissolve carbonates. In contrast precipitation of calcite induced by mixing of brines and freshwater was documented by (Berkowitz et al., 2003; Singurindy and Berkowitz, 2005). (Emmanuel and Berkowitz, 2005) set up a 2D conceptual model, where calcium carbonate vein filling due to mixing of aqueous solutions is suggested to be capable to explain length and distribution of the precipitates. The calcium carbonate formation in veins and its spatial evolution has been previously displayed by (Lee and Morse, 1999), where the ongoing calcium carbonate formation is mostly controlled by the CO_2 partial pressure (P_{CO2}), temperature, composition of the solutions, and flow rates.

For freshwater systems, main focus of research dealing with the $CaCO_3$ - CO_2 - H_2O system under closed system conditions with respect to CO_2 exchange between solution and atmosphere is given on limestone dissolution and related karstification mechanisms (Buhmann and Dreybrodt, 1985; Dreybrodt, 1980; Sanz et al., 2011). Limestone dissolution under closed system conditions (DCS) is based on a spatially separated CO_2 uptake into the solution and dissolution of limestone. For instance one might consider a water charged with CO_2 in the soil zone, which starts to dissolve limestone below the groundwater table, where exchange between $CO_{2(ag)}$ and $CO_{2(g)}$ is inhibited due to the slow diffusion aqueous CO_2 through an aqueous solution (Appelo and Postma, 2007). Once CO_2 is consumed by limestone dissolution, it is not replenished.

In the classical study of (Wigley and Plummer, 1976) the evolution of saturation degree with respect to calcite during mixing of calcite saturated solutions was modelled in a wide view. They distinguished between the mixing approaches with exchange (MOS: mixing at open system conditions) and (ii) without exchange (MCS: mixing at closed system conditions) of CO_2

between the mixed solution and the atmosphere. But in any case the endmember solutions, which they used for mixing, are primary derived from calcite dissolution under open system conditions with respect to CO_2 (DOS). In both situations super- and undersaturation with respect to calcite can be obtained by mixing of solutions saturated with respect to calcite. However supersaturation by mixing of calcite saturated solutions was only documented by the mixing using endmember solutions in the $CaCO_3$ - $CaSO_4$ - CO_2 - H_2O system.
In the pure $CaCO_3$ - CO_2 - H_2O system, precipitation of calcite from natural solutions is rather investigated by means of CO_2 degassing, assuming open system conditions with respect to the atmosphere, e.g. for travertine and speleothem formation (Polag et al., 2010).

In all the above cases the redistribution of dissolved inorganic carbon (DIC) species is the crucial mechanism for whether dissolution or precipitation may occur in the mixed solution. Most relevant parameters for the individual DIC redistribution are the pH, $P_{CO2,}$ DIC and calcium content of the end member solutions as well as their distinct volume fractions in the mixed solution. An additional decisive factor in particular for mixing of freshwater, seawater and/or brines is the impact of ionic strength on ion activities and saturation degrees with respect to calcium carbonates in the merged solution.

In conclusion it is widely accepted that mixing of aqueous solutions is highly relevant for the dissolution and precipitation behaviour of calcium carbonates such as for the interpretation of karst features and sinter formation at near neutral pH and slightly alkaline conditions. But until now less attention has been given to the antagonists in more alkaline environments, where the mixing of two solutions, both saturated with respect to calcite, may cause supersaturation with regards to calcium carbonates in the merged solution. Such alkaline conditions can be easily reached in the $CaCO_3$-CO_2-H_2O system by assuming closed system conditions during limestone dissolution (DCS). Strong alkaline solutions are also highly relevant for carbonate sinter formation in terrestrial lakes and deep seawater horizons (Bonatti et al., 1980) as well as for carbonate scaling through water-concrete interaction (Dietzel et al., 1992).

In the following three distinct mixing approaches are separately discussed, where the end member solutions comprise (i) groundwater originated from open system conditions during dissolution of limestone (DOS), (ii) groundwater originated from respective closed system conditions (DCS), and (iii) additional strong alkaline solutions generated from intensive uptake of alkali e.g. through weathering of silicate or leaching of hydraulic-setting cements.

5.2 Methodology

The hydrogeochemical modelling for mixing of aqueous solutions is referred to the $CaCO_3$-CO_2-H_2O system at 20°C and was carried out by using the program code PHREEQC (Parkhurst and Apello, 1999) with minteq database. $SI_{Calcite}$ and Pco_2 denote the saturation index with respect to calcite and the internal partial pressure of CO_2, respectively. The mixing approach (MIX) is given by the basic equation

$$[\ ]_{Mix} = [\ ]_{S1^*} \cdot (1-x) + [\ ]_{S2} \cdot x \qquad (1)$$

for the mixing of two end member solutions, where [ ] denotes the total concentration of the individual component (e.g. Ca^{2+}, DIC) of the end member solutions S1 and S2 and x is the volume fraction of the solutions, in the mixed solution (Mix).

Reasonable end member solutions for mixing of naturally occurring groundwater are gained from modelling of calcite dissolution under open (DOS) or closed system conditions (DCS) until saturation with respect to calcite is reached ($SI_{calcite} = 0$). Highly alkaline end member solutions are modelled by distinct additions of KOH. Elevated alkali concentrations of K ions comprise a valid approach to equal the high hydroxide concentrations and to simulate typical natural and man-made environments. Note, that the addition of NaOH instead of KOH results in virtually the same results. However in any case an exchange of CO_2 between the mixed solution and the atmosphere is not allowed (MCS).

5.3 Mixing of aqueous solutions

5.3.1 Groundwater originated from open system conditions

The classical diagram for mixing corrosion given by *(Appelo and Postma, 2007; Bögli, 1964)* may provoke a general misinterpretation regarding the behaviour of calcite saturation through mixing of aqueous solutions. This is caused by the scaling for the x-axis ($P_{CO2}/10^{-2}$ atm) and the fact that such diagrams that normally comprise Pco_2 values much lower than that of the Earth's atmosphere ($P_{CO2} = 10^{-3.45}$ atm*;* 0.035 in Fig. 1a) which cannot be resolved appropriately at the chosen scaling of the diagram. Fig.1a displays misleadingly that the mixing of two solutions, which are both saturated with calcite, always yields a mixed solution undersaturated with respect to calcite.

In fact the given dashed line in Fig.1a is not valid for very low P_{CO2} values down to e.g. 10^{-8} atm. Such low partial pressures of CO_2 can occur either during calcite dissolution under closed system conditions (DCS) or through alkali uptake in alkaline environments. In contrast at open system conditions with respect to CO_2 the P_{CO2} through calcite dissolution is mostly limited by $10^{-3.45}$ atm, the modern atmospheric CO_2 content (see Fig. 1b).

Thus a P_{CO2} value below $10^{-3.45}$ atm in natural and man-made environments requires usually (i) the liberation of like Na^+ and K^+ from e.g. silicate weathering or shotcrete leaching or (ii) the uptake of bases e.g. from DCS (see Fig. 2).

Accordingly the boundary conditions to understand mixing behaviour of two distinct solutions comprise highly variable P_{CO2} values at least until ≤ $10^{-1.5}$ atm. The latter value is the upper limit for the soil atmosphere and this value can be even higher values if for instance additional CO_2 from volcanic origin or from decomposition of fossil fuel is considered.

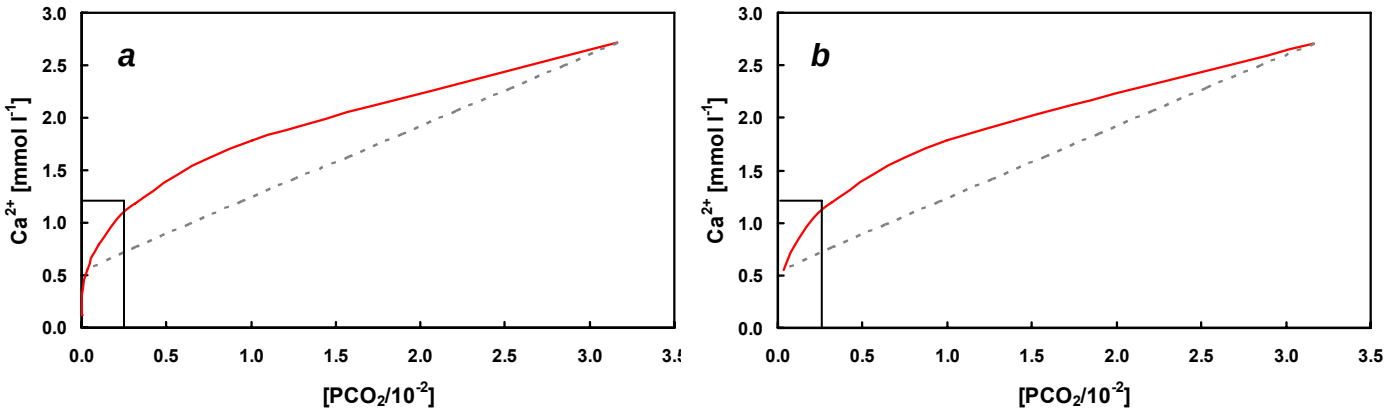

Figure 1: Mixing corrosion considering end member solutions from calcite dissolution under open system conditions (DOS after (Appelo and Postma, 2007) down to a P_{CO2} of 10^{-8} atm (a) and considering DOS down to the atmospheric P_{CO2} of $10^{-3.45}$atm (b). The solid line denotes the concentration of Ca^{2+} ions at equilibrium with respect to calcite at a P_{CO2} between $10^{-1.5}$ (3.16) to 10^{-8} (1.00 E-6) atm (a) and $10^{-1.5}$ (3.16) to $10^{-3.45}$ (0.035) atm (ie. modern Earth's atmosphere) (b). The dashed line displays the mixing of two solutions, both saturated with respect to calcite. The rectangles depict the area for mixing calculations in Fig. 2.

Conclusively there is only minor graphical difference between Figs.1a and b due to poor resolution of data at low P_{CO2} values (ie. below Earth's atmosphere) at the chosen scaling (Note that e.g. a P_{CO2} of 10^{-4} atm results in $P_{CO2}/10^{-2}$ = 0.01). However as shown in chapter 5.2.2 this distinction is crucial for the understanding of all possible processes for such a mixing system. The fact that a mixed solution plots on a nearly straight line in the field of undersaturation with

respect to calcite is based on the assumption that the individual components Ca^{2+} and $CO_{2(aq)}$ can be simply mixed according to equation 1. This is valid for groundwater originated from DOS (see Fig. 1b). But by an increase in pH and accompanied decreasing P_{CO2} values the redistribution of carbonate species may overrule the effect from an approximated linear mixing and may result in mixed solutions supersaturated with respect to calcite (see Fig. 2).

5.3.2 Groundwater originated from closed system conditions

The following calculations provide the modelling for the mixing of two solutions originated via dissolution of limestone at closed system conditions (DCS), but with the same initial P_{CO2} values as given in the above chapter ($10^{-1.5}$ to $10^{-3.45}$ atm). At closed system conditions the groundwater dissolves less $CaCO_3$ as CO_2 is not permanently delivered during the dissolution of limestone.
Figures 2 and 3 display the behaviour for mixing of two individual solutions, which are both in equilibrium with calcite for DCS. The solutions 1_CO2 to 5_CO2 in Tab. 1 are initially equilibrated with CO_2 at a P_{CO2} value between $10^{-1.5}$ and $10^{-3.45}$ atm. Subsequently the solutions dissolve calcite until the equilibrium with calcite is reached without allowing any further exchange of CO_2. The resulting solutions 1_DCS to 5_DCS in Tab. 1 show pH values between 7.72 and 9.95 at P_{CO2} values between $10^{-2.64}$ and $10^{-6.21}$ atm, respectively. The dotted lines in Figs. 2 and 3 indicate mixtures between solution 1_DCS with a pH of 7.72 and more alkaline solutions generated by the dissolution of calcite (2_DCS to 5_DCS).

Comparing Figs. 1 and 2 the change from a linear to nonlinear behaviour of the mixed solutions can be easily seen. This is a result of redistribution of carbonate species where HCO_3^- is converted to CO_3^{2-} and within the chosen variables of the plot the change from linear behaviour to nonlinear redistribution of carbonate species is especially related to the conversion of $CO_{2(aq)}$ into HCO_3^-. Note that the concentration of CO_3^{2-} in the mixed solution is higher than in initial solution 1_DCS, whereas the total inorganic carbon (DIC) decreases (see Tab. 1). Even with a new scaling of the x-axis within the range from 0 to 0.25 (see rectangles in Figs.1a and b) Fig.2 is hardly capable of resolving the evolution in the different mixing calculations because $P_{CO2}/10^{-2}$ results in a value of approximately 0.01, 0.0006, 0.0001 and 0.00006 for the end member solutions 2_CS, 3_CS, 4_CS and 5_CS, respectively.

The higher the initial pH of the alkaline end member is the easier mixed solutions can reach supersaturation with respect to calcite (see Fig. 3 where $SI_{calcite}$ is given as a function of pH). The mixing of solution 1_DCS with 2_DCS results solely in undersaturation with respect to calcite, the typical behaviour mentioned before as mixing corrosion *(grey dotted line in Figs.2*

and 3). For the other mixtures both under- and supersaturation with respect to calcite are possible, depending on the distinct mixing ratios (Fig. 3). The chemical composition of the mixed solution at $SI_{calcite}$ = 0 is given in Tab. 1, where the ratios for 1_CS/3_CS, 1_CS/4_CS and 1_CS/5_CS are approximately 3/7, 7/3 and 8/2 (intersection point in Fig.3).

Solution	pH	Ca^{2+}	DIC	H_2CO_3	HCO_3^-	CO_3^{-2}	P_{CO2}
1_CO2	4.64	-	1.1E+00	1.1E+00	2.3E-02	4.3E-08	$10^{-1.5}$
2_CO2	4.89	-	3.6E-01	3.5E-01	1.3E-02	4.3E-08	$10^{-2.0}$
3_CO2	5.14	-	1.2E-01	1.1E-01	7.2E-03	4.3E-08	$10^{-2.5}$
4_CO2	5.39	-	3.9E-02	3.5E-02	4.0E-03	4.2E-08	$10^{-3.0}$
5_CO2	5.62	-	1.5E-02	1.2E-02	2.4E-03	4.2E-08	$10^{-3.5}$
1_DCS	7.72	1.06	2.2E+00	7.9E-02	2.1E+00	5.5E-03	$10^{-2.6}$
2_DCS	8.59	0.38	7.4E-01	3.9E-03	7.2E-01	1.3E-02	$10^{-4.0}$
3_DCS	9.38	0.17	2.8E-01	2.2E-04	2.5E-01	2.7E-02	$10^{-5.2}$
4_DCS	9.81	0.12	1.6E-01	4.0E-05	1.2E-01	3.6E-02	$10^{-5.9}$
5_DCS	9.95	0.12	1.3E-01	2.2E-05	9.2E-02	3.7E-02	$10^{-6.2}$
1_DCS/3_DCS	8.48	0.43	8.5E-01	5.6E-03	8.3E-01	1.2E-02	$10^{-3.8}$
1_DCS/4_DCS	7.96	0.78	1.6E+00	3.4E-02	1.5E+00	6.8E-03	$10^{-3.0}$
1_DCS/5_DCS	7.88	0.87	1.8E+00	4.6E-02	1.7E+00	6.4E-03	$10^{-2.9}$

Tab. 1: Chemical composition of modelled solutions at a given P_{CO2} value and groundwaters in equilibrium with calcite at DCS ($SI_{calcitre}$ = 0). Concentrations are given mmol l^{-1}. Ratios for 1_CS/3_CS (3/7), 1_CS/4_CS (7/3) and 1_CS/5_CS (8/2) denote the intersection point where the merged solution reaches $SI_{calcite}$ = 0 (see Fig. 3).

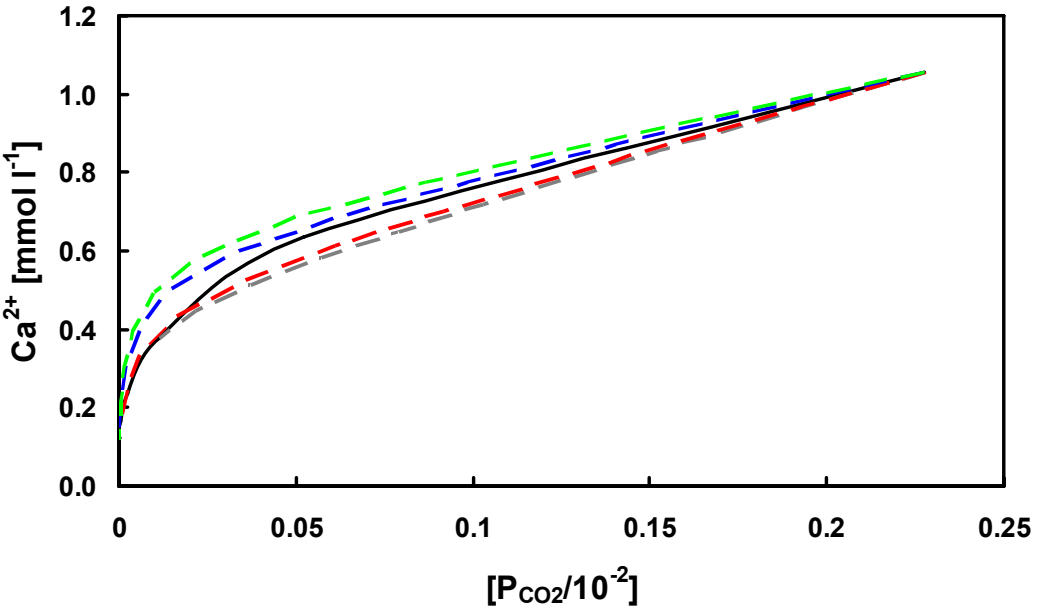

*Figure 2: Mixing.of solutions in equilbrium with calcite derived from closed system conditions (DCS). Solubility of calcite as a function of P_{CO2}. The solid line denotes the concentration of Ca^{2+} ions at equilibrium with respect to calcite at a P_{CO2} between $10^{-2.64}$ to $10^{-6.2}$ atm. Mixed solutions may result in either under- or supersaturation with respect to calcite. 1_DCS/2_DCS (grey),*1_CS/3_CS (red), 1_CS/4_CS (blue) and 1_CS/5_CS (green) (see Tab. 1).

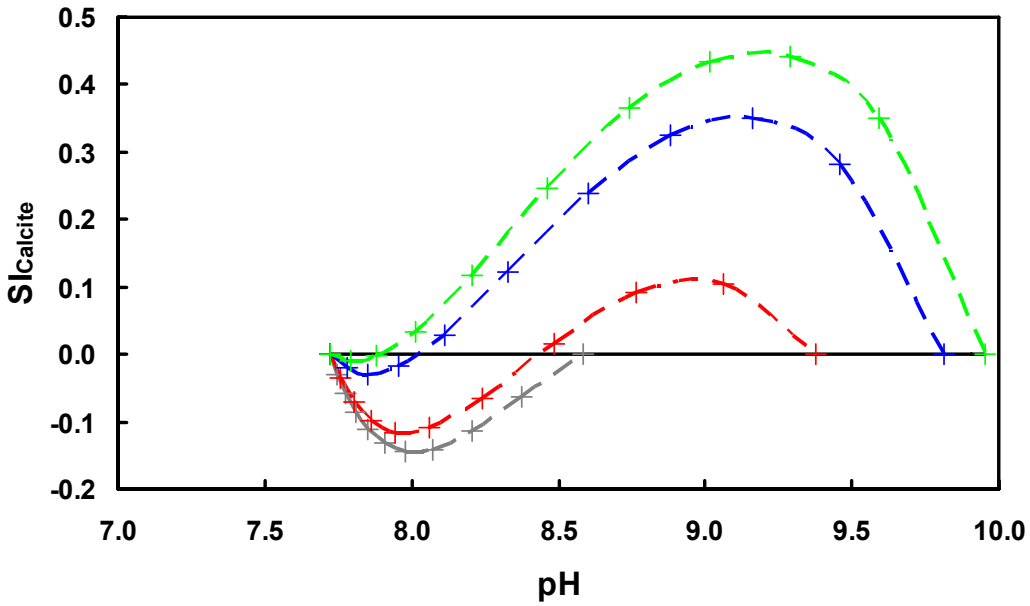

Figure 3: $SI_{Calcite}$ as a function of pH for solutions generated from DCS. Mixed solutions may result in either under- or supersaturation with respect to calcite. 1_DCS/2_DCS (grey),1_DCS/3_DCS (red), 1_DCS/4_DCS (blue) and 1_DCS/5_DCS (green) (see Tab. 1). Mixing was carried out in 10% steps (see marks).

5.3.3 Mixing of groundwater with strong alkaline solutions

The mixing behaviour of groundwater and alkaline solutions is studied for groundwater derived from the dissolution of limestone at open system (DOS; see Chapter 5.2.1) mixed with alkaline solutions gained from the uptake of KOH. Latter solutions simulate environments which may likely occur in tunnel buildings due to hydraulic cement – water interaction or in connection with strong dissolution of Mg- and Ca-bearing silicates from basalt and basaltic glass such as biotite and olivine (Gislason and Oelkers, 2003; Golubev et al., 2005). In principle the behaviour of a groundwater in equilibrium with calcite which is mixed with an alkaline KOH solution follows closely the behaviour plotted for the DCS in Fig. 3 and is therefore not given separately. The pH of the KOH solution is crucial whether mixing results in an under- or supersaturated solution with respect to calcite.

However the use of a single master variable as in Figs. 1 and 2 for comparison of different mixing calculations may be somewhat misleading, due to the fact that different initial solutions differ in their overall chemical composition (e.g. P_{CO2}, pH or DIC). This is exemplarily illustrated by means of the evolution of P_{CO2} in 5 groundwaters equilibrated with calcite under open system conditions (DOS) at their respective P_{CO2} values (Table 2). From these groundwaters respective alkaline solutions are generated by the continuous uptake of KOH considering calcite precipitation and a final P_{CO2} of 10^{-4} atm (Fig. 4). The different groundwaters (EQ_KOH1 to EQ_KOH5) reach the P_{CO2} of 10^{-4} atm at different pH values between 9.3 and 8.68 for addition of KOH into 1_DOS to 5_DOS, respectively. Accordingly the relationship between P_{CO2} and the amount of calcite in equilibrium with the solution is not a suitable tool to study the mixing behaviour in the $CaCO_3$ - CO_2 - KOH - H_2O system.

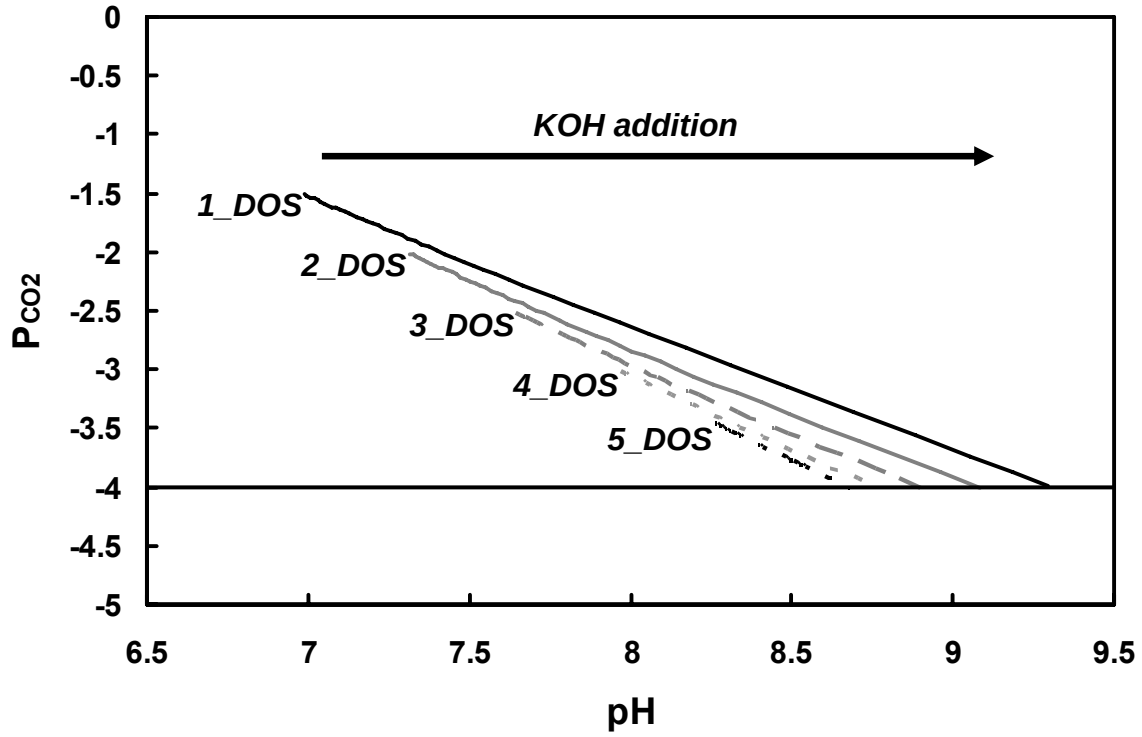

Figure 4: Uptake of KOH into calcite saturated groundwaters with P_{CO2} values between $10^{-1.5}$ and $10^{-3.45}$ atm (1_DOS_to 5_DOS). All solutions are brought to a P_{CO2} of 10^{-4} atm by addition of KOH and simultaneous modelling of calcite precipitation until $SI_{Calcite}$ is 0 (EQ_KOH1 to EQ_KOH5).

solution	pH	Ca^{2+}	DIC	H_2CO_3	HCO_3^-	CO_3^{-2}	P_{CO2}	$SI_{Calcite}$
1_DOS	6.98	2.71	6.5E+00	1.1E+00	5.3E+00	2.8E-03	$10^{-1.5}$	0
2_DOS	7.30	1.79	3.9E+00	3.5E-01	3.5E+00	3.7E-03	$10^{-2.0}$	0
3_DOS	7.63	1.19	2.5E+00	1.1E-01	2.3E+00	5.1E-03	$10^{-2.5}$	0
4_DOS	7.96	0.79	1.6E+00	3.5E-02	1.6E+00	6.9E-03	$10^{-3.0}$	0
5_DOS	8.25	0.56	1.1E+00	1.2E-02	1.1E+00	9.3E-03	$10^{-3.45}$	0
EQ_KOH1	9.30	0.02	3.8E+00	3.5E-03	3.5E+00	3.6E-01	$10^{-4.0}$	0
EQ_KOH2	9.08	0.05	2.2E+00	3.5E-03	2.0E+00	1.2E-01	$10^{-4.0}$	0
EQ_KOH3	8.90	0.11	1.4E+00	3.5E-03	1.3E+00	5.0E-02	$10^{-4.0}$	0
EQ_KOH4	8.76	0.19	1.0E+00	3.5E-03	9.7E-01	2.6E-02	$10^{-4.0}$	0
EQ_KOH5	8.68	0.27	8.3E-01	3.5E-03	8.0E-01	1.8E-02	$10^{-4.0}$	0

*Table 2: *_DOS. Modelling of pure water in equilibrium with calcite and respective P_{CO2} values under open system conditions with respect to CO_2. EQ_KOH*: KOH addition until a P_{CO2} of 10^{-4} atm is reached and simultaneous calcite precipitation until $SI_{calcite}$ = 0 (see Fig. 4). Concentrations are given in mmol l^{-1}.*

The dominant reactions responsible for P_{CO2} changes at the pH range given in Figure 4 mainly involve the carbonate species H_2CO_3 and HCO_3^-. The relation between those species and pH value can be described after (Appelo and Postma, 2007).

$$\left[H_2CO_3^*\right] = 10^{-1.5} * \left[P_{CO2}\right] \quad (1)$$

$$\left[H^+\right] = \frac{10^{-6.3} * \left[H_2CO_3\right]}{\left[HCO_3^-\right]} \quad (2)$$

$$H^+_{(EQ\_KOH)} = \frac{10^{-7.8} * \left[P_{CO2}\right]_{EQ\_KOH}}{(\left[P_{CO2}\right]_{DOS} * 10^{-1.5} - \left[P_{CO2}\right]_{EQ\_KOH} * 10^{-1.5} + \left[HCO_3^-\right]_{DOS})} \quad (3)$$

By combining equation 1 and 2 the relationship between P_{CO2} and pH value for the addition of KOH is obtained by equation 3. Ignoring calcite formation and only considering the addition of KOH, the amount of DIC in the system stays constant during KOH addition. In such a system a decreasing P_{CO2} is connected to decreasing H_2CO_3* (H_2CO_3* = CO_2 + H_2CO_3) and increasing HCO_3^- values. Therefore by assuming [$H_2CO_3^*$] and [HCO_3^-] as the only relevant species, and assuming DIC ≈ [H_2CO_3]* + [HCO_3^-] is constant, one can easily approximate the pH value of a solution with a certain P_{CO2} (H^+) according to equation 3. This equation is valid until a pH of 8.3, when redistribution of [HCO_3^-] to [CO_3^{2-}] becomes a relevant factor. Once a pH of 8.3 is reached, the simple approach in equation 3 by ignoring CO_3^{2-} does not apply for the HCO_3^- concentration, but it still gives a good estimation of the final pH value considering that the ratio of HCO_3^-/CO_3^{2-} is 10/1 at a pH of 9.3. Thus equation 3 describes the relationship between P_{CO2} and pH value of different groundwater solutions in Fig. 4, by showing that the value of the denominator is mainly dominated by the initial concentration of DIC species of a groundwater (DOS). The final pH ($H^+_{(EQ\_KOH)}$) of a solution at a fixed P_{CO2} ($[P_{CO2}]_{EQ\_KOH}$) will be higher, the higher the initial P_{CO2} of the groundwater is.

Consequently it has to be considered that in a KOH containing system equal P_{CO2} values can result in solutions with different chemical properties. The same accounts for pH (see Fig. 5), the total amount of calcium and DIC as well as the distribution of the individual carbonate species in solution. Keeping this in mind mixing of alkaline solutions, saturated with respect to calcite is only carried out exemplarily for one selected groundwater (1_DOS) and two alkaline end member solutions (Alk_EQ1 and Alk_EQ 5)., which are gained by KOH addition into solutions 1_DOS and 5_DOS until a pH of 9.3 is reached (see Tab. 3). Simultaneously calcite

precipitation is carried out until a $SI_{calcite}$ of 0 is reached. Mixing of DOS_1 with Alk_EQ1 reaches strong oversaturation, whereas the mix of DOS_1 with Alk_EQ5 reaches supersaturation only until the fraction of Alk_EQ5 on the mix falls below 96%, whereas any other mixing ratio leads to undersaturation.

As a crucial remark it has to be considered that mixing under closed system conditions (MCS) may be of minor importance in environments such as tunnel drainages, as exchange of mixed solutions with atmospheric CO_2 (MOS) is suggested to be possible in most cases. However for reactions in the cement pore system as well as in areas with constant water pressure – for example the shotcrete/hostrock reaction front of a tunnel building – this model is valuable. In the drainage system itself, such MCS can be ruled out by the effect of CO_2 degassing or absorption from or into the atmosphere, which has to be considered as a crucial factor for the actual chemical evolution of the merged solution in the drainage system.

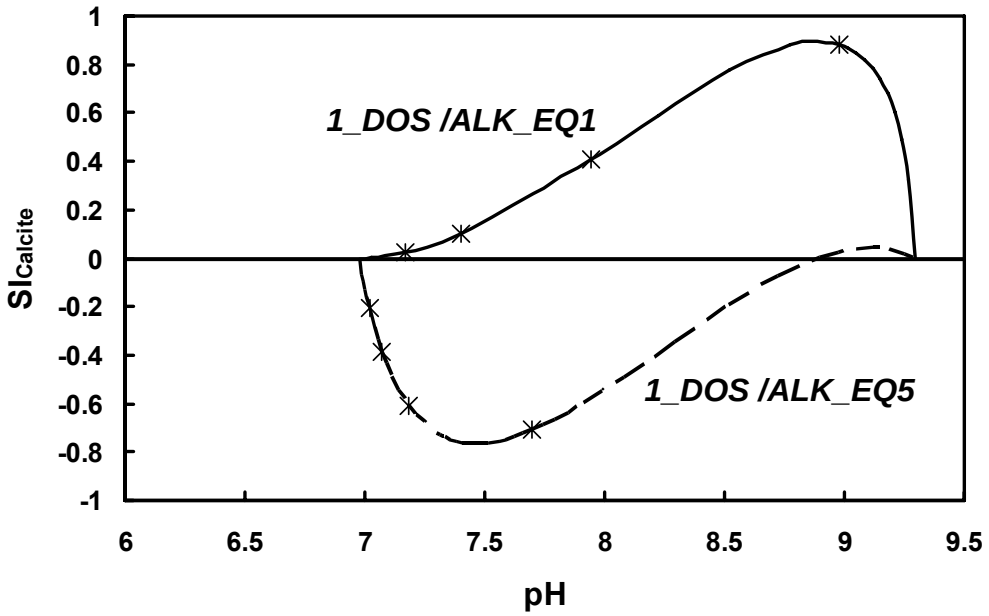

Figure. 5: Mixing of a groundwater (1_DOS; see Tab. 3) with two distinct alkaline solutions with pH 9.3 (see ALK_EQ1 and ALK_EQ5 in Tab. 3). Marks show percentage of solution 1_DOS on the respective mix for 30, 50, 70 and 90 % from left to right.

Solution	pH	ΔKOH	Ca^{2+}	DIC	H_2CO_3	HCO_3^-	CO_3^{2-}	P_{CO2}	$SI_{calcite}$
DOS_1	6.98	0.00	2.71	6.5E+00	1.1E+00	5.3E+00	2.8E-03	$10^{-1.50}$	0
ALK_EQ1	9.30	4.15	0.02	3.8E+00	3.5E-03	3.5E+00	3.6E-01	$10^{-4.00}$	0
ALK_EQ5	9.30	0.54	0.09	6.4E-01	6.1E-04	5.8E-01	5.4E-02	$10^{-4.76}$	0
1_DOS /ALK_EQ1	7.40	2.08	1.37	5.2E+00	3.7E-01	4.7E+00	6.4E-03	$10^{-1.97}$	0.10
1_DOS /ALK_EQ5	7.07	0.27	1.40	3.6E+00	5.1E-01	3.0E+00	1.9E-03	$10^{-1.83}$	-0.39

Tab. 3: Chemical composition of a model groundwater (1_DOS) and two distinct alkaline end member solutions derived from KOH addition and simultaneous calcite precipitation to solution 1_DOS and 5_DOS, respectively (see Tab. 1). Mixtures 1_DOS/ALK_EQ1 and 1_DOS /ALK_EQ5 are calculated for equal proportions. Concentrations are given in mmol l^{-1}.

5.4 Conclusions

Considering closed system condition through the mixing of two aqueous solutions (MCS) in the $CaCO_3$-CO_2-H_2O system our calculations clearly display a more complex behaviour in respect to potential dissolution and precipitation of calcite than commonly expected. Special regard has to be given to the relationship between P_{CO2} and saturation index for calcite. Herein we demonstrate that mixing of aqueous solutions with different chemistry, but both in equilibrium with respect to calcite, may yield in mixed solutions super- or undersaturated with respect to calcite. This is even true for groundwater, which is originated from the dissolution of limestone. The redistribution of DIC species as a function of pH value may well lead to supersaturation with respect to calcite in the mixed solution, as soon as a critical pH value for redistribution of HCO_3^- into CO_3^{2-} is reached. Such pH values can be reached if a groundwater is suggested where calcite was dissolved under closed system conditions (DCS) at elevated pH.

In the $CaCO_3$-CO_2-H_2O-KOH system supersaturation by mixing may be easily obtained for solutions with a low buffer capacity. In principle the buffer capacity of a solution for alkaline waters is higher, the higher the initial P_{CO2}. On the other hand, once supersaturation is reached through mixing calcite precipitation capacities will be also higher for solutions at higher the initial P_{CO2} because of increasing abundance of Ca^{2+} and DIC with increasing P_{CO2}.

5.5 References

Appelo, C.A.J., Postma, D., 2007. Geochemistry, groundwater and pollution, 2nd edition. A.A. Balkema Publishers.

Baceta, J.I., Wright, V.P., Pujalte, V., 2001. Palaeo-mixing zone karst features from Palaeocene carbonates of north Spain: criteria for recognizing a potentially widespread but rarely documented diagenetic system. Sedimentary Geology 139, 205-216.

Berkowitz, B., Singurindy, O., Lowell, R.P., 2003. Mixing-driven diagenesis and mineral deposition: $CaCO_3$ precipitation in salt water - Fresh water mixing zones. Geophysical Research Letters 30, 57-51.

Bögli, A., 1964. Mischungskorrosion: ein Beitrag zum Verkastungsproblem. Erkunde 18, 83–92.

Bonatti, E., Lawrence, J.R., Hamlyn, P.R., Breger, D., 1980. Aragonite from deep sea ultramafic rocks. Geochimica et Cosmochimica Acta 44, 1207-1214.

Buhmann, D., Dreybrodt, W., 1985. The kinetics of calcite dissolution and precipitation in geologically relevant situations of karst areas: 2. Closed system. Chemical Geology 53, 109-124.

Dietzel, M., Usdowski, E., Hoefs, J., 1992. Chemical and $^{13}C/^{12}C$- and $^{18}O/^{16}O$-isotope evolution of alkaline drainage waters and the precipitation of calcite. Applied Geochemistry 7, 177-184.

Dreybrodt, W., 1980. Kinetics of the dissolution of calcite and its applications to karstification. Chemical Geology 31, 245-269.

Emmanuel, S., Berkowitz, B., 2005. Mixing-induced precipitation and porosity evolution in porous media. Advances in Water Resources 28, 337-344.

Gislason, S.R., Oelkers, E.H., 2003. Mechanism, rates, and consequences of basaltic glass dissolution: II. An experimental study of the dissolution rates of basaltic glass as a function of pH and temperature. Geochimica et Cosmochimica Acta 67, 3817-3832.

Golubev, S.V., Pokrovsky, O.S., Schott, J., 2005. Experimental determination of the effect of dissolved CO2 on the dissolution kinetics of Mg and Ca silicates at 25 °C. Chemical Geology 217, 227-238.

Lee, Y.-J., Morse, J.W., 1999. Calcite precipitation in synthetic veins: implications for the time and fluid volume necessary for vein filling. Chemical Geology 156, 151-170.

Parkhurst, D.L., Apello, C.A.J., 1999. User's guide to PHREEQC (V2). U.S. Geol. Sur, 312.

Polag, D., Scholz, D., Mühlinghaus, C., Spötl, C., Schröder-Ritzrau, A., Segl, M., Mangini, A., 2010. Stable isotope fractionation in speleothems: Laboratory experiments. Chemical Geology 279, 31-39.

Romanov, D., Dreybrodt, W., 2006. Evolution of porosity in the saltwater and freshwater mixing zone of coastal carbonate aquifers: An alternative modelling approach. Journal of Hydrology 329, 661-673.

Sanz, E., Ayora, C., Carrera, J., 2011. Calcite dissolution by mixing waters: Geochemical modeling and flow-through experiments. Geologica Acta 9, 67-77.

Singurindy, O., Berkowitz, B., 2005. The role of fractures on coupled dissolution and precipitation patterns in carbonate rocks. Advances in Water Resources 28, 507-521.

Wigley, T.M.L., Plummer, L.N., 1976. Mixing of carbonate waters. Geochimica et Cosmochimica Acta 40, 989-995.

Chapter 6

Sr^{2+} and Mn^{2+} incorporation during $CaCO_3$ cementation on calcitic shells

Thomas Rinder, Martin Dietzel, Artur Deditius

(To be submitted upon completion of the study)

Sr^{2+} and Mn^{2+} incorporation during $CaCO_3$ cementation on calcitic shells

Abstract

A solution supersaturated with respect to calcite was pumped through columns packed with shell fragments of a grain size between 0.5 and 1mm with approximately 68% free pore space. At the given flow rate of 1.6 ml/min the mean retention time of the solution through the column was approximately 3 minutes. Within the total 5400 minutes of experimental runtime the estimated amount of precipitated $CaCO_3$ was 68 mg for experiment 1 and 168 mg for experiment 2. The free pore size was reduced by about 0.3 and 0.8 % for experiment 1 and 2, respectively. Precipitation pattern of $CaCO_3$ within the column was successfully modelled using an overall calcite growth model, where our precipitation rates were approximately 20 times higher than suggested by considered literature data. Sr^{2+} and Mn^{2+} addition was used to trace the temporal and spatial evolution of newly formed precipitates in the pore space. Overall distribution coefficients D_{Sr} (0.68) and D_{Mn} (6.08) which were calculated from aqueous bulk solutions are in good agreement with literature values. However, apparent measured data of the trace element contents in the $CaCO_3$ solids is highly heterogeneous and results in a maximum D_{Sr} and D_{Mn} value of 18 and 163, respectively. We suggest that the incorporation mechanisms which result in bulk ratios that serve as proxies for the reconstruction of environmental conditions during precipitation of $CaCO_3$ do not necessarily apply on the microscale where actual trace element incorporation into $CaCO_3$ may exceed or fall below the average bulk incorporation.

6.1 Introduction

Precipitation of calcium carbonates may cause significant changes in the porosity, permeability and overall physical properties of sedimentary rocks. For instance in sandstone the loss of permeability and porosity negatively influences the potential quality of the hostrock as a hydrocarbon or groundwater reservoir (Taylor and Machent, 2011). In recent years more attention to cementation issues is received for the increasing efforts to reduce CO_2 emission into the atmosphere and the possibility of long term storage by means of underground fixation in carbonates (Gislason et al., 2010; Matter et al., 2009). A controlled carbonate cementation process is also desired to consolidate foundation soils and to stabilise embankments (Lioliou et al., 2007). In contrast chemical clogging and cementation by calcium carbonate adversely

affects the performance of wells and tunnel drainages (Dietzel et al., 2008) and bears problems e.g. for dredging action where slightly lithified layers may inhibit the failure of underwater slopes (Molenaar and Venmans, 1993).

In any case the individual structure and composition of the carbonate cements provide information about the environmental conditions during the formation and subsequent alteration. Thus, the chemical composition as well as microstructure of carbonate cements can be used as an archive for the reconstruction of precipitation conditions and to tailor the cementation progress. The general behaviour of trace element incorporation such as strontium and manganese incorporation in calcite has been extensively studied for the last decades (Dromgoole and Walter, 1990; Franklin and Morse, 1983; Lee and Morse, 1999; Mucci and Morse, 1983; Nehrke et al., 2007; Pingitore Jr et al., 1988; Tang et al., 2008). However progress of carbonate cementation for unconsolidated sediments is less well investigated by using combined microstructural and trace element distribution analyses. In the present study a flow through experiment with traces of strontium and manganese in the solution was carried out to simulate and monitor ongoing calcium carbonate cementation of primary unconsolidated carbonate shell material by the spatial trace element distribution in the precipitated calcium carbonate cement.

6.2 Method

Materials

The column experiments were carried out using calcitic shell fragments. The shells were stored in 30% H_2O_2 (Merk, p.A.) for 24h and subsequently mechanically cleaned to free them from organic residues. After rinsing with deionized water the samples were put in an ultrasonic bath and dried in an oven at 30 °C. Crushing in an agate mortar and subsequent sieving resulted in a grain size from 0.5 - 1 mm in diameter used for the experiments.

Stock solutions A and B were prepared by dissolving $CaCl_2 \cdot 6H_2O$ (Roth, p.A.) and $NaHCO_3/Na_2CO_3$ (Roth; Merck,, p.A.) in distinct concentrations (see input_bulk_* solutions in Tab. 1). $NaHCO_3/Na_2CO_3$ ratio was adjusted to reach a P_{CO2} of the Earth's atmosphere in the solution ($10^{-3.45}$ atm). Stock solutions C and D were prepared with a $CaCl_2$ concentration similar to stock solution A, but additional distinct $SrCl_2$ *$6H_2O$ (Merck) and/or $MnCl_2$*$4H_2O$ (Roth) content.

Analytics

Analysis of the element concentrations of polished sections was carried out by electron microprobe analysis (EMPA) using a Jeol JXA8200 at the Montan University Leoben, Austria. Elements and X-ray lines used for the analysis were Na (Kα), Ca (Kα), Mg (Kα), Mn (Kα), and Sr (Lα). Operating conditions during single spot quantitative analyses included an accelerating voltage of 15 kV and beam current of 10 nA with wave-length dispersive X-ray spectrometers (WDS). In order to improve count rate statistics, counting times were 10 seconds on the peak position and 5 second on the back ground. The size of the electron beam was ~4x3 µm or 8x6 µm, and it depended on the size of the trace-element-rich zones. Standard specimens used for calibration were dolomite (for Ca and Mg), rhodonite (for Mn), celestine (for Sr), and jadeite for Na. The elemental maps were collected using focused bean ~1 µm in size; an accelerating voltage of 15 kV, beam current of 50 nA, and 30 milliseconds counting time at single step; with wave-length dispersive X-ray spectrometers (WDS).

Alkalinity in the experimental solutions was measured by potentiometric titration with 0.05m HCl directly after sampling. Concentration of cations (Na^+, K^+, Mg^{2+}, Ca^{2+} and Sr^{2+}) was analysed by ion chromatography (Dionex ICS-3000) with an analytical error of ±3% in acidified samples, using 2wt. % ultrapure double distilled HNO_3. Concentration of Mn^{2+} was analysed by ICP-OES (Perkin Elmer 4300) with an analytical precision of ±5%. The computer code PHREEQC (Parkhurst and Apello, 1999) with the database minteq.dat was used for hydrogeochemical modelling, e.g. to calculate saturation indices with respect to calcite ($SI_{Calcite}$) aragonite ($SI_{Aragonite}$), strontianite ($SI_{Strontianite}$), rhodochrosite ($SI_{Rhodochrosite}$) and the internal partial pressure of CO_2 (P_{CO2} in atm).

Experimental setup

Both solutions A and B were separately pumped through a mixing unit (Fig. 1) using a DIONEX GP 50 gradient pump and a DIONEX IP20 isocratic pump. Subsequently the merged solution entered a column packed with the above calcitic shell fragments using a SEPACORE cartridge adapter set (Φ = 12 mm).

Additionally distinct concentrations of Sr^{2+} and Mn^{2+} in the merged solution were adjusted by using the stock solutions C and D. For different experiments the solution A was mixed with solutions C and D, using the DIONEX GP 50 gradient pump and a coupled separate mixing chamber, before being mixed with solution B (see Fig.1). For the Sr^{2+} bearing experiment, the mixed input solution (Ca^{2+}, Sr^{2+} and carbonate containing solution) was continuously pumped through the column for the whole experimental runtime (5400 min). In the case of the

experiment with Mn^{2+} the solution D was added at 2700 min of reaction time and continuously pumped until the end of the experiment (5400 min).

In both experiments the flow rate was adjusted to 0.8 ml/min for each of the two mixed experimental solutions, resulting in a total of 1.6 ml/min. This results in total of about 8.64 litres of the mixed input solution passing through the column during the experiment run (5400 min). Fraction sampling at the column inlet and outlet was carried out for analysis of dissolved components.

Characterisation of the flow through behaviour of the packed columns was done by pre-experiments with a KBr bearing solution as a conservative tracer, which was pumped through the column and measured via electric conductivity (DIONEX ED 50 electrochemical fluid cell detector) at the outlet of the column to estimate the flow velocity through the column.

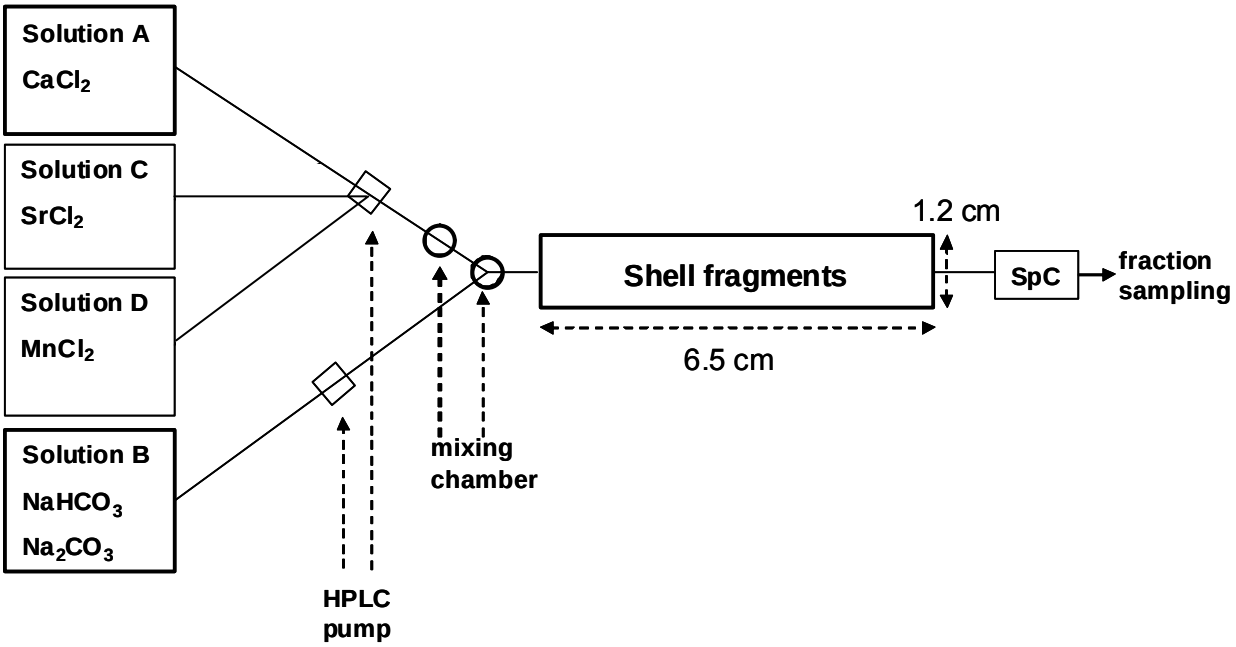

Figure 1. Experimental setup for calcification of shell fragments. SpC: Specific Conductivity cell. Solution A: $CaCl_2$ bearing solution; Solution B: $NaHCO_3$/Na_2CO_3 solution; trace element addition of strontium and manganese into solution A via solution C ($SrCl_2$) and solution D ($MnCl_2$).

6.3 Results

6.3.1 Modelling of $CaCO_3$ precipitation from aqueous solution chemistry

Table 1 displays the bulk chemical composition of the inlet and outlet solutions of the experiments 1 and 2 as well as the results from PHREEQC calculations for calcite precipitation

(EQ_*). Modelling of $CaCO_3$ precipitation was carried out in order to estimate the chemical evolution of the solutions passing through the column and accompanied special precipitation pattern of $CaCO_3$. The solutions EQ_Alk*, EQ_pH* and EQ_Ca* denote the chemical composition of the modelled solutions derived from $CaCO_3$ precipitation from the input bulk_* solution where $CaCO_3$ precipitation is modelled until one of the chosen parameters, the total alkalinity (EQ_Alk*), pH (EQ_pH*) or dissolved Ca^{2+} (EQ_Ca*) reaches the value of the output bulk_* solution. Caclulations were carried out in the pure $CaCO_3$-H_2O system. Therefore Sr^{2+}, Mn^{2+} and Na^{+} incorporation as well as degassing of CO_2 were not considered for these calculations (thus respective values are not given in Tab. 1). For the first experiment with Sr^{2+} as trace element only one input bulk solution is considered, because a single mixed solution with constant chemical composition was pumped through the column continuously throughout the whole experiment (input bulk_1). For the experiment with Mn^{2+} as a tracer two different solutions have to be considered for the first half of the experiment without manganese (see input bulk_2) and the second half including manganese addition (input bulk_3 in Tab. 1).
The difference of measured Ca^{2+} concentrations between inlet and outlet is still within the analytical error of ± 3% (from IC- analysis). However calculating the standard deviation for the individual measurement points of the bulk values results in a Ca^{2+}concentration of 9.28 ±0.04 mmol L^{-1} at the input bulk_1 and 9.10 ±0.07 mmol L^{-1} at output bulk_1 as well as 9.83±0.17 mmol L^{-1} and 9.40±0.01 mmol L^{-1} for input bulk_2 and 3 and output_bulk_2 and 3, respectively.
For the manganese bearing experiment the alkalinity of the $NaHCO_3$ - Na_2CO_3 solution changed during experimental runtime from 6.39 mmol L^{-1} at pH 9.09 to 6.55 mmol L^{-1} at pH 8.97. Interestingly this corresponds to a change in P_{CO2} from $10^{-3.58}$ to $10^{-3.45}$ atm and can therefore be interpreted as equilibration of the solution with P_{CO2} of the atmosphere. In order to investigate the effects of the change in the initial composition on precipitation rates and capacities (i.e. $SI_{Calcite}$), the initial alkalinity is attributed to solution input bulk_2, whereas the alkalinity after equilibration with the Earth's atmosphere is attributed to solution input bulk_3. The decrease in pH in the $NaHCO_3$-Na_2CO_3 solution is accompanied by a decrease in $SI_{Calcite}$ from 1.54 to 1.49 during experimental runtime.

As can be concluded from Tab. 1, calcite precipitation from the input solutions is not capable of explaining the change in chemical composition between inlet and outlet for all 3 investigated master variables (pH, alkalinity and dissolved Ca^{2+}). However the modelling until the pH of the output solution is reached (EQ_pH*) is in good accordance with the P_{CO2}, $SI_{Calcite}$ and $SI_{Aragonite}$. The measured change in alkalinity (EQ_Alk*) is to low in all 3 cases to account for the change in

dissolved Ca^{2+} as $CaCO_3$ precipitation. The modelling for dissolved Ca^{2+} (EQ_Ca*) reaches a pH value much lower than measured.

Since the P_{CO2} of the inlet solution is between $10^{-3.17}$atm and $10^{-3.24}$ atm, degassing of the solution is possible in principle. However, considering initial degassing in the input bulk_* solutions, leads to loss in alkalinity and amount of dissolved carbon and further decreases the difference between input_bulk* and output_bulk* alkalinity. Conclusively, considering the above mentioned analytical error with regard to dissolved Ca^{2+} measurements pH value seems most suitable for modelling with the important parameters P_{CO2}, $SI_{Calcite}$ and $SI_{Aragonite}$ being correctly predicted by the calculations.

Solution	pH	Alk	Ca^{2+}	HCO_3^-	CO_3^{2-}	DIC	SI_{Ca}	SI_{Ar}	SI_{Rh}	P_{CO2}	Rate	Sr^{2+}	Na^+	Mn^{2+}	$CaCO_3$
Input bulk_1	8.16	1.88	9.29	1.65	0.016	1.83	1.11	0.97	-	-3.21	1.3E-10	0.107	2.03	0.010	***3.90*** $^{(1)}$
output bulk_1	7.76	1.78	9.10	1.64	0.007	1.81	0.70	0.56	-	-2.81	3.6E-11	0.106	1.98	0.009	
EQ_Alk_1	7.93	**1.79**	9.24	1.62	0.009	1.78	0.87	0.73	-	-2.98	6.3E-11	-	-	-	40.69 $^{(2)}$
EQ_ pH_1	**7.76**	1.73	9.21	1.59	0.006	1.75	0.69	0.55	-	-2.82	3.4E-11	-	-	-	67.53 $^{(2)}$
EQ_Ca_1	7.28	1.51	**9.10**	1.43	0.002	1.64	0.17	0.03	-	-2.39	1.3E-12	-	-	-	160.16 $^{(2)}$
input bulk_2	8.39	3.21	9.83	2.68	0.04	3.03	1.54	1.40	-	-3.24	4.6E-10	-	3.36	-	***14.46*** $^{(1)}$
output bulk_2	7.81	2.67	9.40	2.46	0.01	2.69	0.91	0.77	-	-2.70	8.9E-11	-	3.28	-	
EQ_pH_2	**7.81**	2.80	9.63	2.58	0.01	2.82	0.94	0.80	-	-2.68	9.9E-11	-	-	-	177.82 $^{(2)}$
EQ_ Alk_2	7.59	**2.67**	9.56	2.50	0.01	2.76	0.70	0.56	-	-2.47	4.6E-11	-	-	-	234.09 $^{(2)}$
EQ_Ca_2	7.20	2.35	**9.40**	2.23	0.00	2.60	0.25	0.11	-	-2.13	4.2E-12	-	-	-	373.56 $^{(2)}$
input bulk_3	8.33	3.27	9.83	2.78	0.04	3.11	1.49	1.35	0.46	-3.17	4.3E-10	-	3.36	0.011	***13.25*** $^{(1)}$
output bulk_3	7.81	2.67	9.40	2.46	0.01	2.69	0.91	0.77	-0.25	-2.70	8.9E-11	-	3.28	0.008	
EQ_pH_3	**7.81**	2.91	9.65	2.68	0.01	2.93	0.95	0.81	-0.08	-2.66	1.1E-10	-	-	-	158.08 $^{(2)}$
EQ_Alk_3	7.45	**2.67**	9.53	2.51	0.00	2.81	0.56	0.42	-0.46	-2.33	2.7E-11	-	-	-	260.32 $^{(2)}$
EQ_Ca_3	7.17	2.41	**9.40**	2.28	0.00	2.68	0.24	0.10	-0.78	-2.09	3.8E-12	-	-	-	373.56 $^{(2)}$

Table 1. Chemical composition of measured (input bulk_* and output bulk_*) and modelled (EQ Alk_*, EQ pH_* and EQ Ca_*) solutions for both experiments. Ca^{2+}, HCO_3^-, CO_3^{2-}, DIC, Sr^{2+}, Na^{2+} and Mn^{2+} in mmol L^{-1}. P_{CO2} in log (atm). Rate in mol s^{-1}; calculation after (Wolthers et al., 2012). SI_{Ca} ($SI_{Calcite}$), SI_{Ar} ($SI_{Aragonite}$) and SI_{Rh} ($SI_{Rhodocrosite}$). Total calcium carbonate precipitation ($CaCO_3$) throughout the experiments in mg calculated according to the precipitation rate (equation 1) from input bulk_* solutions (1), $CaCO_3$ precipitation for EQ Alk_*, EQ pH_* and EQ Ca_* calculated from Ca^{2+} difference between the solution (Input bulk_*) and the respective modelled output solution (equation 2) (2).

6.3.2 Free pore space and flow through behaviour in the column

From the pre-experiments carried out with an electrical conductivity cell and a KBr tracer a mean retention time of approximately 3 minutes and a maximum retention time of approximately

7 minutes can be estimated (see Fig. 2). Similar results are gained from weighting of the dry and wet column, which results in approximately 5 ml of solution in the packed column. The calculated volume of the empty column is 7.35 cm³, which results in a free pore space of 68%.

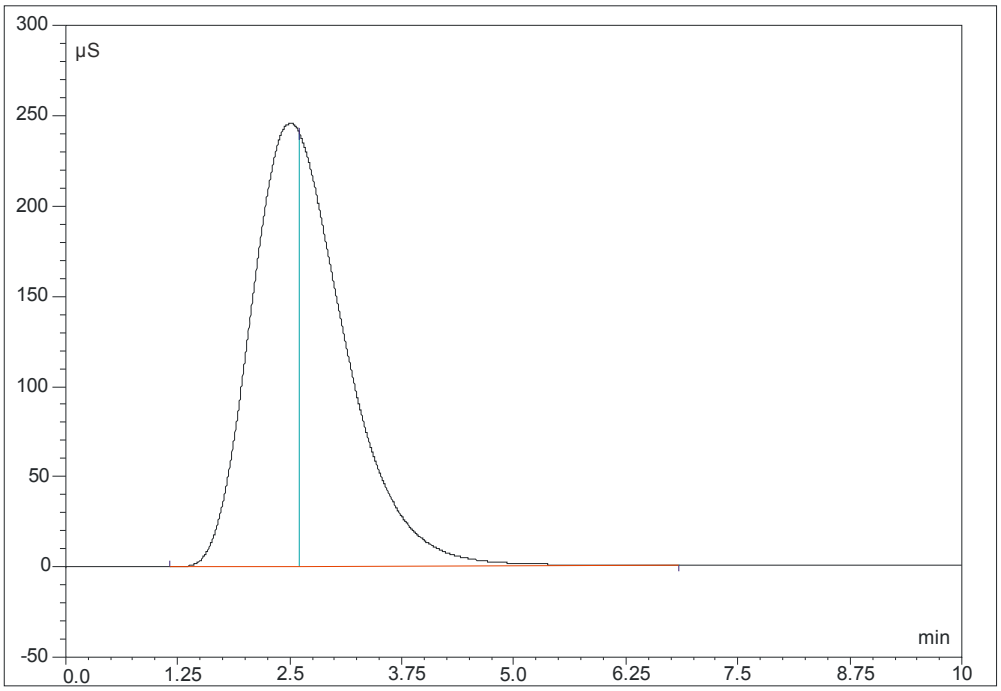

Figure 2. Result from KBr tracer experiment for a typical column experiment. Note that time where maximum concentration is reached, is not equal to mean retention time (i.e. 50% of solution passing the column) of the solution in the column.

6.3.3 Calcite growth rate and distribution of precipitates

Mineralogical composition of precipitates from the experiments 1 and 2 was identified mostly as calcite and with crystals of aragonitic shape found only at the column inlet (see Chapter 6.4.1). Therefore an overall calcite growth rate is introduced to approximate the spatial distribution of precipitated carbonate within the columns at a given experimental time. The precipitation rate for the individual experimental and modelled solutions can be roughly estimated according to the expression

$$R_{Calcite}^{*} = I^{-0.004}pH^{-10.71}(Ca^{2+})/(CO_3^{2-})^{-0.35}((10^{SICalcite})^{0.5} - 1)^2 \quad (1)$$

given by (Wolthers et al., 2012) for a compilation of experimental data from various calcite precipitation experiments. Precipitation rates for the individual solutions are given in mol s^{-1} in Table 1.

Figure 3a displays the evolution of pH and Ca^{2+} within the 3 minutes retention time of the solution in the column for the experiment input bulk_1 (input_bulk_2 and input_bulk_3 deliver comparable results). At the chosen rate equation (1), the amounts of calcite precipitation of 3.9, 14.5 and 13.3 mg $CaCO_3$ in total for the experiment with initial solution input bulk_1, input bulk_2 and input bulk_3 are obtained. This low amount of $CaCO_3$ is neither consistent with the observed amount of precipitations nor with the measured change of pH, alkalinity and dissolved Ca^{2+} between column inlet and outlet. For example figure 3b indicates that the time necessary to precipitate the amount of $CaCO_3$ calculated from change in dissolved Ca^{2+} (9.29 mmol l^{-1} to 9. 10 mmol l^{-1}; see Tab. 1) between input bulk_1 and output bulk_1 from equation 1 is approximately 25 hours. The time needed to reach the chemical composition with regard to dissolved Ca^{2+} (9.29 mmol l^{-1} to 9.21 mmol l^{-1}) of solution EQ_pH_1 is still 95 minutes.

To obtain a more realistic scenario for the precipitation behaviour of calcite within the column the amount of $CaCO_3$ for *EQ Alk_*, EQ pH_* and EQ Ca_** is calculated from the bulk calcite growth rate according to the equation (2)

$$R_{Calcite}=(Ca_{in} - Ca_{out}) *V/t \quad (2)$$

where V/t is the volume of the solution passing through the column per time unit, Ca_{in} is the amount of dissolved Ca^{2+} in the input solution and Ca_{out} the amount of dissolved Ca^{2+} in the respective modelled output solution (see Tab. 1). Assuming that equation 1 correctly describes the overall precipitation kinetics of a calcite precipitating system and the actual measured values in a given experimental setup will deviate more or less linearly (Wolthers et al., 2012) from the overall rate law we may apply a multiplication factor (α) in order to correlate theoretical rate calculation with the measured rate after equation 3

$$\alpha = (R_{meas}) / (R_{Calcite\ input\ bulk\_*} + R_{Calcite\ output\ bulk\_*}) * 0.5 \quad (3)$$

where R_{meas} is the bulk rate according to equation 2 and ($R_{Calcite\ input\ bulk\_*}$ + $R_{Calcite\ output\ bulk\_*}$) * 0.5 is the aritmethic mean of the respective rates calculated according to equation 1. The bulk calcite growth rate for EQ_pH_* solutions calculated from equation 2 results in a rate of 2.08 * 10^{-9} (EQ_pH_1), 5.48 10^{-9} (EQ_pH_2) and 4.87 10^{-9} (EQ_pH_3) mol s^{-1}. This amounts to a factor α of 25.6, 19.8 and 18.9 for for bulk solutions 1, 2 and 3, respectively. In Figs. 3c and 3d the evolution of the parameters dissolved Ca^{2+} and pH is plotted as a function of the reaction time of three minutes, for the mean retention time of the solution in the column, using the

precipitation rate (equation 1) multiplied with the individual correction factor α. In Fig. 3c the chemical composition of the solution after 180 seconds is very close (pH = 7.81, Ca^{2+} =9.22 mmol l^{-1}) to the modelled value for EQ pH_1 (pH = 7.76, Ca^{2+} =9.21 mmol l^{-1}; see Tab. 1) suggesting that the introduction of a correction factor is a α is a suitable tool to link the proposed calcite precipitation rate equation with bulk rates modelled for this study. In principle the same applies for bulk solutions 2 and 3 (see values in Fig. 3d) where pH value and dissolved Ca^{2+} after 180 seconds are also close to the values for EQ pH_2 (pH = 7.81, Ca^{2+} =9.63 mmol l^{-1}) and EQ pH_3 (pH = 7.81, Ca^{2+} =9.65 mmol l^{-1}).

Comparing the similar evolution of bulk_2 and bulk_3, the change in the initial alkalinity of the $NaHCO_3$ -Na_2CO_3 solution over experimental time will have only minor influence on the amount and temporal evolution of precipitation (see Figs 3d and 4b) .

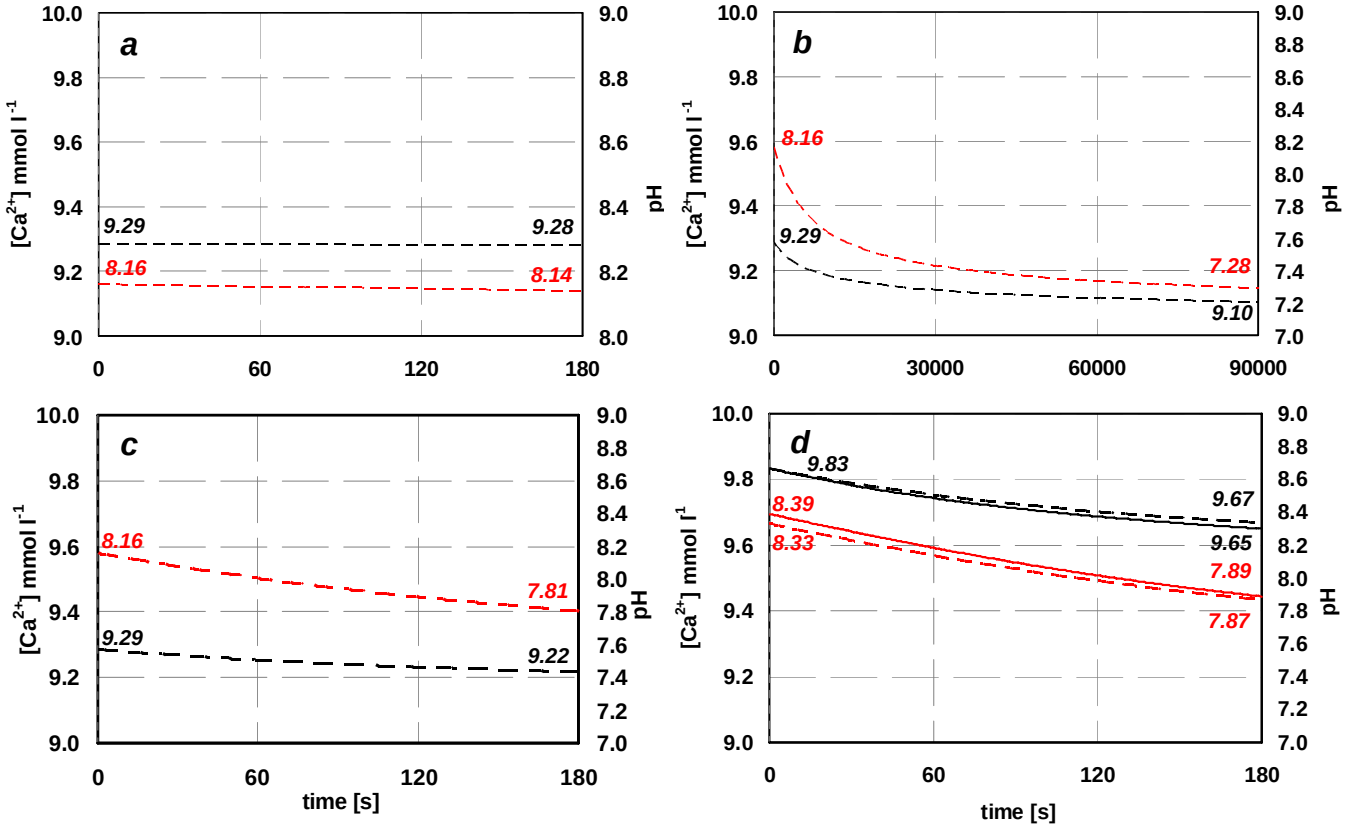

Figure 3. Ca evolution as a function of time, calculated using precipitation rate after (Wolthers et al., 2012); Ca^{2+} in mmol l^{-1}(black), pH value (red). (a) original rate for mean retention time (180 s) calculated from input bulk_1,(b) until Δ Ca^{2+} (input bulk_1 – output bulk_1) is reached, (c) original rate multiplied by α (25.6; see equation 3) for mean retention time (180 s) and (d) original rate for input bulk_2 (lines) and input bulk_3 (dotted lines) multiplied by α (19.8 and 18.9).

For both columns the macroscopic investigation of thin sections clearly indicates a decrease in the amount of newly precipitated material from the inlet to the outlet of the column. Therefore the above introduced model is used to investigate the distribution of cumulative precipitation pattern within the columns as percentage of the total precipitation in Figs. 4a and b. Again, equation 1 is not capable of reproducing the spatial distribution of the observed precipitation pattern, resulting in uniformly distributed calcite throughout the whole column (see solid line in Figs. 4a and b). The distribution pattern after equation 1 corrected by α results in 47% (Fig. 4a), 49 % (red line in fig 4 b) and 48% (black line in Fig. 4b) of the total precipitated $CaCO_3$ precipitated within the first third of the column for input bulk_1 *α, 2* α and 3 *α, respectively. Despite the fact that the precipitated amount of $CaCO_3$ is much higher for input bulk_2 and input bulk_3 compared to input bulk_1, the relative distribution within the columns is nearly constant, according to the chosen model.

Conclusively, introducing a correction factor α to the overall rate law (equation 1) for calcite precipitation, modelled and observed evolution of solution chemistry as well as modelled and observed precipitation pattern are in good accordance. The introduction of such a multiplication factor seams reasonable considering the huge specific calcite surface in our experiments, whereas the chosen overall rate law is a result from seeded and unseeded calcite growth experiments. Additionally the difference between our measured rate and predicted rate after equation (1) is in a similar range as for calcite growth rate experiments by (van der Weijden et al., 1997), which has used a similar experimental setup, using K_2CO_3 instead of Na_2CO_3. They reported an initial growth surge, which is agreement with thin section analyses of our cementated column. This precipitation surge was attributed to healing of e.g the rounded corners of the seed crystals (van der Weijden et al., 1997). $CaCO_3$ precipitation surge immediately after mixing was also challenging with regards to clogging of the tube inlet as reported by (Emmanuel and Berkowitz, 2005). Degassing at the inlet, which is caused by strong change in pressure due to change in diameter of tubes may be considered as an explanation for such inlet clogging in our case.

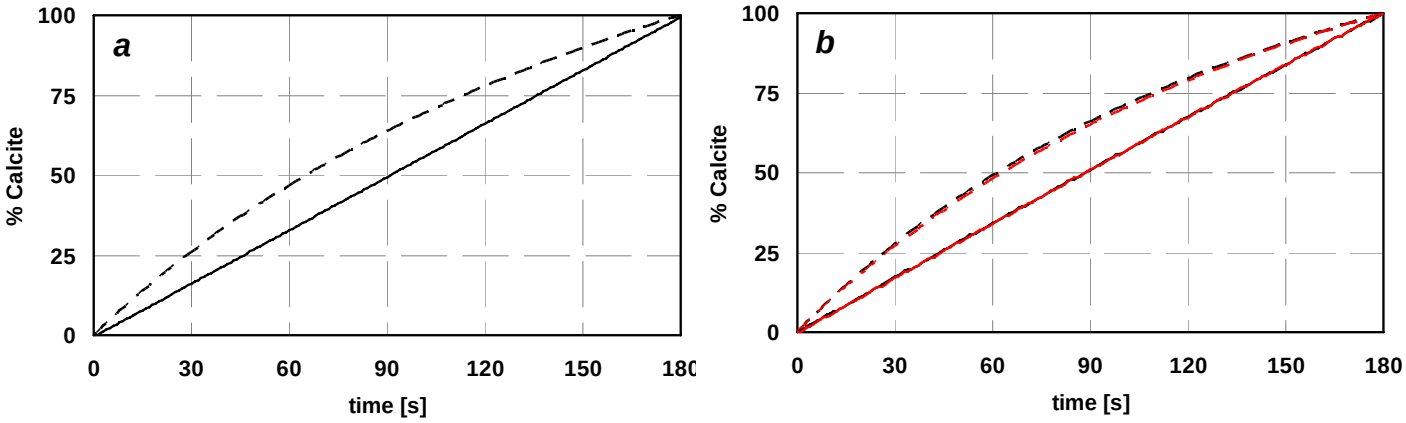

*Figure 4. Distribution of calcite calculated after equation 1 (continuous line) and equation 1*α (dashed line) for initial solution input bulk_1 (Fig. a), input bulk_2 (black lines in Fig. b) and input_bulk3 (red lines in Fig. b).*

6.4 Incorporation of strontium and manganese into $CaCO_3$

6.4.1 Strontium distribution

A total of 45 microprobe measurements have been made at the column inlet as well as 28 measurements after approximately 1 cm (see Tab. A1). From Figures 5a and b different crystal morphologies can be deduced. Needle like shapes were identified as aragonite based on their characteristic morphology and were only found at the column inlet. Small anhedral crystals were also limited to the column inlet, whereas the majority of precipitates showed calcitic shapes.

The Sr^{2+} incorporation in the calcitic shapes varies between 1.14 and 2.78 wt.% as Sr^{2+} (Table A1). Within the calcite crystal zonal structures are obvious (see Fig. 6f). In the small anhedral crystals (see Fig. 6e) the amount of Sr^{2+} incorporation lies between 5.38 and 7.15 wt.%. Needle like shapes do not show a preferential incorporation of Sr^{2+} (see Fig. 6e) compared to solids with the calcitic shape.

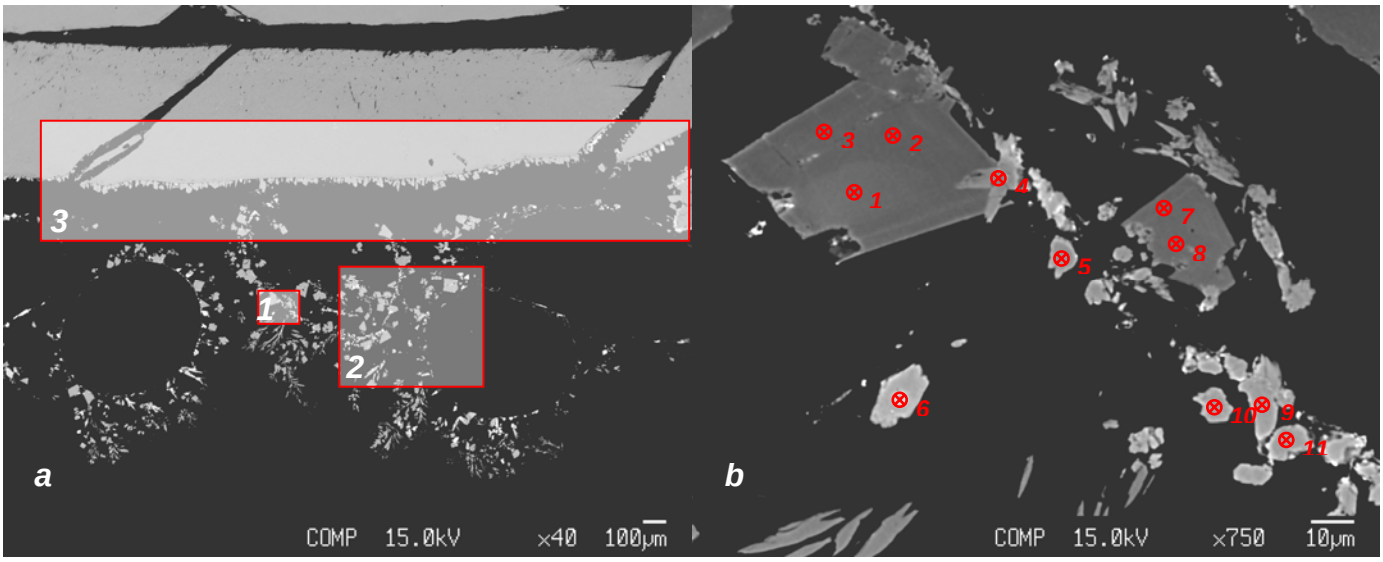

Figure 5. BSE image showing distribution of measurement points from Table A1. (a) column inlet with flow through from bottom up. Frame No. 1 depicts area with measurements 1 - 11, No. depicts 12 - 21 , No. 3 depicts 22 - 44; (b) closeup of area No. 1 in Fig. 4a.

In principle Sr^{2+} incorporation in $CaCO_3$ polymorphs occurs via isomorphic substitution of Ca^{2+}. This incorporation can be followed by the distribution coefficient according to the equation

$$D_{Sr} = ([Sr^{2+}]/[Ca^{2+}])_s/([Sr^{2+}]/[Ca^{2+}])_{aq} \quad (4)$$

where D_{Sr} is the distribution coefficient for Sr into a $CaCO_3$ modification. It is well known from literature that the apparent D - value is a function of environmental conditions during crystal growth, especially temperature and precipitation rate (Nehrke et al., 2007; Tang et al., 2008). Discrimination of Sr^{2+} versus Ca^{2+} during precipitation of calcite leads to an ongoing accumulation of Sr^{2+} versus Ca^{2+} in the solution. The bulk input_1 ratio of $([Sr^{2+}]/[Ca^{2+}])_{aq}$ was 0.012. The $([Sr^{2+}]/[Ca^{2+}])_{ss}$ ratio, which is calculated from decrease of dissolved Ca^{2+} and Sr^{2+} between input bulk_1 and output bulk_1 is 0.008. According to the equation 4 a D_{Sr} value of 0.68 is obtained.

D_{Sr} values from (Tang et al., 2008) are between 0.055 and 0.17, in which calcite was the only precipitated phase. On the other hand aragonite precipitation experiments from (Niedermayr, 2011) showed values close to 1. Since aragonitic and calcititic shapes have been identified within this column experiment the D_{Sr} value of 0.68 seems reasonable. The $([Sr^{2+}]/[Ca^{2+}])_s$ ratios from microprobe measurements give ratios ranging from 0.0022 to 0.0046 for the shells, 0.011 to 0.073 for calcite and 0.154 to 0.208 for the anhedral Sr rich crystals at the column inlet. The

thereby calculated D_{Sr} values range from 0.95 to 6.37 and 13.31 to 17.98 for calcitic and anhedral crystals, respectively.
Note that the above calculated D_{Sr} values do not give a representative distribution of the Sr^{2+} incorporation throughout the whole column. All measured points are referred to the beginning of the column. Additionally the points were chosen to analyse the chemical composition of the high Sr^{2+} areas. On that account the difference between the calculated D_{Sr} values from bulk aqueous solutions and the D_{Sr} values derived from microprobe analysis may be explained by areas with a very low incorporation degree, which have not been measured.

Difference in chemical composition between shells, newly formed calcite and anhedral crystals is best illustrated by a plot of Na^+ vs. Sr^{2+} (Fig. 7). High Na^+/Sr^{2+} ratios are clearly correlated to marine environment (i.e. shells), whereas the anhedral crystals show a higher incorporation of Na^+ than calcite does. High Na^+ content in the shells might be caused by high Na^+ in seawater for shell formation. On the other hand despite the fact that the Sr/Ca ratio in seawater is the same as in our experiments Sr^{2+} incorporation into inorganic new precipitates strongly exceeds the values measured in our shells. From (Ishikawa and Ichikuni, 1984) it is suggested that two atoms of Na^+ replace Ca^{2+} to maintain charge balance. In general the amount of Na^+ for incorporation is suggested to be limited by the crystal defects. Additionally the Na^+ content in calcite increases for precipitation at elevated supersaturation caused by preferentially irregular crystal structures at elevated precipitation rates (Busenberg and Plummer, 1985). Thus besides distinguishing between shells and newly formed $CaCO_3$ the Na^+/Sr^{2+} ratios might be used to discover precipitation condition during growth. The inhomogeneous distribution of Na/Sr let us suggest that the initial $CaCO_3$ precipitation surge at the inlet may be accompanied with continuous precipitation at low rates in the same area. The amount of Sr^{2+} increased in crystals which were not attached to the shell surface (see Fig. 6d). This could imply that crystals which are not attached to the shell surface grow faster. Moreover increasing Sr^{2+} incorporation on the outer rims of the calcitic precipitates can be seen from Figs. 6d and f. Increasing precipitation rate in the ongoing experiment could explain the latter behaviour.

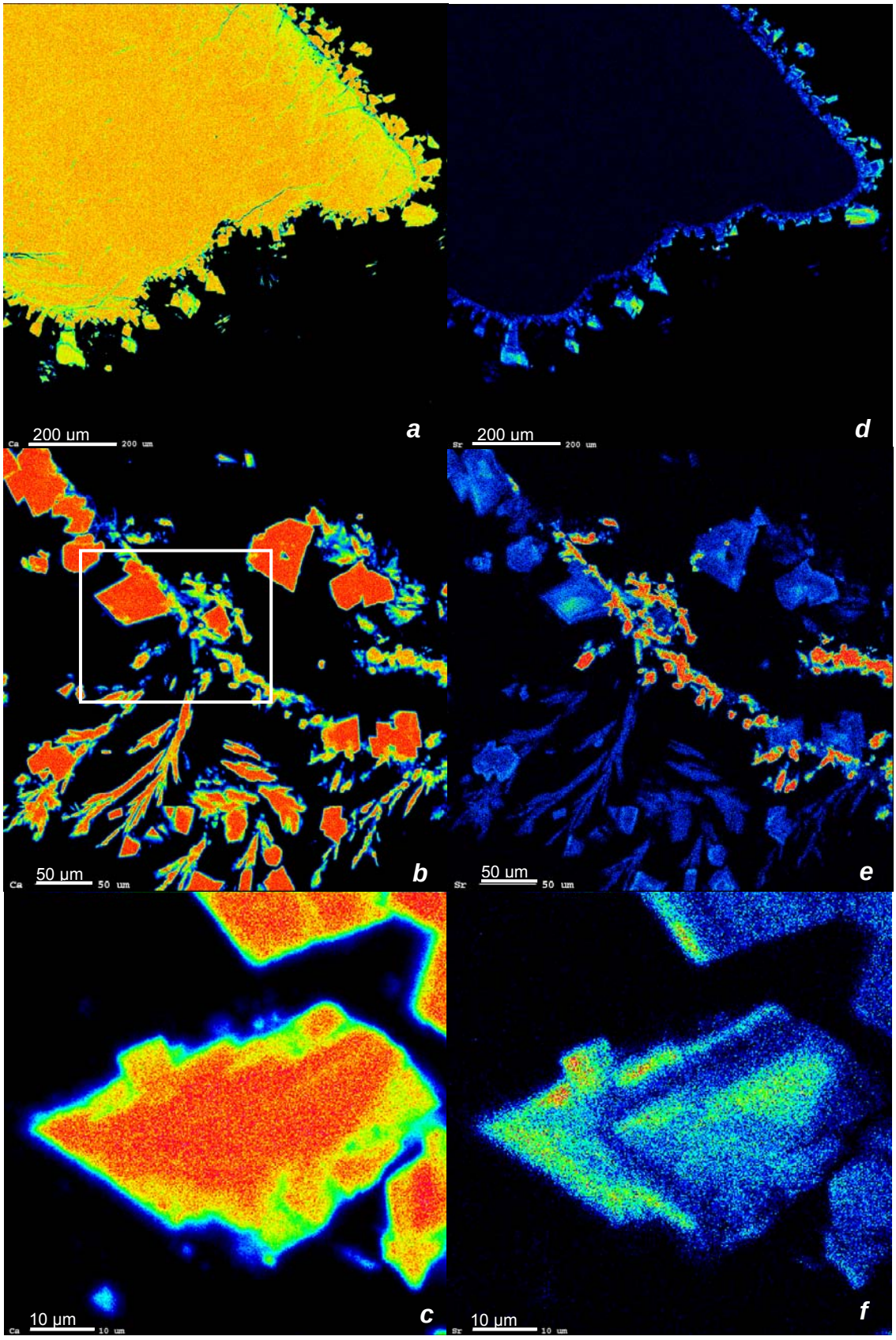

Figure 6. Elemental Map of Ca^{2+} (a-c) and Sr^{2+} distribution (d-f) from column experiment 1. Frame in Fig 4b depicts area of BSE picture (Fig. 5b). Measurement points 45 - 74 (Tab. A1) taken from area in Fig 6d.

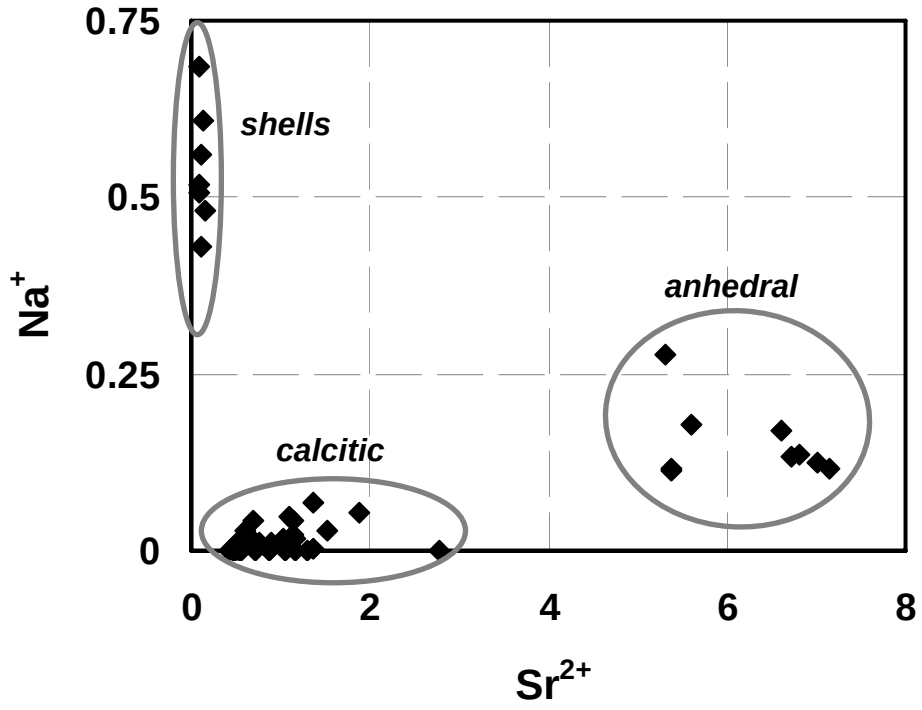

Figure 7. Plot of Na^+ versus Sr^{2+} in wt.% from samples No. 1 to 44 (see Tab. A1) indicating high sodium content for the shells, high Sr^{2+} content for anhedral crystals (see Fig. 6e) and low trace element incorporation for calcitic structures.

6.4.2 Manganese distribution

A total of 26 microprobe measurements have been carried out in the column, analysing the manganese poor or virtually free core as well as the manganese rich rims (see areas in Figs. 8a and b; Tab. A1). Fig. 9b shows very heterogeneous behaviour of calcite crystals concerning incorporation of Mn^{2+}. In analogy to the experiment for Sr^{2+} incorporation (see Chapter 6.4.1) manganese incorporation seems to increase with crystal size as well as with increasing distance from shells. Manganese incorporation in $CaCO_3$ polymorphs occurs via isomorphic substitution of Ca^{2+}. In alagogy to Sr, the Mn incorporation into $CaCO_3$ can be followed by the distribution coefficient D_{Mn}.

The $([Mn^{2+}]/[Ca^{2+}])_{aq}$ ratio in the input solution is 0.0011. Based on the difference in aqueous solution chemistry between solution input bulk_3 and outputbulk_3 the $([Mn^{2+}]/[Ca^{2+}])_{ss}$ ratio in the precipitated solid is 0.0067. The thereby calculated amount of manganese in the precipitated material is 0.36 wt%. The partition coefficient

$$D_{Mn} = ([Mn^{2+}]/[Ca^{2+}])_{ss}/([Mn^{2+}]/[Ca^{2+}])_{aq} \quad (4)$$

calculated after (Böttcher, 1998) is 6.08, which is in good accordance with the presented partition coefficients with D_{Mn} values between 2 and 13 for his experiments. However recalculating the molecular weight of the microprobe analysis, results in a maximum of 5.6 wt% of Mn in the precipitated material (sample Nr. 83 in Tab. A1). The calculated D_{Mn} value from the latter micro probe measurement is 163.

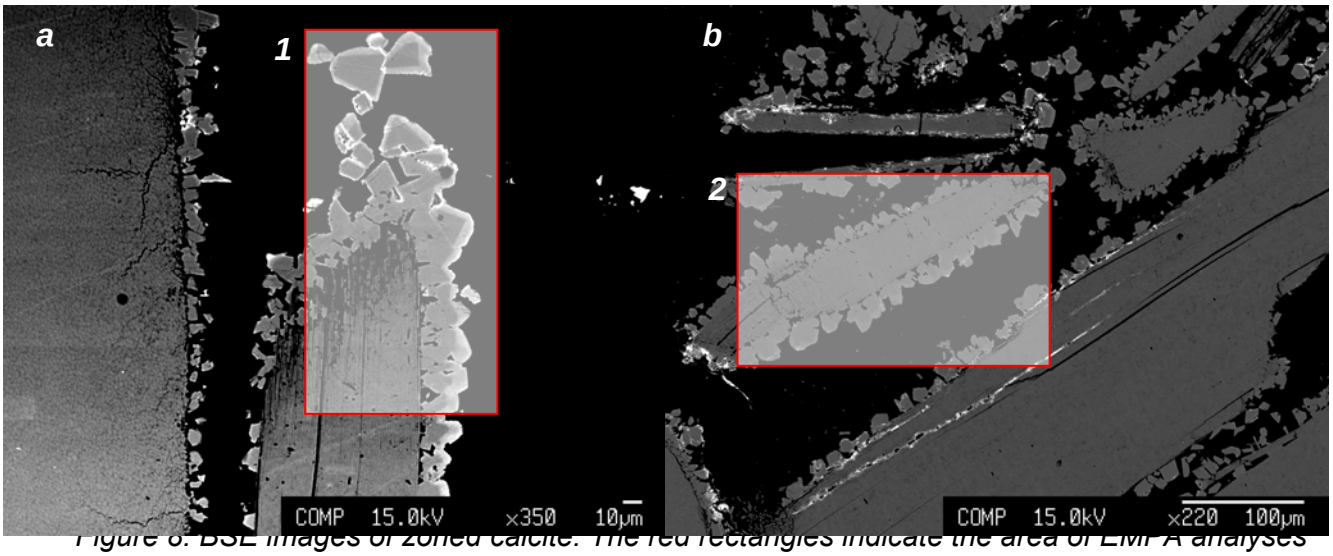

Figure 8. BSE images of zoned calcite. The red rectangles indicate the area of EMP A analyses from Table A1. Flow through from bottom up. Frame No. 1 depicts the area with measurements 75 - 86 (a), Nr.2 depicts 87 - 100 (b).

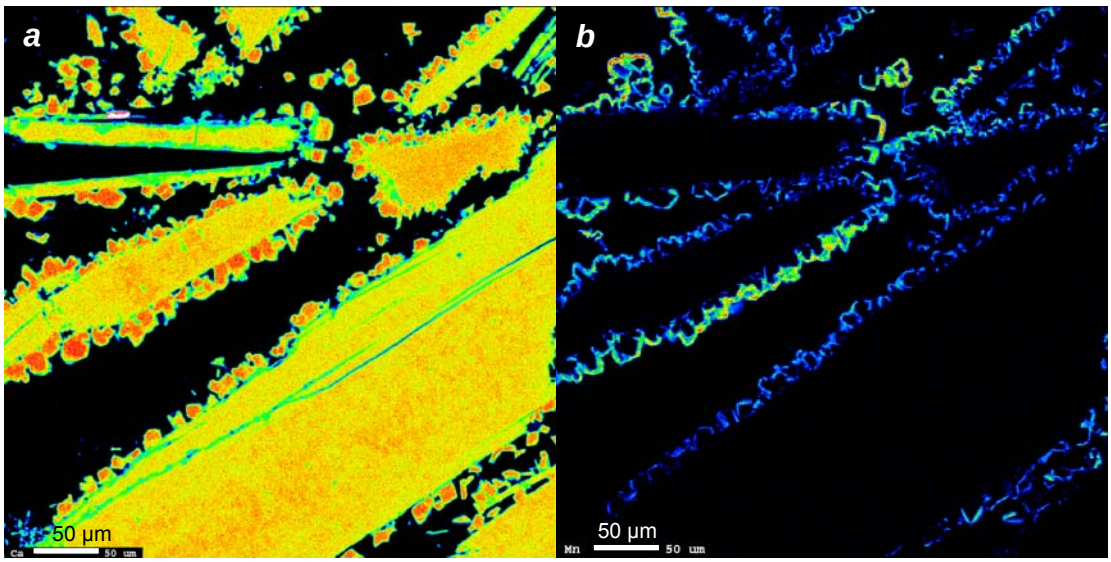

Figure 9. Elemental map showing distribution of Ca^{2+} (a) and Mn^{2+} content (b) for the cementated carbonate shells from column experiment 2.

(Franklin and Morse, 1983) studied the incorporation of manganese into calcite by using distilled water in equilibrium with calcite and distinct amounts of $MnCO_3$. They reported a rapid incorporation of 10 to 15 % of the total Mn^{2+} within the first 10 minutes of their calcite seeded experiment, increasing with initial amount of calcite seeds. Within our column experiment 27% of the dissolved Mn^{2+} was removed from the solution in the experiment (see input bulk_3 and output bulk_3 in Tab. 1), which may be due to the relatively large surface area of the used shells for precipitation and increased precipitation rate.

6.5 Conclusions

A supersaturated solution with respect to calcite was pumped through columns packed with shell fragments of a grain size between 0.5 and 1mm, which resulted in approximately 68% free pore space. At the given flow rate of 1.6 ml/min the mean retention time of the solution was approximately 3 minutes in the column. Within the total 5400 minutes of experimental runtime the estimated amount of $CaCO_3$ precipitated was 68 mg for the first experiment and 168 mg for the second experiment. Therefore the free pore size was reduced by 0.3 and 0.8 % for experiments 1 and 2, respectively. The $CaCO_3$ precipitations are not homogeneously distributed. The preferential occurrence of $CaCO_3$ precipitation close to the inflow indicates a precipitation surge as typically observed in such kind of experimental approaches ((Lee and Morse, 1999; Noiriel et al., 2012; van der Weijden et al., 1997)).

The modelling of the change in aqueous solution chemistry between column inlet and outlet with the proposed model of calcium carbonate formation as the solely factor influencing solution chemistry can be best followed by change in pH from input to output.

Interestingly the calcite precipitation rate estimated from the given empirical approach by (Wolthers et al., 2012) fails to reproduce the observed precipitation rates and to explain the spatial inhomogeneous distribution and the amount of $CaCO_3$ precipitates in the columns. Overall precipitation rates are in the order of 20 times higher than predicted with the proposed model. This can be attributed to the initial precipitation surge which could be induced by CO_2 degassing effects at the column inlet and the huge reactive surface area of the provided shells.

However applying a multiplication factor α to the model, it correctly reproduces temporal evolution of solution chemistry as well as spatial distribution of precipitates within the columns.

Beside crystal shapes the Sr^{2+} and Mn^{2+} as well as Na^{+} content of the solids can be easily used to distinguish shell fragments from newly formed $CaCO_3$ cement. The range of the distribution of Sr^{2+} and Mn^{2+} concentrations in the precipitates suggests temporally and locally different $CaCO_3$

precipitation rates within adjacent areas of the column. These rates seem to increase with crystal size and distance from the shells (i.e. in the free pore space).

For both, the Sr^{2+} and Mn^{2+} bearing experiment the overall bulk D_{Sr} (0.68) and D_{Mn} (6.08) values calculated from aqueous solutions are in good agreement with literature values. However, the apparent measured data of the trace element content in the $CaCO_3$ solids is very heterogeneous and results in a maximum D_{Sr} and D_{Mn} value of 18 and 163, respectively.
Despite the fact that the concentrations of Ca^{2+} and Sr^{2+} in solution input bulk_1 were in the range of seawater, the D_{Sr} values of the newly formed precipitates are much higher than reported for precipitates from natural environments (Ortega et al., 2005). High amounts of Sr^{2+} in calcite are commonly referred to recrystallisation of aragonite to calcite, whereas our results indicate that such incorporation may occur even without transformation.

The alternating trace element rich and poor growth zones even at a constant solution composition, temperature and flow through point to the difficulty inherent with tracing environmental conditions during formation of $CaCO_3$. This layer formation can not be satisfyingly explained within our experiments, but may be related to individual and distinct flow behaviour. The incorporation mechanisms which result in bulk ratios that serve as proxies for the reconstruction of environmental conditions during precipitation of $CaCO_3$ do not necessarily apply on the microscale where actual trace element incorporation into $CaCO_3$ may exceed or fall below the average bulk incorporation.

6.6 References

Böttcher, M.E., 1998. Manganese(II) partitioning during experimental precipitation of rhodochrosite and calcite solid solutions from aqueous solutions. Marine Chemistry 62, 287-297.

Busenberg, E., Plummer, N., L., 1985. Kinetic and thermodynamic factors controlling the distribution of SO_3^{2-} and Na^+ in calcites and selected aragonites. Geochimica et Cosmochimica Acta 49, 713-725.

Dietzel, M., Rinder, T., Niedermayr, A., Mittermayr, F., Leis, A., Klammer, D., Köhler, S., Reichl, P., 2008. Mechanisms of Sinter Formation in Drainage Systems. BHM Berg- und Hüttenmännische Monatshefte 153, 369-372.

Dromgoole, E.L., Walter, L.M., 1990. Iron and manganese incorporation into calcite: Effects of growth kinetics, temperature and solution chemistry. Chemical Geology 81, 311-336.

Emmanuel, S., Berkowitz, B., 2005. Mixing-induced precipitation and porosity evolution in porous media. Advances in Water Resources 28, 337-344.

Franklin, M.L., Morse, J.W., 1983. The interaction of manganese(II) with the surface of calcite in dilute solutions and seawater. Marine Chemistry 12, 241-254.

Gislason, S.R., Wolff-Boenisch, D., Stefansson, A., Oelkers, E.H., Gunnlaugsson, E., Sigurdardottir, H.I., Sigfusson, B., Broecker, W.S., Matter, J.M., Stute, M., Axelsson, G., Fridriksson, T., 2010. Mineral sequestration of carbon dioxide in basalt: A pre-injection overview of the CarbFix project. International Journal of Greenhouse Gas Control 4, 537-545.

Ishikawa, M., Ichikuni, M., 1984. Uptake of sodium and potassium by calcite. Chemical Geology 42, 137-146.

Lee, Y.-J., Morse, J.W., 1999. Calcite precipitation in synthetic veins: implications for the time and fluid volume necessary for vein filling. Chemical Geology 156, 151-170.

Lioliou, M.G., Paraskeva, C.A., Koutsoukos, P.G., Payatakes, A.C., 2007. Heterogeneous nucleation and growth of calcium carbonate on calcite and quartz. Journal of Colloid and Interface Science 308, 421-428.

Matter, J.M., Broecker, W.S., Stute, M., Gislason, S.R., Oelkers, E.H., Stefansson, A., Wolff-Boenisch, D., Gunnlaugsson, E., Axelsson, G., Bjornsson, G., 2009. Permanent Carbon Dioxide Storage into Basalt: The CarbFix Pilot Project, Iceland. Energy Procedia 1, 3641-3646.

Molenaar, N., Venmans, A.A.M., 1993. Calcium carbonate cementation of sand: A method for producing artificially cemented samples for geotechnical testing and a comparison with natural cementation processes. Engineering Geology 35, 103-122.

Mucci, A., Morse, J.W., 1983. The incorporation of Mg^{2+} and Sr^{2+} into calcite overgrowths: influences of growth rate and solution composition. Geochimica et Cosmochimica Acta 47, 217-233.

Nehrke, G., Reichart, G.J., Van Cappellen, P., Meile, C., Bijma, J., 2007. Dependence of calcite growth rate and Sr partitioning on solution stoichiometry: Non-Kossel crystal growth. Geochimica et Cosmochimica Acta 71, 2240-2249.

Niedermayr, A., 2011. Effect of Magnesium. polyaspartic acid, carbonate accumulation rate and temperature on the crytallization, morphology, elemental incorporation and isotopic fractionation of caclium carbonate phases, Institute of Applied Geosciences. Graz University of Technology, Graz.

Noiriel, C., Steefel, C.I., Yang, L., Ajo-Franklin, J., 2012. Upscaling calcium carbonate precipitation rates from pore to continuum scale. Chemical Geology 318-319, 60-74.

Ortega, R., Maire, R., Devès, G., Quinif, Y., 2005. High-resolution mapping of uranium and other trace elements in recrystallized aragonite and calcite speleothems from caves in the Pyrenees (France): Implication for U-series dating. Earth and Planetary Science Letters 237, 911-923.

Parkhurst, D.L., Apello, C.A.J., 1999. User's guide to PHREEQC (V2). U.S. Geol. Sur 312.

Pingitore Jr, N.E., Eastman, M.P., Sandidge, M., Oden, K., Freiha, B., 1988. The coprecipitation of manganese(II) with calcite: an experimental study. Marine Chemistry 25, 107-120.

Tang, J., Köhler, S.J., Dietzel, M., 2008. Sr^{2+}/Ca^{2+} and $^{44}Ca/^{40}Ca$ fractionation during inorganic calcite formation: I. Sr incorporation. Geochimica et Cosmochimica Acta 72, 3718-3732.

Taylor, K.G., Machent, P.G., 2011. Extensive carbonate cementation of fluvial sandstones: An integrated outcrop and petrographic analysis from the Upper Cretaceous, Book Cliffs, Utah. Marine and Petroleum Geology 28, 1461-1474.

van der Weijden, R.D., van der Heijden, A.E., Witkamp, G.J., van Rosmalen, G.M., 1997. The influence of total calcium and total carbonate on the growth rate of calcite. Journal of Crystal Growth 171, 190-196.

Wolthers, M., Nehrke, G., Gustafsson, J.P., Van Cappellen, P., 2012. Calcite growth kinetics: Modeling the effect of solution stoichiometry. Geochimica et Cosmochimica Acta 77, 121-134.

6.7 Appendix

Table A1. Chemical composition of microprobe analysis.1-11 (Fig. 5b), 12 -44 (Fig. 5a) 45-74 (Fig. 4a); 75 -86 (Fig. 7a), 87 - 100 8Fig. 7b).

No.	MgO	CaO	SrO	MnO	Na_2O
1	0.01	52.67	3.28	bdl.	bdl.
2	0.02	53.85	1.55	bdl.	bdl.
3	0.01	53.37	1.36	0.02	0.03
4	bdl.	48.83	6.36	0.02	0.15
5	bdl.	48.54	8.28	bdl.	0.17
6	bdl.	51.70	8.45	0.05	0.16
7	0.01	54.74	1.61	0.02	0.09
8	bdl.	53.45	2.21	0.03	0.07
9	0.02	47.33	7.83	0.02	0.23
10	0.02	45.80	8.06	0.04	0.18
11	0.01	49.62	7.95	bdl.	0.18
12	bdl.	53.23	0.85	0.02	bdl.
13	0.01	53.94	1.03	0.03	bdl.
14	bdl.	47.82	6.35	bdl.	0.16
15	0.01	46.63	6.28	bdl.	0.37
16	bdl.	53.33	1.24	0.01	bdl.
17	bdl.	46.84	6.62	0.04	0.24
18	0.01	52.86	1.31	0.03	0.06
19	bdl.	53.66	0.91	bdl.	0.02
20	bdl.	53.64	0.84	0.03	0.02
21	0.02	49.40	0.82	0.02	0.06
22	bdl.	52.20	0.11	0.08	0.93
23	bdl.	52.73	0.85	0.02	0.01
24	0.01	52.69	1.81	bdl.	0.04
25	0.02	52.13	0.15	0.01	0.82
26	bdl.	54.20	0.64	bdl.	0.02
27	0.29	52.50	0.13	0.05	0.75
28	0.23	52.29	0.12	0.00	0.58
29	bdl.	53.34	1.37	bdl.	bdl.
30	0.01	53.07	0.64	0.02	bdl.
31	0.01	54.36	0.55	bdl.	bdl.
32	bdl.	54.08	0.67	bdl.	0.01
33	0.05	51.01	1.38	0.01	0.02
34	bdl.	52.81	1.61	0.03	bdl.
35	bdl.	53.69	0.57	bdl.	bdl.
36	bdl.	53.47	0.72	bdl.	0.04
37	bdl.	53.41	0.86	bdl.	0.01
38	bdl.	53.59	1.36	bdl.	0.06
39	bdl.	53.71	0.66	bdl.	bdl.
40	bdl.	53.52	0.50	0.03	bdl.
41	0.01	49.86	1.22	bdl.	0.02
42	0.13	51.26	0.10	bdl.	0.70
43	0.13	51.34	0.20	bdl.	0.65
44	0.08	50.83	0.11	bdl.	0.68
45	0.01	50.48	1.96	0.06	
46	0.02	51.25	1.46	0.03	
47	bdl.	49.04	0.66	bdl.	
48	bdl.	54.09	1.30	bdl.	
49	bdl.	52.81	0.80	bdl.	
50	bdl.	53.87	0.96	0.04	

51	0.01	52.48	2.50	0.01	
52	bdl.	48.45	1.95	0.04	
53	0.03	52.90	1.87	0.02	
54	bdl.	52.58	2.36	0.01	
55	bdl.	52.54	2.16	bdl.	
56	0.03	53.23	1.02	bdl.	
57	bdl.	53.06	0.80	bdl.	
58	0.01	53.45	0.92	bdl.	
59	bdl.	51.15	2.39	0.02	
60	0.01	51.02	3.15	0.01	
61	bdl.	52.31	2.86	0.00	
62	bdl.	52.36	2.17	0.01	
63	bdl.	52.46	1.89	bdl.	
64	0.02	53.63	1.53	bdl.	
65	0.01	54.11	0.93	bdl.	
66	bdl.	52.00	1.68	0.01	
67	0.02	53.32	1.07	bdl.	
68	bdl.	53.93	1.02	bdl.	
69	bdl.	53.16	1.13	bdl.	
70	0.02	53.63	0.75	0.03	
71	0.01	53.43	1.06	0.03	
72	0.02	52.07	2.47	bdl.	
73	bdl.	52.61	1.66	0.02	
74	0.03	49.90	0.64	0.01	
75	bdl.	53.29	0.06	3.89	bdl.
76	bdl.	55.68	0.02	0.06	0.03
77	bdl.	50.79	bdl.	4.87	0.01
78	0.01	55.11	bdl.	0.17	bdl.
79	bdl.	44.86	0.01	5.02	0.01
80	bdl.	55.41	0.01	0.58	0.02
81	bdl.	51.93	0.03	2.51	0.01
82	0.02	55.52	bdl.	0.05	0.02
83	bdl.	44.24	0.03	7.30	bdl.
84	bdl.	55.29	bdl.	0.03	0.06
85	bdl.	55.11	0.01	0.10	bdl.
86	0.01	54.89	bdl.	0.08	bdl.
87	bdl.	59.40	0.02	bdl.	bdl.
88	bdl.	57.14	bdl.	1.21	bdl.
89	bdl.	51.88	bdl.	2.79	bdl.
90	bdl.	56.68	bdl.	0.42	0.05
91	0.01	49.28	0.01	4.49	bdl.
92	bdl.	54.82	bdl.	3.68	0.01
93	bdl.	56.29	bdl.	0.41	0.02
94	bdl.	59.38	0.01	bdl.	0.03
95	bdl.	58.17	bdl.	0.78	0.02
96	0.04	55.28	bdl.	4.52	0.01
97	0.03	59.21	bdl.	0.04	0.01
98	bdl.	50.47	0.04	0.16	0.47
99	0.02	56.83	0.02	0.17	bdl.
100	bdl.	56.63	0.01	0.03	bdl.

bdl. below detection limit

7. Concluding remarks

This thesis comprises a series of field and lab studies and aims to improve our understanding of calcium carbonate precipitation in natural and man-made environments. Overall key questions are:

1. Can we trace the evolution of carbonate formation from elemental and isotopic composition of aqueous solutions and solids?

2. What are the effects of pH, CO_2 exchange with the atmosphere, and mixing issues on the calcite precipitation capacities of a solution?

3. May trace element incorporation of Sr^{2+} and Mn^{2+} be applied in laboratory experiments to follow the evolution of carbonate formation in porous media?

(1) The main mechanisms, which are responsible for calcium carbonate scaling in the present alkaline environments, were successfully discovered by using multi-proxy and modelling approaches. Water-cement interaction is primarily connected to an increase of pH and in particular of highly soluble K^+ (Na^+) ions. Ongoing dissolution of alkali and calcium hydroxide, may even lead to supersaturation with respect to brucite even at very low Mg^{2+} concentrations.
The application of stable carbon isotope distribution has shown to be a very useful tool to gain an advanced understanding of the formation of $CaCO_3$ induced by cement-water reactions. $CaCO_3$ sinter formation was identified to be referred to both the bicarbonate of the groundwater and the absorption of atmospheric CO_2. Absorption phenomena were also studied by $CaCO_3$ sinter formation in the drainage along a flow path via isotopic $^{13}C/^{12}C$ evolution in the DIC and in the $CaCO_3$ precipitates.

(2) The uptake of CO_2 in alkaline solutions can either lead to an increase or decrease of the saturation index with respect to calcite, where the internal P_{CO2} ($10^{-6.15}$ atm at 25°C) marks the respective boundary conditions. Mixing of highly alkaline solutions with groundwater-like solutions in the drainage can cause a dramatic increase of calcite supersaturation in the resulting solution, which stimulates calcite formation. Both the increase and decrease of $SI_{Calcite}$ values through mixing is caused by the non-linear behaviour of redistribution of DIC species as a function of pH.

Supersaturation may even occur, if both endmember solutions are in equilibrium with respect to calcite. In the pure $CaCO_3$ - CO_2 - H_2O system the required pH values can be reached if a groundwaters are suggested where calcite is dissolved under closed system conditions with respect to CO_2 exchange between the solution and the surrounding atmosphere - i.e. the CO_2 which is consumed by limestone dissolution is not replenished.

In general calcite precipitation capacities of drainage solutions increase at elevated pH. But the apparent amount of calcite formation in a tunnel drainage depends on additional parameters, like CO_2 uptake rate, calcite precipitation rates and the residence time of drainage solution in the tunnel. Highest calcite precipitation rates are estimated at pH 10.2 ±0.3, which may cause relatively low abundance of moderate alkaline drainage solutions due to rapid calcite formation and corresponding pH decrease. The mixing of alkaline solutions and groundwater-type solutions increases both, calcite precipitation capacities and rates.

In conclusion a sustainable prevention of calcium carbonate scaling in tunnel drainage systems may be reached by (i) the use of hydraulic cements for concrete and shotcrete application with reduced content of portlandite and leachable alkalies, e.g. by adding fly ash with latent hydraulic silica, (ii) avoiding mixtures of high alkaline type 1 and type 3 solutions, e.g. by separating flow channels, (iii) decreasing residence times of solutions within the tunnel, e.g. by tailored design of the drainage system, (iv) increasing the CO_2 exchange rates between the solution and the atmosphere for solutions with internal P_{CO2} values between $10^{-3.45}$ and $10^{-6.15}$ atm (25°C), e.g. by ventilation with air, (v) decreasing the respective CO_2 exchange rates for solutions with internal P_{CO2} values $<10^{-6.15}$ and $> 10^{-3.45}$ atm, e.g. by laminar flow and (vi) adding substances to inhibit calcium carbonate formation, like polyaspartic acid, if applicable.

(3) For the $CaCO_3$ precipitation experiments using columns filled with shells, trace element addition of Sr^{2+} and Mn^{2+} was used to investigate the evolution of newly formed precipitates within the free pore space. The distribution coefficients D_{Sr} and D_{Mn} for the formation of calcite resulted in values of 0.68 and 6.1 in the column experiments from the bulk material at $SI_{Calcite}$ values of 1.1 and 1.5, respectively. Whereas the calculated bulk D values from aqueous solutions are in good agreement with literature values, the spatial incorporation of the trace elements is very heterogeneous delivering a maximum D_{Sr} and D_{Mn} value of 18 and 163, respectively. The latter D_{Sr} values of the newly formed precipitates are much higher than reported for precipitates from natural environments. Extraordinary high amounts of Sr^{2+} in calcite are commonly interpretated to be caused by recrystallisation of aragonite to calcite,

whereas our results indicate that the accumulation of Sr in calcite occurred without transformation.

The alternating trace element rich and poor growth zones even at a constant solution composition, temperature and flow through point to the difficulty inherent with tracing environmental conditions during formation of $CaCO_3$. This layer formation can not be satisfyingly explained within our experiments, but may be related to individual and distinct flow behaviour. The incorporation mechanisms which result in bulk ratios that serve as proxies for the reconstruction of environmental conditions during precipitation of $CaCO_3$ do not necessarily apply on the microscale where actual trace element incorporation into $CaCO_3$ may exceed or fall below the average bulk incorporation.

From observed high D_{Mn} values it is suggested that trace amounts of Mn^{2+} already have an impact of calcite precipitation kinetics. Conclusively the impact of Mn^{2+} addition at the used concentration level on precipitation kinetics may disqualify such an approach for tracing $CaCO_3$ precipitation evolution in a porous media.

Appendix - List of publications

Articles

Rinder, T.; Dietzel, M.; Leis, A.: Calcium Carbonate Scaling under Alkaline Conditions - Case Studies and Hydrochemical Modelling. - Submitted to Applied Geochemistry (2012)

Dietzel, M.; Harer, G.; Klammer, D.; Köhler, S. J.; Leis, A.; Mittermayr, F.; Niedermayr, A.; Reichl, P.; Rinder, T.: Karbonatabscheidungen in Drainagesystemen von Tunnelbauten. - in: Beiträge zur Hydrogeologie 57 (2010) , S. 143 - 153

Dietzel, M.; Rinder, T.; Leis, A.; Reichl, P.; Sellner, P. J.; Draschitz, C.; Plank, G.; Klammer, D.; Schöfer, H.: Koralm Tunnel as a Case Study for Sinter Formation in Drainage Systems - Precipitation Mechanisms and Retaliatory Action. - in: Geomechanik und Tunnelbau 1 (2008) 4, S. 271 - 278

Dietzel, M.; Rinder, T.; Niedermayr, A.; Mittermayr, F.; Leis, A.; Klammer, D.; Köhler, S. J.; Reichl, P.: Ursachen und Mechanismen der Versinterung von Tunneldrainagen. - in: Berg- und hüttenmännische Monatshefte 153 (2008) 10, S. 369 - 372

Dietzel, M.; Rinder, T.; Niedermayr, A.; Köhler, S. J.; Leis, A.: Versinterungen in Drainagesystemen von Tunnelbauten - Mechanismen, Monitoring und Prognosen. - in: Geotechnik 34 (2008), S. 89 - 100

Dietzel, M.; Rinder, T.; Leis, A.; Köhler, S. J.; Klammer, D.; Reichl, P.: $^{13}C/^{12}C$ and $^{18}O/^{16}O$ signatures of calcite sinter in alkaline drainage solutions - Proxy for precipitation mechanisms. - in: Berichte des Institutes für Erdwissenschaften der Karl-Franzens-Universität Graz 11 (2006) , S. 16 - 18

Conference contributions

Mittermayr, F.; Rinder, T.; Klammer, D.; Leis, A.; Dietzel, M.:
A carbon isotope study of thaumasite and calcite sinter formation in underground constructions. - in: International Congress on Durability of Concrete ; 1 (2012)

Turpin, M., Rinder, T., Dietzel, M., Bahamonde. J.R., Immenhauser, A., (2011):
Granulometry and geochemistry of micritic carbonates along a Carboniferous and a Jurassic platform to basin transects. Geophysical Research Abstracts, Vol. 13, EGU

Wagner, T.; Mayaud, C.; Oswald, S.; Rinder, T.; Leis, A.; Stadler, H.; Benischke, R.; Birk, S.: Understanding intercatchment flow in a karst aquifer – using the Lurbach system example (Eastern Alps - Austria). - in: 8th EGU General Assembly. (2011), S. 7962 - 7962

Rinder, T.; Dietzel, M.; Spatzenegger, J.; Abdalla, R.: Calcium carbonate cementation of unconsolidated materials - An experimental approach. - in: EGU 2010. (2010), S. 12395 - 12395

Oswald, S.; Birk, S.; Winkler, G.; Benischke, R.; Leis, A.; Dietzel, M.; Stadler, H.; Klock, E.; Köhler, S. J.; Rinder, T.: Künstliche und natürliche Tracer in einem Karsteinzugsgebiet mit allochthoner Neubildung (Lurbach, Österreich). - in: Grundwasser für die Zukunft - Tagung der Fachsektion Hydrogeologie (2010), S. 130 - 130

Abdalla, R.; Rinder, T.; Dietzel, M.; Leis, A.: Quality of groundwater in the shallow and deep aquifers of the Gefara Plain, Tripoli region, Libya. - in: Groundwater Quality Sustainability, Extended Abstracts (2010), S. 2182 - 2182

Abdalla, R.; Rinder, T.; Dietzel, M.; Leis, A.: Seawater Intrusion and groundwater quality of the coastal area in Tripoli region, Libya. - in: EGU 2010. (2010), S. 11911 - 11911

Rinder, T.; Dietzel, M.; Köhler, S. J.; Leis, A.: Multi proxy approach for the formation of calcium carbonates in alkaline man-made environments. - in: Awards Ceremony Speeches and Abstracts of the 19th Annual V.M. Goldschmidt Conference (2009), S. A1103 - A1103

Rinder, T.; Dietzel, M.; Leis, A.: Multi proxy approach for the formation of calcium carbonates in alkaline man-made environments. - in: 6th EGU General Assembly. (2009), S. 13782 - 13782

Oswald, S.; Benischke, R.; Leis, A.; Winkler, G.; Klock, E.; Stadler, H.; Rinder, T.; Köhler, S. J.; Dietzel, M.; Birk, S.: Responses of artificial and natural tracers to a storm event in a karst catchment with allogenic recharge (Lurbach, Austria). - in: 6th EGU General Assembly. (2009), S. 9255 - 9255

Dietzel, M.; Rinder, T.; Leis, A.; Köhler, S. J.: Stable Carbon and Oxygen Isotope Values of Secondary Calcite from Cement Water Interaction - Proxies for Origin and Environmental Conditions. - in: EGU Vienna. (2008), S. 1 - 2

Dietzel, M.; Rinder, T.; Niedermayr, A.; Köhler, S. J.; Leis, A.: Versinterungen in Drainagesystemen von Tunnelbauten - Mechanismen, Monitoring und Prognosen. - in: Beiträge zum Symposium "Drainagesysteme im Tunnelbau - Design, Versinterung und Instandhaltung". (2008), S. 89 - 100

Dietzel, M.; Draschitz, C.; Harer, G.; Klammer, D.; Köhler, S. J.; Leis, A.; Mittermayr, F.; Niedermayr, A.; Reichl, P.; Rinder, T.; Sellner, P.: Versinterungen von Tunneldrainagen - Ursachen, Risikoabschätzung, Gegenmaßnahmen. - in: Tagungsband "Wasserressourcen und deren Bewirtschaftung- Die Bedeutung von Netzwerken. (2008), S. 236 - 243

Dietzel, M.; Rinder, T.; Leis, A.; Köhler, S. J.; Klammer, D.; Reichl, P.: $^{13}C/^{12}C$ and $^{18}O/^{16}O$ Signatures of Calcite Sinter in Alkaline Drainage Solutions. - in: EGU. (2007)

Rinder, T.; Dietzel, M.; Leis, A.; Köhler, S. J.; Klammer, D.; Reichl, P.: Calcite sinter formation in alkaline drainage solutions of tunnel buildings - chemical evolution and distribution of 13C/12C and 18O/16O isotopes. - in: EGU (2006), S. 0294 - 0294

Rinder, T.; Dietzel, M.; Köhler, S. J.; Klammer, D.; Leis, A.; Reichl, P.: Ursachen der Karbonatversinterung von Tunneldrainagen. - in: Sediment 2006 (2006), S. 143 - 143

Rinder, T.; Dietzel, M.; Köhler, S. J.; Klammer, D.; Leis, A.; Reichl, P.: Ursachen der Karbonatversinterung von Tunneldrainagen. - in: Meeting of SEPM Central European Section ; 2006 (2006), S. 143 - 143